General Disclaimer

One or more of the Following Statements may affect this Document

- This document has been reproduced from the best copy furnished by the organizational source. It is being released in the interest of making available as much information as possible.

- This document may contain data, which exceeds the sheet parameters. It was furnished in this condition by the organizational source and is the best copy available.

- This document may contain tone-on-tone or color graphs, charts and/or pictures, which have been reproduced in black and white.

- This document is paginated as submitted by the original source.

- Portions of this document are not fully legible due to the historical nature of some of the material. However, it is the best reproduction available from the original submission.

Produced by the NASA Center for Aerospace Information (CASI)

PHASE II FINAL REPORT

STUDY OF A LOW ALTITUDE SATELLITE
UTILIZING A DATA RELAY SATELLITE SYSTEM

AUGUST 1969

Contract No. NAS 5-11602

Prepared By:

Project Manager/Dennis Eggert
Hughes Aircraft Company
Space Systems Division
For
Goddard Space Flight Center
Greenbelt, Maryland

HUGHES

HUGHES AIRCRAFT COMPANY
SPACE SYSTEMS DIVISION

07

PHASE II FINAL REPORT
STUDY OF A LOW ALTITUDE SATELLITE
UTILIZING A DATA RELAY SATELLITE SYSTEM

AUGUST 1969

Contract No. NAS 5-11602

Goddard Space Flight Center
Contracting/Grafton Young
Technical Monitor/Sheldon Wishna

Prepared By:

Project Manager/Dennis Eggert
Hughes Aircraft Company
Space Systems Division
For
Goddard Space Flight Center
Greenbelt, Maryland

HUGHES

HUGHES AIRCRAFT COMPANY
SPACE SYSTEMS DIVISION

ACKNOWLEDGMENT

PRECEDING PAGE BLANK NOT FILMED

CONTENTS

ILLUSTRATIONS

TABLES

1. INTRODUCTION

This document presents the results of Phase II of the Study of a Low Altitude Satellite Utilizing a Data Relay Satellite System conducted by Hughes Aircraft Company Space Systems Division for the National Aeronautics and Space Administration, Goddard Space Flight Center, under Contract NAS 5-11602.

The purpose of this study (19 July 1968 to 22 September 1969) was to investigate the technical considerations associated with a low altitude satellite (LAS) operating in conjunction with a data relay satellite system (DRSS). The study was conducted in two phases. Phase I consisted of analysis and trade studies dealing with LAS-DRSS communication and with LAS subsystems. The results of this phase were published in January 1969. Phase II consisted of a spacecraft conceptual design based upon the results of Phase I. The satellite concept developed during Phase II is presented in this report.

The basic spatial relationships of an LAS-DRSS system are illustrated in Figure 1-1. The DRSs are at geostationary altitude in an equatorial orbit, while the LAS is relatively near the earth. With two or more properly located DRSs, an LAS is in view of one at all times, and all DRSs can be seen from two ground stations. These properties make an LAS-DRSS system extremely attractive because they offer the potential for continuous communication between the LAS and a small number of ground stations. Two fundamental consequences of the continuous communication capability are:

1) Elimination of the need for LAS data storage

2) Reduction in the cost of ground equipment by providing continuous command, telemetry, tracking, and experiment data transmission with a small number of ground stations that transmit to and receive from geostationary relay satellites

To take advantage of the continuous communication potential of an LAS-DRSS, the satellite must be able to establish a communication link capable of handling the type and quantity of data required. A number of technical problems for the LAS and DRSS accompany this requirement. This study dealt only with the LAS and with the impact on its design of providing the capability of transmitting data to and receiving from a system of DRSs.
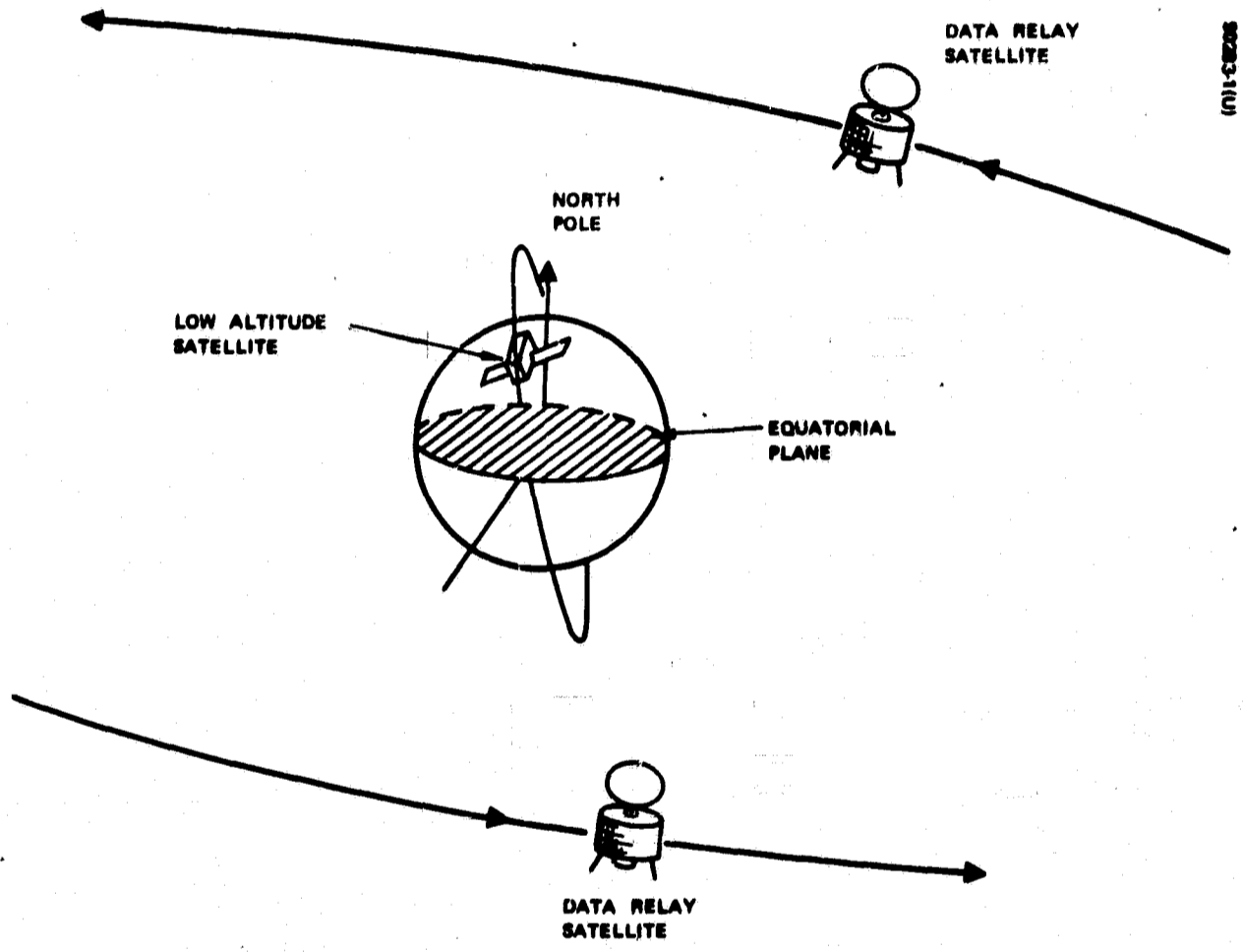
Figure 1-1.   LAS-DRSS System

The low altitude satellite concept developed during Phase II, and presented here, has the capability of providing high quality optical imaging and of transmitting 10 MHz of baseband information to the ground via a DRSS.

REPORT ORGANIZATION

A logical process of development resulted in this satellite concept. The organization of material is arranged sequentially in this report in an attempt to recreate this process. Section 2 is a summary of the major aspects of the spacecraft design.

The first topic that must be considered is the mission of the LAS and the corresponding payload. The mission was chosen in Phase I to be earth observation; the payload is the subject of Section 3. The LAS mission and payload will influence the orbit chosen. In Section 4, the LAS-sun relationship, imaging resolution, and global coverage considerations play an important part in selecting the orbital parameters. With the orbital parameters determined, the basic elements of the communication system can be chosen based upon the payload data requirements. Thus, the antenna, carrier frequency, RF power, and link capacity are treated in Section 5. Especially critical to the LAS-DRSS communication link are the techniques associated with, and the design of, the antenna control system. Section 6 deals with antenna gimbaling, tracking, and acquisition.

Section 7 presents a description and analysis of the attitude and velocity control system. The power system is discussed in Section 8, and some of the fundamental considerations involved in the LAS configuration are discussed in Section 9.

The principal aspects and considerations in each of these areas are presented in the following section.

2. SUMMARY

This section presents, in condensed form, the major considerations, aspects, and conclusions of the LAS conceptual design which are amplified in greater detail in Sections 3 through 9.

2.1 MISSION AND PAYLOAD

During Phase I, it was determined that earth observation is the most meaningful mission on which to base this satellite study. The potential uses of earth observation data are many and varied including geographic studies, cartography, earth resources, and weather prediction. The most popular and generally agreed upon information is that obtained by multispectral scanning in the visible and infrared regions of the electromagnetic spectrum. Thus, the major payload item is a multispectral scanning camera. This device images a small spot field of view onto several point detectors such as photomultiplier tubes or photodiodes. . A different detector is used for each spectral band to be imaged. A vibrating mirror optically scans this spot across the orbit track at a rate selected so that the movement of the spacecraft along the orbit causes the consecutive sweeps to be contiguous. An illustration of this scanning process is shown in Figure 3-1 on page 3-2.

The second payload item is a data collection system (DCS). This system will allow measurement data to be collected by the LAS from ground or balloon-carried sensors and relayed to the ground via the DRSS. Examples of measurements include water depths, flow rates, rainfall, snow depths, soil moisture, wind velocities, and air and soil temperatures. Also, the locations of the ground or balloon instrument packages can be determined. This function, while not important for fixed sensor locations, is extremely useful for sensors on drifting buoys or balloons. Furthermore, transponders aboard aircraft or ships would allow their location by satellite in emergencies.

The third payload item is called a radar scatterometer. Basically, this device measures the strength of radar signal return and the angle of incidence. This information yields a signature that can be matched to a "library" of known sea states. Consequently, wave height and hence, wind fields can be inferred.

The principal features of each payload system are listed in Table 2-1. This combination was chosen as representative of the type of payload most likely to be employed on a low altitude satellite which has the capability to transmit all data to a geostationary data relay satellite. This payload establishes a representative data baseband communication requirement and spacecraft stabilization and control requirements which will arise in future low altitude missions.

TABLE 2-1. PAYLOAD

	Multispectral Scanning Camera	Data Collection System	Radar Scatterometer
Weight, pounds	100	25	50
Power, watts	45	25	50
Baseband or data rate	≤8 MHz	2560 bits/sec	200 Hz
Resolution, feet	150	–	–

2.2 BOOSTER AND CONFIGURATION

After choosing the representative payload, a brief iterative process followed, whose objective was a preliminary estimate of the weight and power of the various spacecraft components and systems. Based on previous experience, it became evident that the above payload could be easily supported by a spacecraft whose weight was within the capability of the improved Thor-Delta booster. This booster has a relatively low cost which makes it especially attractive.

Following this choice, the analysis and design of the major subsystems proceeded. Weight and power requirement estimates were updated; the results are presented in Table 2-2, which shows that a large margin exists between the booster capability and the spacecraft weight.

The basic spacecraft configuration was developed in a logical process starting with the above booster choice, together with spacecraft requirements and design objectives. With the size allowed by the shroud, power by conversion from incident solar energy would be inadequate for the estimated loads if only the surface of the main body was available for energy collection. Thus, solar arrays are required. Since the solar arrays are the largest appendage to the spacecraft, it was decided to provide an orientation mechanism to obtain the greatest efficiency.

TABLE 2-2. SPACECRAFT WEIGHT AND POWER ESTIMATES

Spacecraft Component	Weight, pounds	Load Power, watts
Payload		
Multispectral scanning camera	100	45
Data collection system	25	25
Radar scatterometer	50	50
Data Transmission System		
Antenna	20	—
Antenna steering	15	15
Transmitters (2)	40	50
Receiver	5	4
Telemetry and Command System (VHF)		
Transmitter	30	35
Receiver	5	4
Processing	10	5
Antenna	10	—
Attitude Control System		
Momentum wheel and motor	25	6
Magnetic torquers	10	6
Electronics and sensors	6	5
Nutation damper	5	—
Orbit Control System		
Dry hardware	15	—
Propellant	80	—
Electronics	2	3
Power System		
Solar array	53	—
Solar array drive system	40	15
Batteries	64	—
Control electronics	5	5
Structure and Thermal Control	140	10
Adapter	50	—
Total	805	283
Improved Thor-Delta Capability (DSV-2L)	1300	—

The momentum wheel technique for angular momentum bias was chosen as the basic stabilization concept with magnetically produced torques to maintain the angular momentum and to orient its direction. A mirror, mounted to the wheel, scans the earth and reflects its field of view through the hollow wheel shaft to two sensors, thus allowing determination of the earth's leading and trailing edges at two different latitudes. These signals are then processed to provide the required attitude error signals.

Considering basic spacecraft shape, a flat surface facing the earth has advantages for mounting instruments and sensors. A flat side parallel to the orbit plane will allow space between it and the shroud for the protruding, earth scanning mirror. If both sides parallel to the orbit plane are flat, the stowage of the solar arrays is facilitated. In particular, if the solar arrays are flexible and rolled in tubes for stowing during launch, the tubes can be readily accommodated between flat spacecraft surfaces and the cylindrical shroud. Based upon these considerations, as well as structural simplicity, a rectangular box shape was chosen. The flexible solar array, deployable from a cylindrical tube, was chosen both for packaging ease and growth capability.

The solar arrays must be rotated 360 degrees with respect to the spacecraft body in order to maintain their sun orientation. To avoid interference with the data transmission system antenna, which covers the hemisphere outward from the LAS away from the earth, the solar arrays must be limited in their dimension that is parallel to the orbit plane. Then, in order to provide the desired power level, the solar arrays must have a much longer dimension normal to the orbit plane.

Both the solar arrays and the momentum wheel have their axis of rotation normal to the orbit plane. Since these items are relatively large, it is apparent that the sides parallel to the orbit plane must be longer than the dimensions perpendicular to the orbit plane. To accommodate both the solar arrays and the momentum wheel with its earth-scanning requirements, the length was set at 88 inches. The shroud diameter then limited the cross section to 36 by 36 inches, which is a larger volume than needed for the above payload, but which allows excellent growth potential.

The basic spacecraft in orbital operation, with its major appendages, is illustrated in Figure 2-1.

2.3 ORBITAL PARAMETERS

The imaging mission of the LAS presents the overriding constraints for most spacecraft parameters and subsystems. The orbital parameters, in particular, are chosen to support this mission. Three fundamental aspects of the imaging-orbit relationship are listed below.

1)   Uniformity of pictures and ground lighting
     conditions
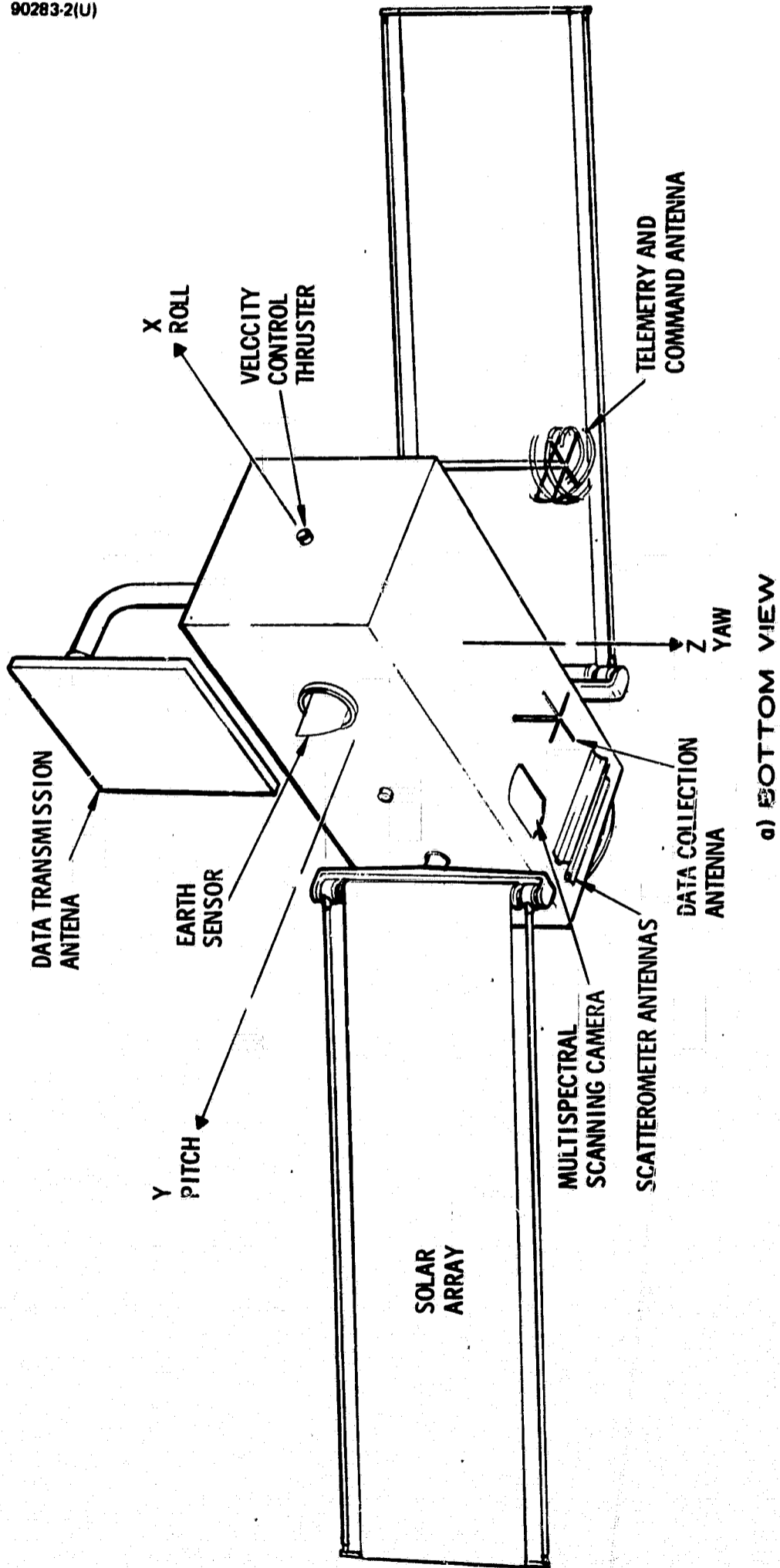
Figure 2-1. Low Altitude Satellite Configuration

X
ROLL

VELOCITY
CONTROL
THRUSTER

TELEMETRY AND
COMMAND ANTENNA

Z
YAW

a) BOTTOM VIEW

DATA TRANSMISSION
ANTENA

EARTH
SENSOR

Y
PITCH

SOLAR
ARRAY

MULTISPECTRAL
SCANNING CAMERA

SCATTEROMETER ANTENNAS

DATA COLLECTION
ANTENNA

90283-3(U)

ADAPTER RING

AXIS OF SOLAR
ARRAY ROTATION

SOLAR
ARRAY

DATA
TRANSMISSION
ANTENNA

INCLINATION
CONTROL
THRUSTER

YAW   Z
(TOWARD EARTH)

b) TOP VIEW

PITCH Y
(NORMAL TO
ORBIT PLANE)

VELOCITY
CONTROL
THRUSTER

ROLL   X
(VELOCITY)

VHF
TELEMETRY AND
COMMAND ANTENNA

Figure 2-1 (continued).   Low Altitude Satellite Configuration

2-6

2) Complete earth coverage and the time required

3) Image resolution

The desire for image uniformity leads to circular, sun-synchronous orbits. Complete earth coverage in minimum time restricts altitude, and image resolution improves with lower satellite attitudes.

A sun-synchronous orbit is characterized by an orbital precession rate, caused by the oblateness of the earth, equal to the angular rate of the earth's travel about the sun. Thus, the sunline makes a constant angle with the spacecraft orbital plane throughout the year. The main advantage of such an orbit is that lighting conditions on the ground can be maintained at the desired level for optical imaging missions. In addition, this orbit is desirable from the standpoint of solar power and thermal control design aspects of the spacecraft.

An orbit is determined by six basic quantities: the semimajor axis, the eccentricity, the inclination, the longitude of the ascending node, the argument of perifocus, and the time of perifocal passage. However, because the mission here includes uniform optical imaging of the earth's surface, only circular orbits are considered, and for these orbits, the above six quantities reduce to three: the altitude, the inclination, and the longitude of the ascending node. These are the three quantities which appear as parameters in orbit related analyses. For the sun-synchronous orbit discussed above, the inclination is determined by the altitude, and the ascending node longitude is determined by the desired sun aspect angle. Thus, the orbital altitude is the remaining parameter.

The closer the LAS is to the earth, the better the potential quality of the picture. Thus, a low altitude is preferred from an image resolution standpoint, but the disturbances on the satellite due to atmospheric drag increase as the altitude decreases. Analysis indicates that altitudes below 250 n. mi. will result in excessive disturbances. Global coverage analysis shows that an altitude near 300 or 480 n. mi. results in a desirable and convenient coverage pattern. Altitudes just below these allow more tolerance in the correction of injection errors than altitudes just above. Based upon all these considerations, an altitude of 293 n. mi. was chosen. This is in the center of the altitude range allowable for a camera with a 100-mile swath width and is also included in the allowable altitude range for a 75-mile swath width camera.

The following parameters are the result of choosing a 293 n. mi. circular sun-synchronous orbit:

Orbit inclination	97. 5 degrees
Altitude sensitivity to inclination	141. 6 n. mi. /degree
Satellite velocity	24, 898 fps

Orbital period	95.5 minutes
Subsatellite velocity	4.35 mi./sec
Maximum LAS-DRS range	23,955 n. mi.
Minimum LAS-DRS range	19,015 n. mi.
Minimum LAS/DRS visibility	58 percent

2.4 COMMUNICATION SYSTEM

The LAS communication system consists of two subsystems, designated as the VHF system and the data transmission system (DTS). The primary function of the VHF system is to provide telemetry and command communication, while the DTS is used for transmitting the payload sensor data. There is a reliability and convenience advantage in providing the capability to transmit and receive some data through both systems. The concept presented here has that capability.

The emphasis in this study was on the basic system parameters which include the antenna carrier frequency, RF power, and baseband or information data rate capacity. Modulation is considered only as to its influence on postdetection signal-to-noise ratios and, hence, the link capacity.

The data to be received by the LAS includes spacecraft commands, data collection interrogation commands, and satellite tracking signals. Those data to be transmitted include housekeeping data, data collection messages, tracking signals, radar scatterometer data, and the camera data. Table 2-3 lists these data along with their baseband or bit rate and the system or systems handling each.

TABLE 2-3. LAS DATA

Receive	Transmit	Baseband or Bit Rate	Communication Subsystem
Commands	Housekeeping	500 bits/sec	VHF and DTS
Data collection system	Data collection system	2560 bits/sec	VHF and DTS
Tracking	Tracking	5 kHz	DTS
	Radar scatterometer	200 Hz	DTS
	Multispectral scanning camera	8 MHz	DTS

2.4.1 VHF System

The principal function of the VHF system, as mentioned above, is to provide command and housekeeping telemetry communication. Inasmuch as this communication is critical to the mission and operation of the spacecraft, it is desirable to have the VHF communication link operational for as much of the time as possible. Consistent with this objective is an omnidirectional antenna on the LAS and an earth-coverage antenna on the DRSs.

Omnidirectional radiation from the LAS is difficult to achieve because of the many appendages to the spacecraft, as well as its size. The most critical time for command capability is when the LAS is near the earth's poles. At this point, the DTS antenna must be commanded to change its transmission from one DRS to another. At other times, the commands and housekeeping data can be transmitted via the DTS system. Based upon this, a spiral dipole antenna was selected. Since the DTS antenna must be located on the side of the spacecraft facing away from the earth, the VHF antenna must be located on the other side to prevent blockage of one by the other. Mounted, as shown in Figure 2-1, the antenna gain toward the DRSs is maximum when the LAS is near the poles.

If both the LAS and DRS have VHF transmitters with 10 watts of RF power, the link capacity in both directions is 50.9 dB-Hz, which for a carrier-to-noise ratio of 10 dB, allows an RF bandwidth of 11.5 kHz.

2.4.2 Data Transmission System

The DTS must transmit and receive all data, providing a redundant capability for housekeeping data, commands, and data collection messages. Table 2-3 shows that the camera provides the major bandwidth requirement. All of the other data have much smaller bandwidth requirements and can be multiplexed within a 2 MHz baseband. Thus, the requirements of the DTS are:

1) 10 MHz baseband

2) No storage

3) Good quality reception

The reception requirement is a constraint on the carrier-to-noise ratio and the test tone-to-noise ratio at the receiver for an FDM/FM system, or the error probability for digital transmission.

The primary factors in choosing the DTS antenna are packaging constraints, weight, and radiation pattern. Packaging is the major factor, and based mainly upon this consideration, a square planar array, 3 feet on a side, was chosen for the antenna.

In choosing the carrier frequency, the trades involved DRS antenna sizes, LAS RF power requirements, and antenna pointing requirements. Based upon a link analysis, 15.3 GHz was chosen as the carrier frequency. Lower frequencies required a large DRS antenna, while at higher frequencies, the noise figure of state-of-the-art receivers was significantly higher, requiring either greater transmitter power or a higher gain DRS antenna with its attendant smaller beamwidth and more stringent pointing requirements. Also, at higher frequencies, the gain of the LAS antenna must be greater, requiring better pointing accuracy than at 15.3 GHz. At the frequency chosen, 16 watts of RF power are required to transmit the 10 MHz baseband.

A summary of the communication system parameters is given in Table 2-4, and a block diagram of the system is shown in Figure 5-9 on page 5-13.

TABLE 2-4. COMMUNICATION SYSTEM SUMMARY

	VHF System	DTS
Antenna	Spiral dipole omnidirectional (see Figure 5-1, Section 5)	Square planar array, 3-foot side
Gain	See Figure 5-2, Section 5	41 dB
Beamwidth	—	1.6 degrees
Carrier frequency	136 MHz	15.3 GHz
RF power	10 watts	16 watts
Data rate capacity	10 kilobits/sec	—
Baseband capacity	—	10 MHz
Reception quality	—	C/N $\gtrsim$10 dB
		TT/N $\geq$40 dB

2.5 ANTENNA CONTROL

In developing an antenna control system concept, a logical order of design choices occurs. The number of DTS antennas to be employed must be determined and then the scheme for mechanical gimbaling must be selected. Following these choices, the method of tracking the DRS must be chosen and finally, the problem of changeover and acquisition must be dealt with.

Two DTS antennas allow communication without interruption, however, they present packaging difficulties, which, although not insurmountable, require considerably more complex stowage and deployment schemes than a single antenna. Furthermore, for the primary optical imaging mission of the representative payload, it was felt that short interruptions are tolerable. Thus, it was decided to use only one DTS antenna. And since pictures of major interest will occur at the lower latitudes rather than at the poles, it was decided to have the changeover from one DRS to another occur near the poles. Simple geometrical considerations indicated that the antenna should be mounted on a structural member away from the spacecraft surface that faces away from the earth. This allows coverage of the "outer" half-space defined by a plane tangent to an earth-centered sphere of orbital radius at the LAS position.

2.5.1 Gimbaling

The fundamental choice in antenna gimbaling design is between two or three gimbals.

It can be shown that a two-gimbal, antenna steering system with the primary axis normal to the orbit plane can provide the required rotational motion and that large gimbal rates can be avoided with certain DRSS configurations. However, with other DRSS configurations or under some special communication requirements, the gimbal rate problem cannot be avoided. Further, the relationship between the gimbal angles and the LAS and DRS orbital parameters is not simple. Thus, the changeover and acquisition is not as simple and easily conceived as is possible with a three-gimbal system. Since changeover will usually occur once an orbit, this is an important consideration. Also, the complexity of computation in the control system is greater for a two-gimbal system than for the three-gimbal system.

A three-gimbal system provides an additional gimbal axis, allowing another degree of rotational freedom and eliminating the gimbal rate problem. Consider now the conceptual simplicity of the three-gimbal system represented in Figure 2-2. Gimbal axis 1 is the "outer" gimbal axis, i.e., it is fixed rigidly to the spacecraft body and is parallel to the orbit normal. The second gimbal axis is mounted to the first with an angle between the two axes equal to the orbital inclination angle. The third, or innermost axis is mounted orthogonal to the second.

This configuration allows operation in the following manner: the gimbal drive about the first axis maintains a constant speed equal to the orbital angular velocity, keeping the second gimbal axis always parallel to the earth's polar axis. Then, this second gimbal axis provides "azimuthal" motion and compensates for the motion of the DRS. The third gimbal axis provides "elevation" motion and compensates for angular movement of the line of sight due to the translational motion of the LAS in its orbit. The motion about the third axis is relatively small — about ±9.4 degrees during one LAS orbit.
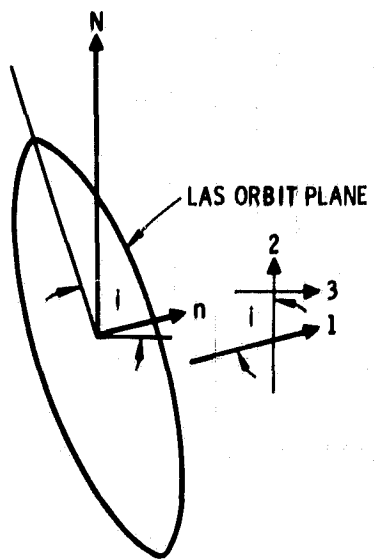
Figure 2-2. Three-Gimbal System
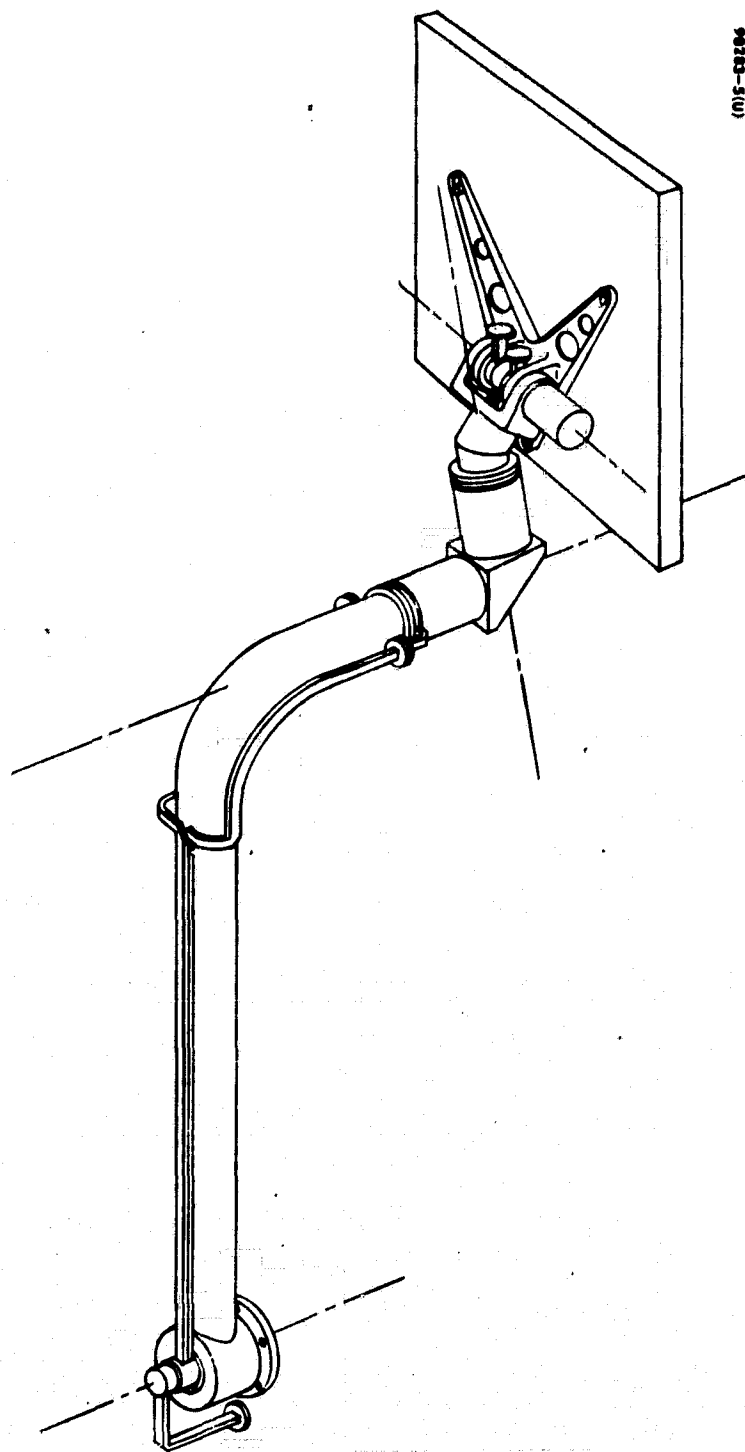
Figure 2-3. Data Transmission Antenna and
Three-Gimbal System

Since the second gimbal axis tracks the DRSs in the equatorial plane, 360-degree rotation is desirable; and, since the first axis compensates for the rotation resulting from the LAS earth pointing requirement and is driven at constant speed, 360-degree rotation about this axis is also desirable.

A three-gimbal system introduces additional mechanical and RF feed problems, which tend to offset its advantages. However, a very limited comparison led to a decision that the advantages of the three-gimbal system outweighed its disadvantages; thus, a three-gimbal system was selected. A design concept for such a system is shown in Figure 2-3.

2.5.2 Tracking

Although the DTS antenna, with a 1.6-degree, 3-dB beamwidth, could be steered open-loop with programmed control, it was felt that automatic tracking would ease ground processing requirements, increase the reliability and quality of the LAS-DRSS data link, and provide for future growth to higher gain antennas.

The square planar array chosen lends itself easily to monopulse tracking. The antenna is divided into four quadrants which, for the monopulse concept, can be thought of as four separate antennas. The received inputs are combined in RF circuits attached to the antenna to produce three signals. Two of these correspond to the pointing errors in azimuth and elevation and the third is the sum of the outputs from all four of the quadrants. This monopulse signal generation is illustrated in Figure 6-13 on page 6-12. The two difference signals are used in a control system to drive the second and third gimbal motors so as to make the antenna boresight axis and the line of sight coincide.

The generation of the monpuulse signals and the antenna control system techniques are well established technology. The major problem with monopulse tracking is in getting the monopulse signals to the receiver and signal processor. The two extreme methods are: 1) place the receiver and signal processor on the antenna structure and feed the resulting signals to the spacecraft through slip rings, or 2) send all three RF signals through rotary joints associated with the three gimbals.

There are a number of intermediate methods which are discussed in Section 6, but the one chosen requires two RF channels to be fed through the gimbal system. The rotary joints necessary for a two-channel feed have more loss than single feed joints, but a 3-dB transmit power loss is avoided. This scheme is illustrated in Figure 6-15 on page 6-12.

2.5.3 Changeover

Changeover refers to the process of discontinuing data transmission to one DRS and repositioning the antenna in order to transmit to another. Acquisition follows this procedure and involves the re-establishment of the communication link and the automatic tracking system operation.

2-13

If a DRS lies nearly 90 degrees from the LAS line of nodes, it is possible to transmit to this DRS for an entire orbit without interruption. However, this situation will occur infrequently, and for most LAS orbits, changeover will be required once per orbit if data transmission is desired on only one side of the earth and twice if transmission on both sides of the earth is desired. The LAS concept presented in this report does not have the power capability for data transmission on the dark side of the earth. During eclipse, the camera, radar scatterometer, and DTS must be turned off. Hence, DTS antenna tracking is required only on the sunlit side of the earth. For this case, the geometry of changeover with the three-gimbal system is particularly simple. This geometry is shown in Figure 6-16 on page 6-12.

During each orbit as the LAS reaches the point nearest the north pole, the second-gimbal axis is rotated $\Delta g_2 = 11.94 - 2.42 \cos \phi_1$ degrees, and the third-gimbal axis is rotated 9.3 degrees, while the first axis continues its constant speed rotation at orbital angular velocity. This orients the antenna so that it is nominally pointing at the DRS when the LAS reaches the point of its orbit nearest the south pole. If there are three data relay satellites spaced 120 degrees apart, then approximately every ten orbits, the second gimbal axis must be rotated in the opposite direction by $120 - \Delta g_2$ degrees to begin transmission to a different DRS. Since these changeover motions are simple and there are only three basic maneuvers, it is an easy matter to make the changeover procedure completely automatic.

2.5.4 Acquisition

With the antenna repositioned to point toward a DRS as the LAS reaches the southernmost point of its orbit, approaching the sunlit side of the earth, the tracking system must be reactivated and lock-on must be achieved. This can be accomplished by lowering the gain of the antenna beam, increasing its beamwidth. With the planar array, this is most easily done by dividing each of the four quadrants into four subquadrants. The gain of the reduced antenna is approximately one-fourth of the entire antenna, which implies a gain of 35 dB and a 3-dB beamwidth of about 3 degrees, which is sufficient to achieve acquisition. Once lock-on has been accomplished with the reduced antenna, the other antenna modules are activated and the data link is reestablished. A functional block diagram of the acquisition/antenna control system is shown in Figure 6-18 on page 6-15.

2.6 ATTITUDE AND VELOCITY CONTROL

The primary objective of the attitude control system is to provide a stable platform for earth oriented sensors. Sensor earth pointing accuracy and rate limitation requirements significantly influenced the design of the attitude control system. Additionally, a velocity control (ΔV) capability is provided to reduce injection errors and to periodically control orbital parameters in order that total earth coverage be ensured.

2-14

The design presented here minimizes on-board equipment complexity by placing the emphasis for control activation and execution on infrequent ground commands. A design lifetime exceeding 1 year was the objective.

2.6.1 System Description

The system selected to control and stabilize the spacecraft employs a dual spin configuration — a high speed rigid momentum wheel and an earth oriented, or despun, platform for the mission sensors. A large angular momentum is generated by the wheel to provide sufficient gyroscopic stability so that spacecraft motion is reasonably insensitive to cyclical precession torques. Magnetic torquing is utilized to trim secular disturbance torques as well as the effects of ΔV thruster firings. The configuration of the spacecraft is illustrated in Figure 7-1 on page 7-2, which also defines the coordinate axes of the body and shows the arrangement of system elements including earth horizon scanner geometry. Mission sensors are aligned relative to the yaw (z_b), which is nominally earth pointed along the local geocentric vertical. Earth sensing is accomplished by a horizon scanner that utilizes the momentum wheel to generate a conical scan pattern. This sensor provides sufficient information to determine the satellite attitude. The wheel spins about an axis which is parallel to the satellite's pitch (y_b) axis, nominally oriented normal to the orbit plane.

Attitude control of the satellite is effected by wheel speed control and by the interaction of current-carrying coils, fixed to the body, and the earth's magnetic field. Multiturn coils are arranged so that their planes are normal to the pitch axis for precession control or parallel to the pitch axis for control of the angular momentum. These coils are attached to the inner structure of the spacecraft. A coil, designated as the orientation coil, is utilized to precess the angular momentum vector for large reorientation maneuvers, as well as to provide for precession at regular prescribed intervals to achieve earth pointing. Additionally, the orientation coil is used to trim disturbance torques during ΔV maneuvering. A bias coil, arranged parallel to the orientation coil, provides for continuous precession of the momentum vector and compensates for a component of solar disturbance torque. The spin control coil is frequently cycled to compensate for pitch disturbances and thereby maintain the angular momentum of the wheel within prescribed limits. Pitch control is achieved by a wheel controller that very accurately controls pitch attitude.

A pair of opposed ΔV thrusters are aligned parallel to both the pitch and roll axes such that their thrust vectors nominally pass through the satellite's center of gravity. These thrusters are used to correct injection errors and to provide orbit control capability.

An eddy current nutation damper, which is free to oscillate about an axis of rotation parallel to the velocity vector, reduces transverse attitude rates following orbital injection and damps motion of the satellite's spin axis caused by disturbance and control impulses.

Figure 2-4. Attitude and Velocity Control System

90283-6(U)

2-16

A summary of the attitude and velocity control system parameters is given in Table 2-5, and a functional block diagram of the attitude and velocity control system is shown in Figure 2-4.

TABLE 2-5.   SUMMARY OF ATTITUDE AND VELOCITY CONTROL
SYSTEM PARAMETERS

Item	Requirement
Attitude control	
Pointing accuracy	≤±0. 5 degree (3σ) about all three earth referenced coordinate axes.
Pointing stability	≤±0. 03 deg/sec (3σ) about body pitch and roll axes.
Precess satellite momentum vector	≈1 deg/day about line of nodes (continually).
Period, between altitude corrections (normal mode)	≥1 week
System lifetime	>1 year
Velocity control	
Correct injection errors	$\Delta V \leq 200$ fps (3σ)
Control orbital period error	≤± 1 second

2. 7   POWER SYSTEM

Flexible solar arrays were chosen as the power source because of their packaging characteristics and growth capability. For the power level under consideration here, there is no weight advantage to the flexible arrays, but if more power should be required, they will provide better weight efficiency than rigid arrays.

A battery, charged during the sunlit portion of the orbit, is the source of power during solar eclipse by the earth. This battery is protected by a diode network against failure due to a malfunctioning cell. A charge-discharge controller and array boost electronics complete the system as shown in Figure 8-7 on page 8-8. The system design is summarized in Table 2-6.

TABLE 2-6.   POWER SYSTEM DESIGN SUMMARY

Sunlight capability	350 watts
Eclipse capability	129 watts
Beginning of life solar array capability	590 watts
End of life array capability (after 1 year)	500 watts
Bus voltage	25 volts
Solar panel voltage	27 volts
Number of battery cells	24
Depth of discharge	13. 2 percent
Solar array weight	53 pounds
Deployment and orientation mechanisms	40 pounds
Electronics	5 pounds
Battery weight	64 pounds

3. PAYLOAD

The representative payload chosen consists of three separate functional elements: a multispectral scanning camera, an earth data collection system, and a radar scatterometer. This selection was made in order to provide guidelines for the spacecraft and subsystem designs and to allow the impact of the payload on the design to be more clearly and specifically delineated.

3.1   MULTISPECTRAL SCANNING CAMERA (MSC)

For illustrative purposes, the basic camera parameters are discussed in this subsection. The objective is to arrive at the requirements which this camera places on the communication, power, and control systems. The camera system parameters set forth here do not necessarily represent any existing camera design unless so specified.

This device images a small spot field-of-view onto several point detectors, such as photomultiplier tubes or photodiodes. A different detector is used for each spectral band to be imaged. A vibrating mirror optically scans this spot across the orbit track at a selected rate so that the movement of the spacecraft along the orbit causes the consecutive sweeps to be contiguous. This scanning process is illustrated in Figure 3-1.

Consider a swath width of 100 miles with a 10-mile overlap capability, yielding an effective swath width of 90 miles. The relationship between swath width and minimum earth coverage time is shown in Figure 3-2. It can be shown that 19 days are required to provide global coverage with a 300 n.mi. orbit.

The required communication system capability is now determined by the resolution required. The subsatellite velocity on the earth's surface is 2.28×10^4 ft/sec so that $(2.28 \times 10^4)(5.28 \times 10^5) = 1.2 \times 10^{10}$ square feet are scanned per second. However, allowing for a mechanical scanning efficiency of 50 percent, the required effective scanning rate is 2.4×10^{10} square feet. If the resolution is 150 feet, then the scan rate can be expressed as 1.07×10^6 resolution elements per second. The dwell time per revolution element is the reciprocal of this number, and the bandwidth of the analog signal corresponding to this resolution is approximately equal to this scan rate. Allowing for multiplexing inefficiencies and additional bandwidth for
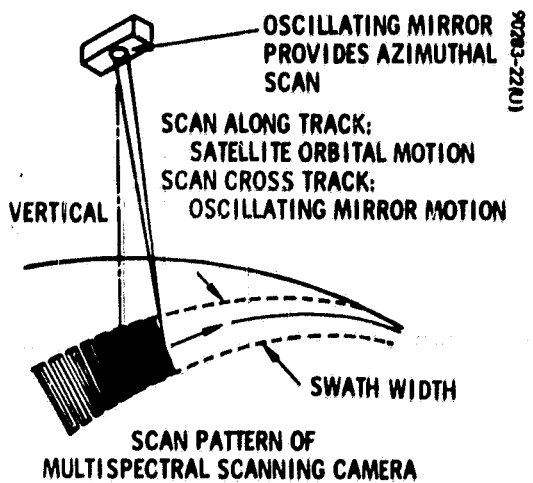
Figure 3-1. Scan Pattern of Multispectral Scanning Camera
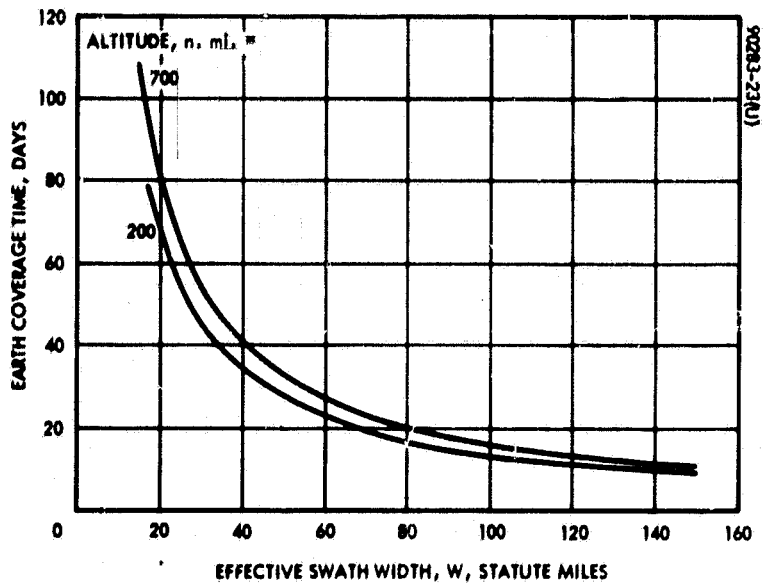
Figure 3-2. Earth Coverage Time
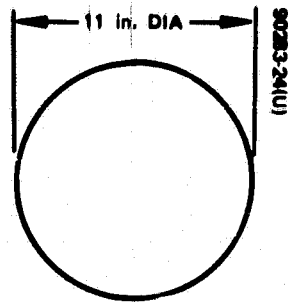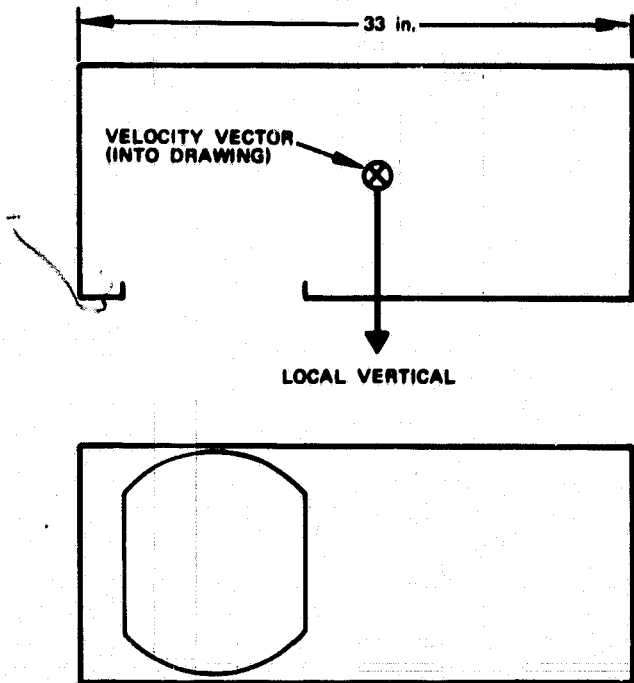
Figure 3-3. Multispectral Scanning Camera Dimensions

filtering considerations, the total bandwidth for a single spectral channel is less than 2 MHz. If four spectral bands are imaged, then the total baseband can be limited to less than 8 MHz.

If better resolution or a different swath width is desired, the bandwidth per spectral channel may be estimated roughly by

$$B = \frac{SW}{r^2} (2.4 \times 10^8) \text{ Hz}$$

where SW is the swath width in statute miles and r is the resolution in feet. Allowances must then be made for multiplexing and filtering.

The initial design objective for the communication system is a 10 MHz baseband capability. Thus, a camera system with a swath width of 100 miles and 150-foot resolution is compatible with this capability.

An MSC is presently being designed by Hughes for operation at approximately 500 n.mi. altitude. The characteristics of this camera, although somewhat dependent on the data quantity, will provide useful guidelines for power, environmental, and mechanical considerations. These characteristics are as follows:

Weight (scanner and signal processor)	100 pounds
Power	-24.5 volts (regulated ±0.5 volt)
Power consumption	45 watts
Scanner clear viewing aperture	A truncated elliptical cone enclosing a 9-inch column rotating ±15 degrees perpendicular to orbit track and a 9-inch column rotating ±10 degrees parallel to orbit track
Disturbing impulse	Scanning mirror assembly results in 10^{-3} slug ft^2 moment of inertia scanning at a rate of 15 Hz
Operating temperature range	+10 to +35 °C
Commands	41 functions
Telemetry (housekeeping)	15 digital, 16 analog

A sketch of the camera's primary dimensions is shown in Figure 3-3.

TABLE 3-1. SAMPLE MESSAGE FORMATS

Message 1 — Ground to DRS to LAS to RIP

Synchronization Word	RIP Address	RIP Address	Unmodulated Carrier
24 bits	16 bits	16 bits	200 bit periods

Message 2 — RIP to LAS

Unmodulated Carrier	Synchronization Word	RIP Address	Information
16 bit periods	24 bits	16 bits	200 bits

Message 3 — LAS to DRS to Ground

Synchronization Word	RIP Address	Information	Range Data
24 bits	16 bits	200 bits	16 bits
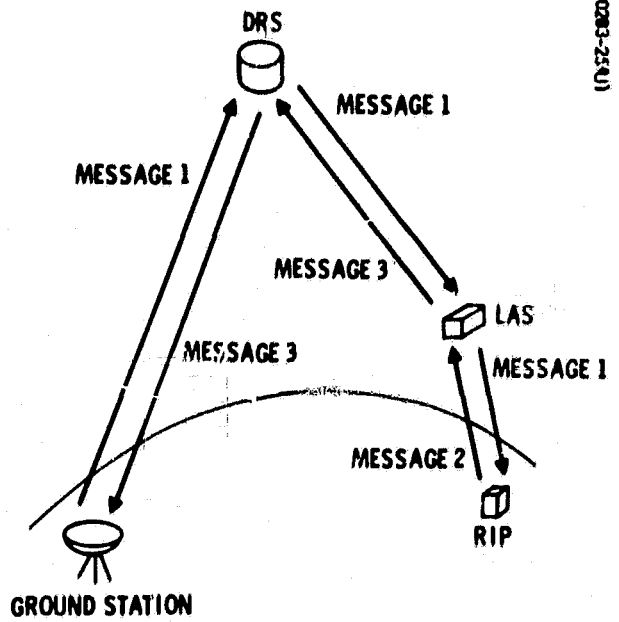
Figure 3-4. Data Collection System
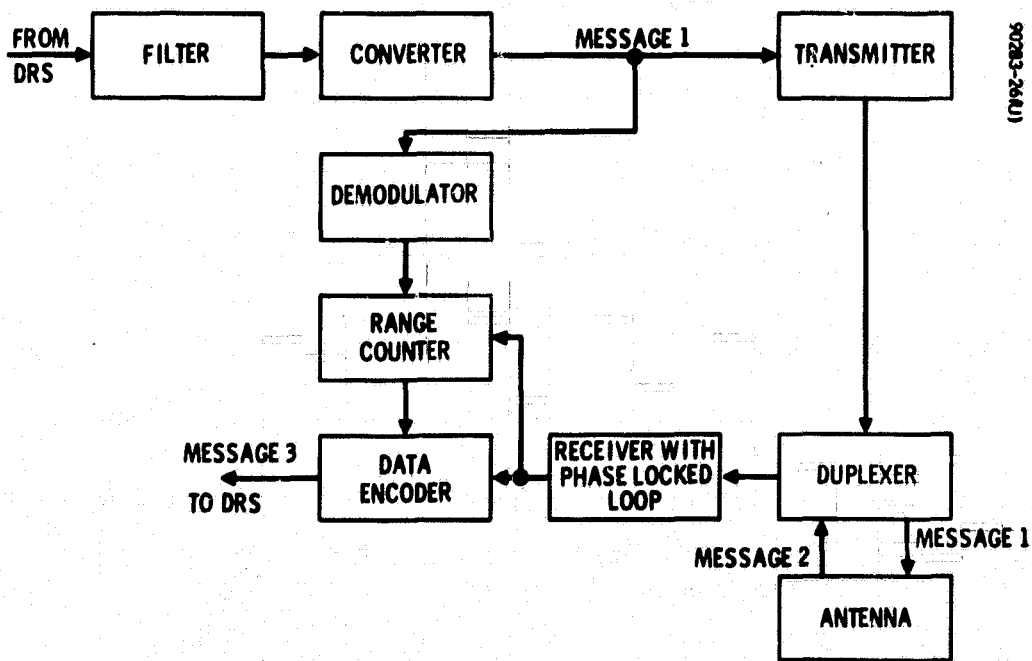
Figure 3-5. Data Collection System Block Diagram

3-4

3.2   DATA COLLECTION

The data collection system (DCS) will allow measurement data to be collected from ground or balloon-carried sensors and relayed to the ground via the DRSS. Examples of measurements that might be made include water depths, flow rates, rainfall, snow depths, soil moisture, wind velocities, and air and soil temperatures. Furthermore, the locations of the ground or balloon instrument packages can be determined. This function, while not important for fixed sensor locations, is extremely useful for sensors on drifting buoys or balloons. Also, transponders aboard aircraft or ships would make it possible to locate them by satellite in emergencies. A concept for such a data collection system is presented in the following paragraphs to illustrate the concepts involved and to provide a basis for determining space-craft requirements.

At 300 n. mi. altitude, the horizon has a range of 1700 miles. The range from the LAS to a remote instrument platform (RIP) may be determined by measuring the time between the transmitted interrogation signal and the received information signal. Counting clock pulses in a 16-stage counter would provide theoretical accuracy of about 0.25 mile.

Three message formats are shown in Table 3-1. Message 1 is sent to the DRS, then to the LAS, and finally to the remote instrument platform. It consists of 24 synchronization bits and 16 RIP address bits repeated twice, followed by unmodulated carrier for 200 bit periods. Message 2 is transmitted from the RIP to the LAS and consists of 16 bit periods of unmodulated carrier, 24 synchronization bits, the RIP address, and 200 bits of information. The initial unmodulated carrier allows the phase-lock loop of the LAS receiver to acquire and lock on the RIP transmission, permitting coherent reception. Message 3 consists of 24 synchronization bits, the RIP address, the 200 information bits, and the output of the range counter. Figure 3-4 illustrates this data collection concept.

The data collection system on the LAS is shown in Figure 3-5. The interrogation signal from the ground via a DRS is filtered from the combined signal and converted to the data collection interrogation frequency, which has been chosen to be in the vicinity of 450 MHz. This is the nominal carrier frequency for the presently planned Earth Resources Technology Satellite data collection system, as well as the frequency used for several other proposed data collection systems. This converted signal is then transmitted toward the earth.

In order to measure the range of the RIP being interrogated, the converted signal is demodulated and used to trigger the range counter which counts clock pulses until the signal from the RIP is received. Both the reviewed message 2 from the RIP and the range counter results are sent to the data encoder which adds the range counter data to message 2 and sends the combined message to the LAS transmitter with the unmodulated or blank portion of message 2 eliminated.

Range rate can also be measured if desired. This can be accomplished by counting zero crossings of the signal received from the RIP to measure the doppler shift. This may be useful for determining the drift rate of balloons or the velocity of moving surface vehicles. Ground processing would be needed to account for the LAS velocity at the time of measurement. The results of this measurement could then be added to message 3, following the range measurement data. It appears that knowledge of range rate is less important than that of range and has a greater possibility of error. Consequently, range rate measurement has been omitted from the above data collection concept but could be easily implemented if desired.

From the preceding discussion, it can be inferred that LAS/RIP detection is performed coherently. For coherent PSK, it can be seen from Figure 3-6 that a bit energy per noise density (E/N) of 10 dB results in a bit error rate of less than 10^{-6}. If the gain of both the LAS and RIP is assumed to be 0 dB, and the maximum range is taken to be 1500 miles, then a simple application of the range equation for microwave transmission yields the following expression:

$$RF \text{ power} = P = (2.88 \times 10^{-4})(\text{bit rate}) \qquad (1)$$

where the noise temperature of the LAS data collection system is taken to be 1000 °K. This noise temperature includes both the receiver noise and the earth background noise.

The above messages have 256 bits or the equivalent in information and unmodulated carrier. An arbitrary but reasonable choice for a message length is 0.1 second. This requires that the messages be transmitted at a rate of 2560 bits per second which, from Equation 1, requires 0.74 watts of RF power. Thus, a 4-watt transmitter is more than sufficient and is recommended to allow for contingencies.

Tentative estimates of weight and power for such a system are 25 pounds and 25 watts load to the prime power source. For packaging, based on proposed designs and past experience, it will be assumed that the LAS data collection system consists of five basic modules requiring 126 cubic inches each (6 x 7 x 3 inches).

The antenna selected is an earth-oriented, crossed dipole antenna with a reflection plane.

The data collection system characteristics are given in Table 3-2.

TABLE 3-2. DATA COLLECTION SYSTEM CHARACTERISTICS

Weight	25 pounds
Power	25 watts prime power
Size	Five 126 cubic inch modules
Transmit/receive frequency	Near 450 MHz
Viewing requirements	68 degrees, half-angle cone about local vertical through the antenna
Temperature range	0 to 40° C
Commands	10
Telemetry	15 digital
Data bit rate	2560 bits/sec

3.3 RADAR SCATTEROMETER

Earth resources investigators have suggested that sea state be measured from a satellite by means of a radar scatterometer, although experimental verification of such a device is still lacking. It was postulated that radar signal return from a patch of ocean plotted against aspect angle would have a shape that could be correlated with the wave height. It was also surmised that the electromagnetic wavelength should be long enough to capitalize on any resonance effects. Subsequently, successful experiments were conducted at 13.3 GHz, in which it was possible to correlate returns with wind speeds at 28 and 5 knots. (A substantial amount of work had already been done to correlate wind speeds with wave height.)

Basically, this device measures the strength of radar signal return versus the angle of incidence. This information yields a signature that can be matched to a "library" of known sea states so that wave height and, hence, wind fields can be inferred. The optimum frequency to be used is still under consideration, so a frequency that has been used successfully for aircraft experiments was selected and a radar configuration was calculated.

Rough calculations were made to determine the nature and power requirements for a 13 GHz radar operating from a 300 n.mi. orbit. Lower frequencies would permit all-weather operation, but the antenna lengths would increase proportionately.

It was assumed that a patch located on the orbit track could be sampled by pulse measurements from the time it lies 45 degrees before the nadir, through the nadir, and to the corresponding position behind the nadir. A

CURVE
A PSK–COHERENT
B PSK–DIFFERENTIAL COHERENT
C PCM–FM MATCHED FILTER COHERENT

D { PSK SYNCHRONOUS
FSK MATCHED FILTER COHERENT
ASK MATCHED FILTER COHERENT

E PCM–FM DISCRIMINATOR DETECTION

F { FSK MATCHED FILTER NONCOHERENT
PSK PHASE COMPARISON

G ASK SYNCHRONOUS DETECTION

H { ASK LINEAR ENVELOPE DETECTION
FSK MATCHED FILTER (MARK) NONCOHERENT

AVERAGE SIGNAL ENERGY PER BIT/
NOISE POWER DENSITY PER HERTZ OF BANDWIDTH, ONE SIDED SPECTRUM,
$\frac{E}{N_o}$, DECIBEL

Figure 3-6.   Probability of Bit Error
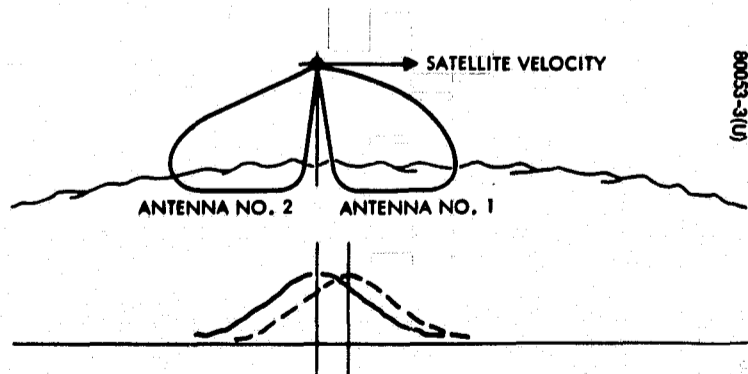
Figure 3-7.   Radar Scatterometer Track

3-8

sidelooking method was investigated, so that the radar could be simplified, but was abandoned when the promise on which it is based proved to be unjustified. In order to obtain signal returns throughout a variety of incidence angles, it must be assumed that patches 500 miles off track are similar to those near the nadir. However, nautical practitioners assure Hughes that this is not true. Since patch size is also controversial, it was decided to be guided by feasibility.

The 13.3 GHz design can utilize a 120-microsecond pulse for 20-mile resolution in range and a 2.5-degree antenna beam for azimuth resolution of 21 n.mi. across the track. The very low and unconventional pulse repetition rate of 130 per second results from the long range and attendant long transit times that are typical of orbiting spacecraft.

The radar was designed to obtain profiles for a sea patch 20 miles square, spaced every 50 miles along the satellite track, as indicated schematically in Figure 3-7. The high frequency chosen (13.3 GHz) permits the use of conventional radar techniques. The antennas are compatible with the other sensor requirements, and power consumption can be kept around 30 to 50 watts.

Characteristics of this radar scatterometer are shown in Table 3-3.

TABLE 3-3. RADAR SCATTEROMETER CHARACTERISTICS

Frequency	13.3 GHz
Ground patch size	20 x 20 n.mi.
Method for resolving	
Along track	120-microsecond pulse
Cross track	Antenna beam
Pulse repetition rate	135 pps
Integration time	0.75 second
Antenna	24-inch linear array
Sample spacing	50 to 100 miles
Angle range	±45 degrees
Minimum reflectivity, σ_o	-20 dB
Prime power	50 watts
Weight	50 pounds
Baseband	200 Hz

4. ORBITAL PARAMETERS

Orbital considerations are discussed in detail in the Phase I report. Several of the basic results are repeated here in an effort to make this report self-contained.

An orbit is determined by six basic quantities: semimajor axis, eccentricity, inclination, longitude of ascending node, argument of perifocus, and time of perifocal passage. However, because the mission here includes uniform optical imaging of the earth's surface, only circular orbits are considered and, for these, the above six quantities reduce to three: altitude, inclination, and longitude of ascending node. These are the three quantities which appear as parameters in orbit related analyses. For a sun-synchronous orbit, discussed in the following subsection, the inclination is determined by the altitude, and the ascending node longitude is determined by the desired sun aspect angle. Thus, the orbital altitude is the principal parameter in LAS orbits under consideration here.

4.1 IMAGING REQUIREMENTS

The imaging mission of the LAS presents the overriding constraints for most spacecraft parameters and subsystems. The orbital parameters, in particular, are chosen to support this mission. There are three fundamental aspects of the imaging-orbit relationship.

1) Uniformity of pictures and ground lighting conditions

2) Complete earth coverage and the time required to obtain it

3) Image resolution

The desire for image uniformity leads to circular, sun-synchronous orbits. Although image resolution is better at lower satellite altitudes, the requirement for complete earth coverage in minimum time restricts this choice.

4-1
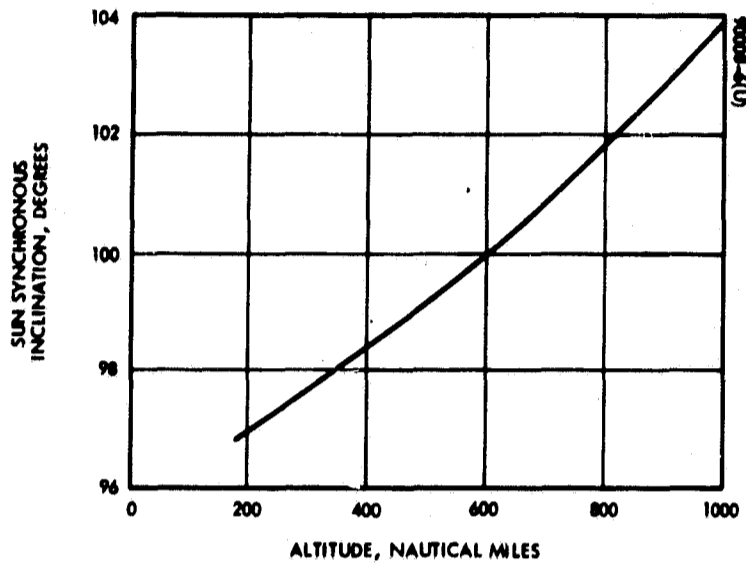
Figure 4-1. Attitude and Inclination for
Sun-Synchronous Orbit
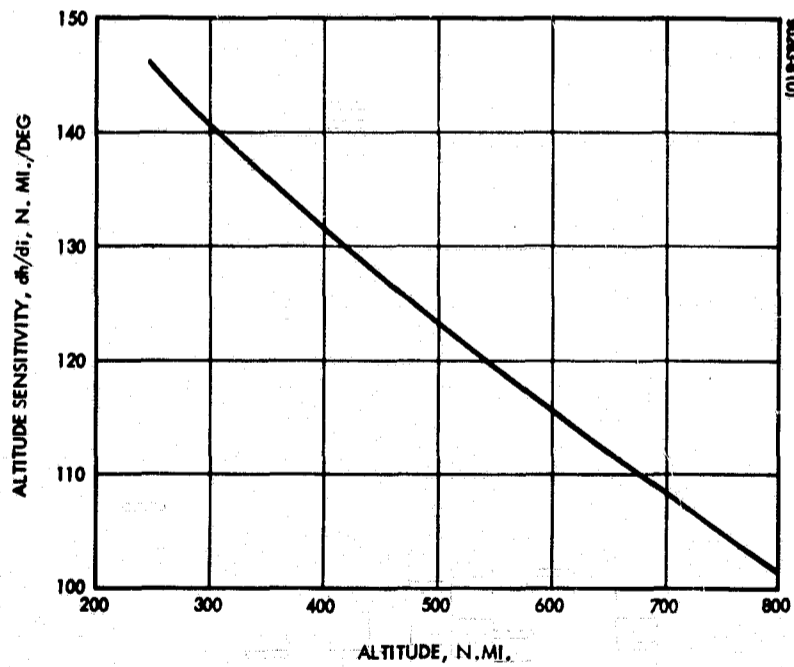
Figure 4-2. Altitude Sensitivity to
Changes in Inclination

4.2 SUN-SYNCHRONOUS ORBITS

A sun-synchronous orbit is characterized by an orbital precession rate, caused by the oblateness of the earth, equal to the angular rate of the earth's travel about the sun. Thus, the sunline makes a constant angle with the spacecraft orbital plane throughout the year. The main advantage of such an orbit is that lighting conditions on the ground can be maintained at the desired level for optical imaging missions. In addition, this orbit is desirable from the standpoint of solar power and thermal control design aspects of the spacecraft.

For circular orbits, the altitude and inclination are related.

$$\cos i = -(4.09105 \times 10^{-14}) (R_e + h)^{\frac{7}{2}} \tag{1}$$

where R_e is the earth's equatorial radius and h is the satellite altitude, both in nautical miles. This relationship is shown in Figure 4-1.

Of interest for orbit control is the sensitivity of altitude to changes in inclination. From Equation 1

$$\frac{dh}{di} = \frac{(2)}{7} \frac{\sin i}{(4.09105 \times 10^{-14}) (R_e + h)^{\frac{5}{2}}} \tag{2}$$

Using Equations 2 and 1, this sensitivity can be calculated as a function of altitude. The results of such a calculation are shown in Figure 4-2.

The angle between the earth-sun line and the line of nodes is determined at orbit injection. Establishing and maintaining the altitude-inclination relationship of Equation 1 will keep this angle nearly constant. Only slight variations will occur caused by the motion of the sun line with respect to the equatorial plane.

4.3 GLOBAL COVERAGE

The scan pattern and the swath imaged by the camera are shown in Figure 3-1. The number of orbits per day as a function of altitude is shown in Figure 4-3. Note that an integer number of orbits per day is possible at altitudes near 150, 300, 480, and 680 n.mi. The significance of these altitudes will be pointed out later.

The global coverage problem was treated in the Phase I report, but the analysis has been refined and clarified since publication of that report. Inasmuch as global coverage considerations will influence orbit control and injection error correction requirements, a brief but comprehensive analysis is presented here.
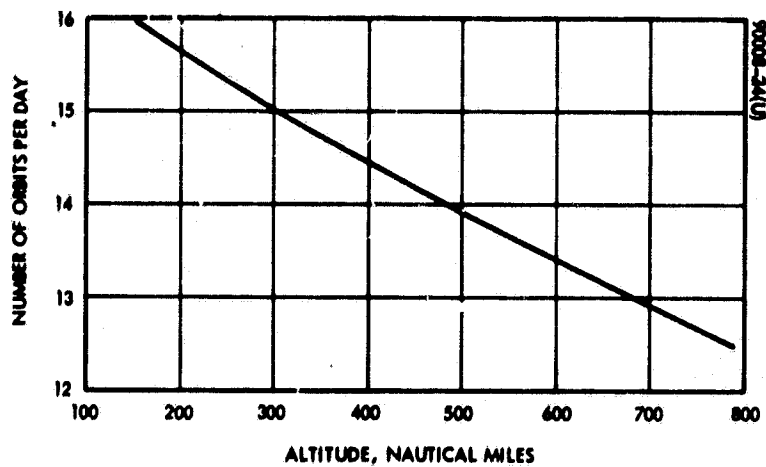
Figure 4-3. Number of Orbits Per Day
as Function of Altitude
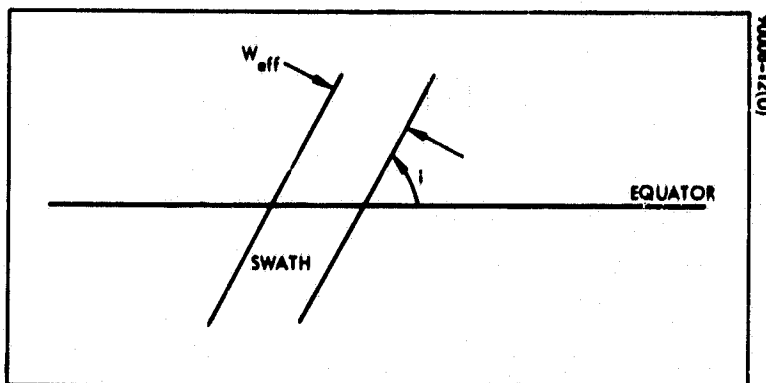
Figure 4-4. Swath and Equator
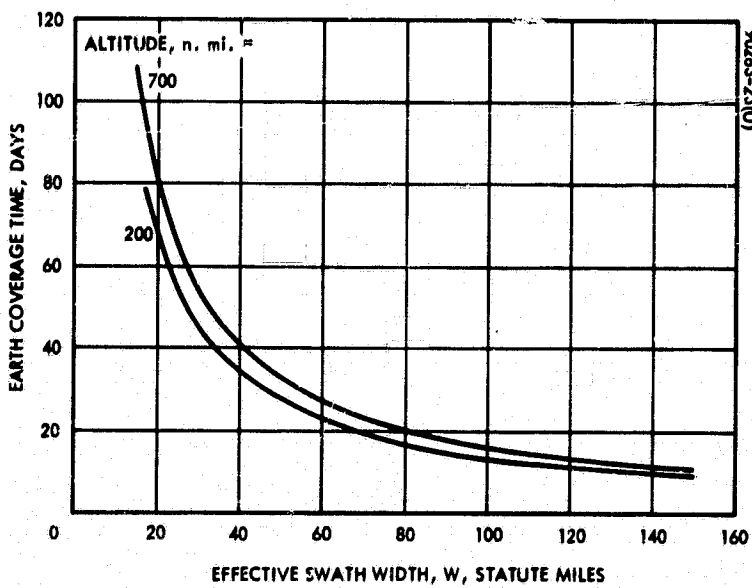
Figure 4-5. Earth Coverage Time

4.3.1 Analysis

The width of the swath is denoted by SW (for swath width). Usually some overlap of one swath by another is desired, and so an effective swath width, W, may be defined as SW minus the desired amount of overlap.

For inclined orbits, global coverage is defined as coverage of the equator. From Figure 4-4, it can be seen that each swath covers $W / \sin i$ of the equator. Since the sun will be shining only on one-half of the earth, usually only one equator crossing per orbit is useful for imaging. Thus, the minimum time for global coverage at the ascending mode is given by

$$T_g = \frac{\sin i \, (R_e + h)^{1.5}}{W} \tag{3}$$

where R_e and h are the earth's radius and the satellite altitude, respectively, in nautical miles. For sun-synchronous circular orbits

$$\cos i = -(4.09099 \times 10^{-4}) \, (R_e + h)^{3.5} \tag{4}$$

For convenience define the swath segment

$$L = \frac{W}{\sin i} \tag{5}$$

Figure 4-5 shows the minimum global coverage time as a function of effective swath width and altitude.

The distance, D, between equator crossings on the earth's surface is given by

$$D = (7.22928 \times 10^{-3}) \, (R_e + h)^{1.5} \text{ statute miles} \tag{6}$$

where R_e and h are in nautical miles. Figure 4-6 illustrates D in addition to the quantities n and a, defined by

$$n + a = \frac{C}{D} \tag{7}$$

where C = 24,902 mi = 21,639 n. mi. is the equatorial circumference and n is the largest integer less than C/D. Thus n orbits are completed before the possibility of an overlap or duplication occurs. The n + 1 orbit track falls somewhere between the tracks of orbits 1 and 2, n + a is the number of orbits completed per day. There will be a large area of the earth's surface between orbit tracks 1 and 2 (k and k + 1) which must be covered
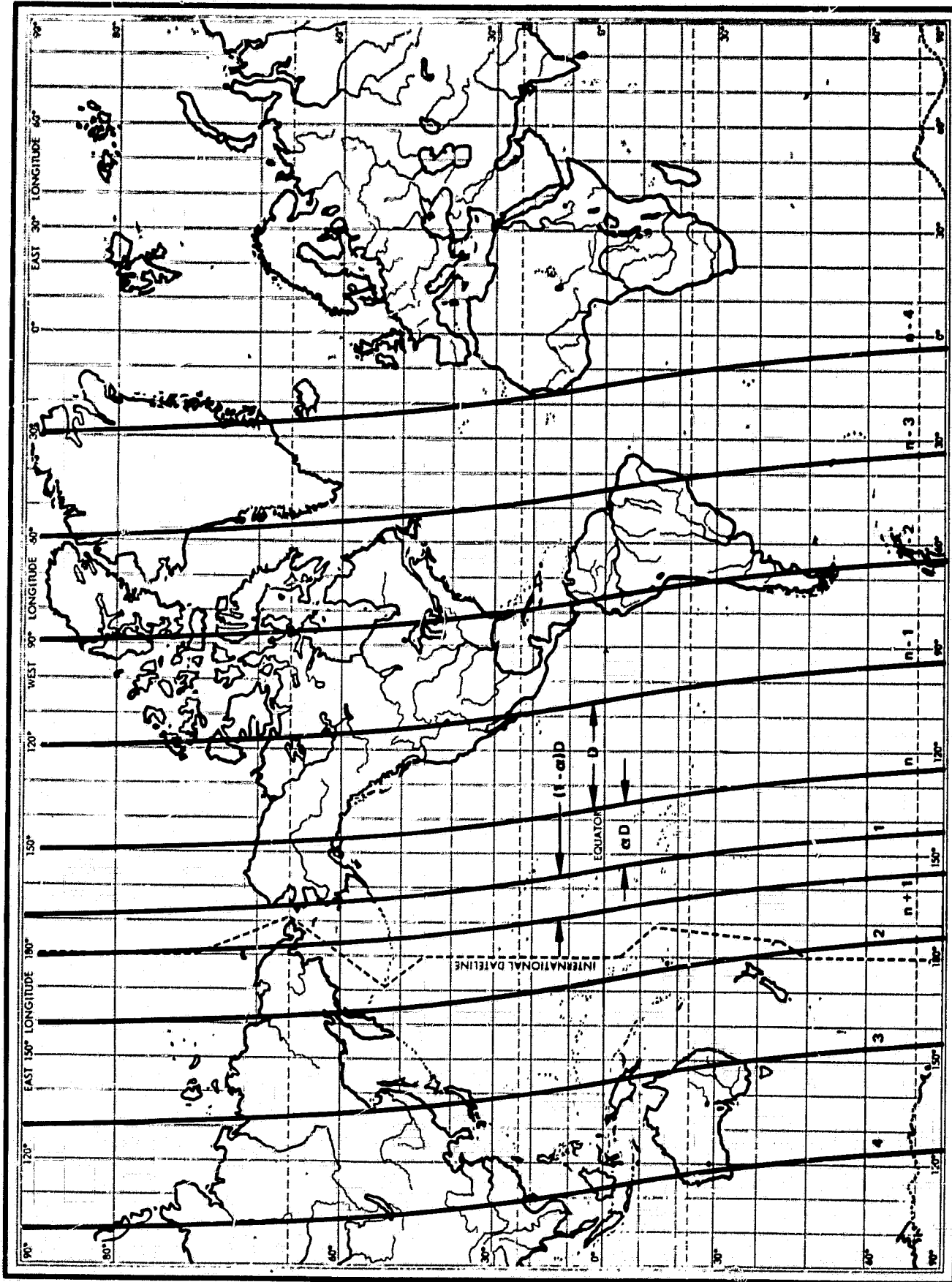
Figure 4-6. Distance Between Equator Crossings

on successive days. The minimum number of days required to complete global coverage is given by

$$N - \beta = \frac{D}{L} \tag{8}$$

i.e., where N is the smallest integer greater than D/L and represents the nearest integer number of days required for global coverage. The distance between any two orbit tracks at the equator may be divided into N "gaps" of equal width, each of which be equal to or smaller than a swath segment, L. Then each of these gaps must be covered by a swath in order to ensure minimum time global coverage.

In order to cover all the gaps and accomplish global coverage, the quantity, a, must be chosen correctly. The following discussion will illustrate the principles involved in choosing a and will lead to the final criterion. For ease in explanation, the discussion will be separated into two cases: 1) $\beta = 0$, i.e., D/L an integer, and 2) $\beta \neq 0$.

$\beta = 0$ (D/L an integer)

Let N = 18 and choose a = 0.5. Then aD/L = 9 and the orbit tracks have the pattern illustrated in Figure 4-7a. Orbit 2n + 1 will coincide exactly with the first orbit, and the third day will be a repeat of the first, and large areas will not be covered.

Now let aD/L = 6. Then the orbit track pattern will correspond to that shown in Figure 4-7b. For this case, orbits 3n + 1 and 3n + 2 will coincide with orbits 1 and 2, respectively, with large areas not covered. If aD/L = 12, then $(1 - a) D/L$ = 6 and a similar pattern occurs with the same areas not covered. Consider a more complex case where aD/L = 14. The orbit tracks are shown in Figure 4-7c where it can be seen that on the tenth day orbits 9n + 7 and 9n + 8 coincide with orbits 1 and 2, respectively, and nine of the gaps are not covered before the pattern begins to repeat.

Integer values of aD/L were used above not only for ease of illustration but because with D/L an integer, aD/L must be an integer for minimum-time coverage. This fact becomes apparent after a brief consideration of orbit track patterns. However, as just shown, not any integer will do.

Some deduction from the above analysis leads to the rule that the integer aD/L and N must be relative primes, i.e., they must have no common integer divisor except unity. And furthermore, it can be shown that if aD/L and N have a common divisor, q, then the orbit tracks on day $(N/q) + 1$ will coincide with those of the first day.

N = 18, β = 0
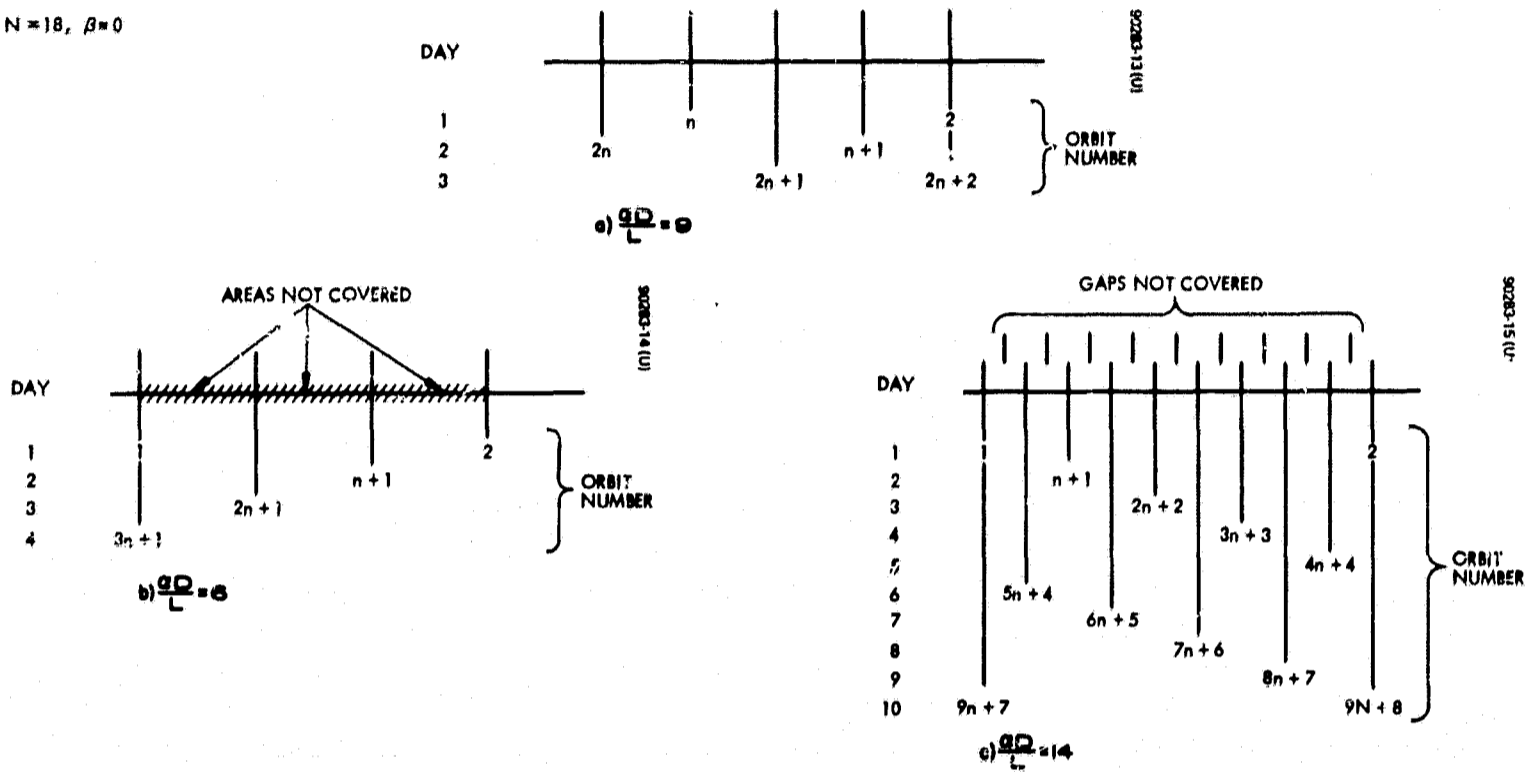
Figure 4-7. Orbit Track Patterns
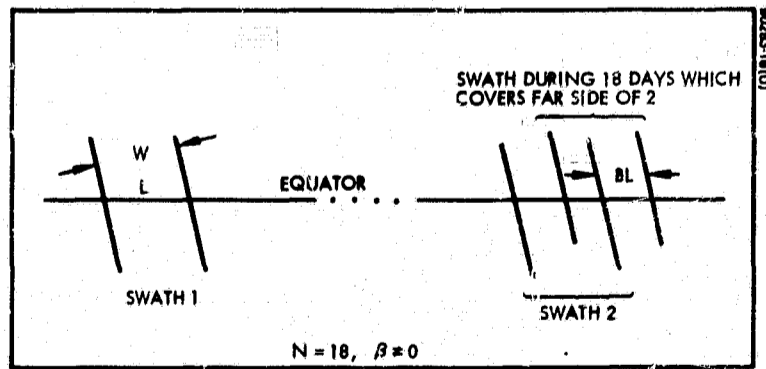
Figure 4-8. Coverage Pattern for β ≠ 0

$\beta \neq 0$ (D/L not an integer)

When D/L is not an integer, $N > D/L$ and, consequently, N crossings of the equator have the potential of covering more than D, the distance between two successive orbits, i.e.,

$$NL > D$$

Since $N - \beta = D/L$, the quantity

$$\beta L = D - NL$$

may be thought of as the "slack" in the coverage capability. That is, for a given N, D may be varied so as to vary β between the values of 0 and 1 with no variation in the number of days required for global coverage. If the imaging swaths could be placed exactly next to each other, then $\beta \neq 0$ implies that there is some coverag. capability left over. This is illustrated in Figure 4-8. The slack per gap, S, is given by

$$S = \frac{\beta L}{N} = \frac{D}{N} - L$$

and can be thought of as additional overlap capability.

With this slack, it is no longer necessary that $\alpha D/L$ be an integer to accomplish global coverage in minimum time. The total slack, βL, may be spread throughout the region between two successive orbits such that the region is covered in N successive days. Thus, by deduction from the above definitions and Figures 4-6 and 4-8, $\alpha D/L$ may be increased somewhat in proportion to itself. It may be shown that if P is an integer ($0 \leq P \leq N$), then $\alpha D/L$ may be as large as

$$\frac{\alpha D}{L} = P + (N - P)\left(\frac{\beta}{N}\right)$$

$$= P\left(1 - \frac{\beta}{N}\right) + \beta = P + \beta\left(1 - \frac{P}{N}\right) \qquad (9)$$

But, for global coverage in minimum time, P and N must be relative primes, as shown above.

4.3.2 Conclusions

From the preceding discussion, the following conclusion is derived:

Criterion

Global coverage in minimum time will be accomplished if P and N are relative primes, i.e., they have no common divisor except unity, and the following relationship is satisfied:

$$P \le \frac{aD}{L} \le P + \beta \left(1 - \frac{P}{N}\right) \tag{10}$$

4.3.3 Consequences

D is a function of altitude and, for sun-synchronous orbits, so is L (see Equations 4 through 6). From Equations (7) and (8), n, a, N, and β are also functions of the satellite altitude. Thus, Equation (10) is a restriction on the satellite altitude. This equation is difficult to solve explicitly for altitude; however, for a given effective swath width, W, various altitudes can be tested to see if they satisfy Equation (10).

Consider now several cases which might arise in determining the requirements for global coverage. Only circular, sun-synchronous orbits are used.

Case 1

For a swath width, SW, of 75 statute miles with a required overlap of 7 miles, which altitudes will allow global coverage in minimum time? The above criterion was applied to altitudes varying from 250 to 650 n.mi. The results are shown in Table 4-1.

Case 2

Similar to Case 1, for a swath width of 100 statute miles with a 10-mile overlap, which altitudes will accomplish global coverage in minimum time? The results are shown in Table 4-2. This case is consistent with swath width chosen for the camera in Section 3.1.

Case 3

For a camera designed to image a 75-mile swath from a 300 n.mi. altitude with a 7-mile overlap (effective swath width equals 68 miles), at which altitudes will global coverage be achieved in minimum time? The results are shown in Table 4-3.

Case 4

Identical to Case 3, except the design swath width is 100 miles with a 10-mile overlap. Table 4-4 presents the results.

TABLE 4-1. ALTITUDES FOR GLOBAL COVERAGE WITH 68-MILE EFFECTIVE SWATH WIDTH

Altitude, n. mi.	P	N
257	7	24
271	5	24
285 to 292	2	25
292 to 299	1	25
307	24	25
314	23	25
322	22	25
329	21	25
344	19	25
351	18	25
358	17	25
366	16	25
380	14	25
388	13	25
399 to 402	11	26
414 to 417	9	26
429 to 431	7	26
444 to 446	5	26
459 to 460	3	26
474 to 475	1	26
489	25	26
504	23	27
512	22	27
527	20	27
534 to 535	19	27
550	17	27
558	16	27
573 to 574	14	27
581	13	27
597	11	27
604	10	27
608 to 612	9	28
639 to 643	5	28

TABLE 4-2.   ALTITUDES FOR GLOBAL COVERAGE WITH 90-MILE
EFFECTIVE SWATH WIDTH

Altitude, n. mi.	P	N
260	5	18
266 to 269	4	19
272 to 278	3	19
281 to 287	2	19
290 to 296	1	19
308	18	19
318	17	19
328	16	19
337	15	19
347	14	19
357	13	19
366 to 367	12	19
376	11	19
386	10	19
396	9	19
405	8	19
410 to 415	7	20
448 to 453	3	20
468 to 472	1	20
487	19	20
508	17	20
549	13	20
566 to 569	11	21
576 to 579	10	21
596 to 600	8	21
628 to 630	5	21
638 to 640	4	21

TABLE 4-3. ALTITUDES FOR GLOBAL COVERAGE WITH CAMERA
DESIGNED TO IMAGE 68-MILE EFFECTIVE SWATH WIDTH
FROM A 300-N.MI. ORBIT

Altitude, n.mi.	P	N
252 to 253	9	29
272 to 274	5	27
276	4	27
284 to 286	3	26
292	2	25
296 to 299	1	25
309	23	24
319	21	23
324	20	23
329	19	23
341	17	22
347	16	22

TABLE 4-4. ALTITUDES FOR GLOBAL COVERAGE WITH CAMERA
DESIGNED TO IMAGE 90-MILE EFFECTIVE SWATH WIDTH
FROM 300-N.MI. ORBIT

Altitude, n.mi.	P	N
250 to 252	7	22
264 to 265	5	21
268 to 270	4	21
278 to 280	3	20
294 to 296	1	19
311	17	18
332	14	17
340	13	17
347 to 348	12	17
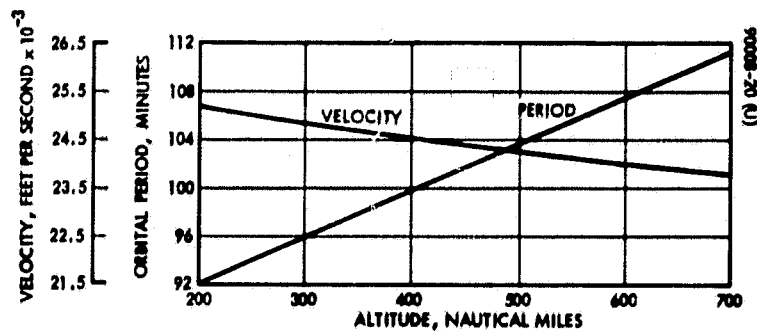
Figure 4-9. V_O and T_O as Function of Altitude
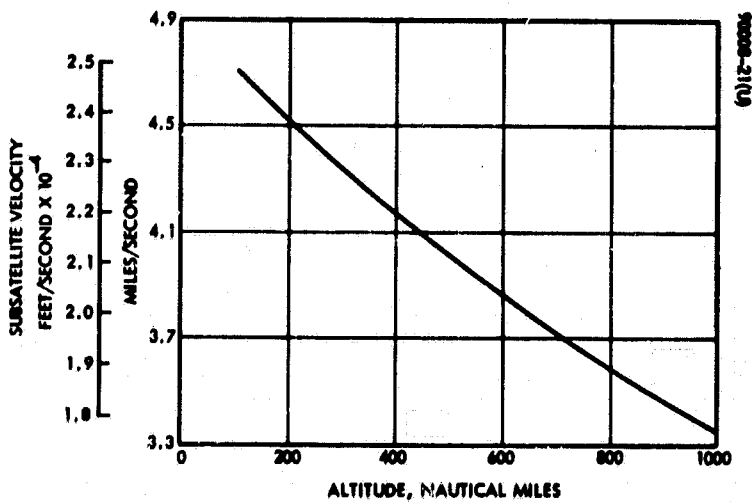
Figure 4-10. Subsatellite Velocity Versus Altitude
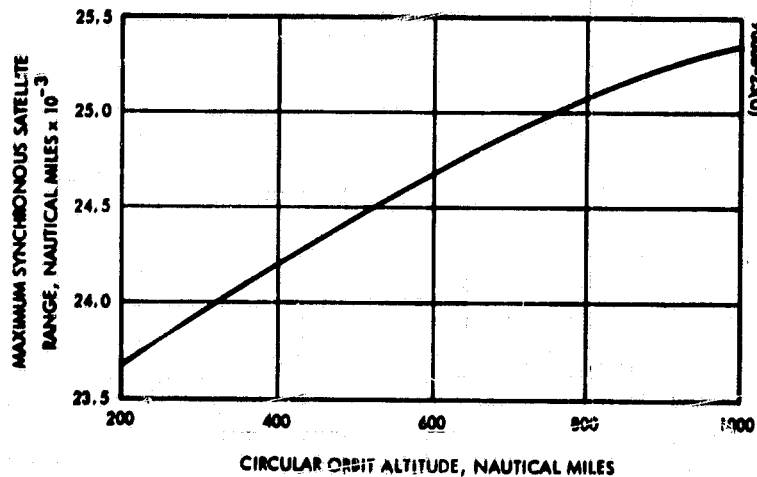
Figure 4-11. Maximum Synchronous Satellite Range as Function of Circular Orbit Altitude
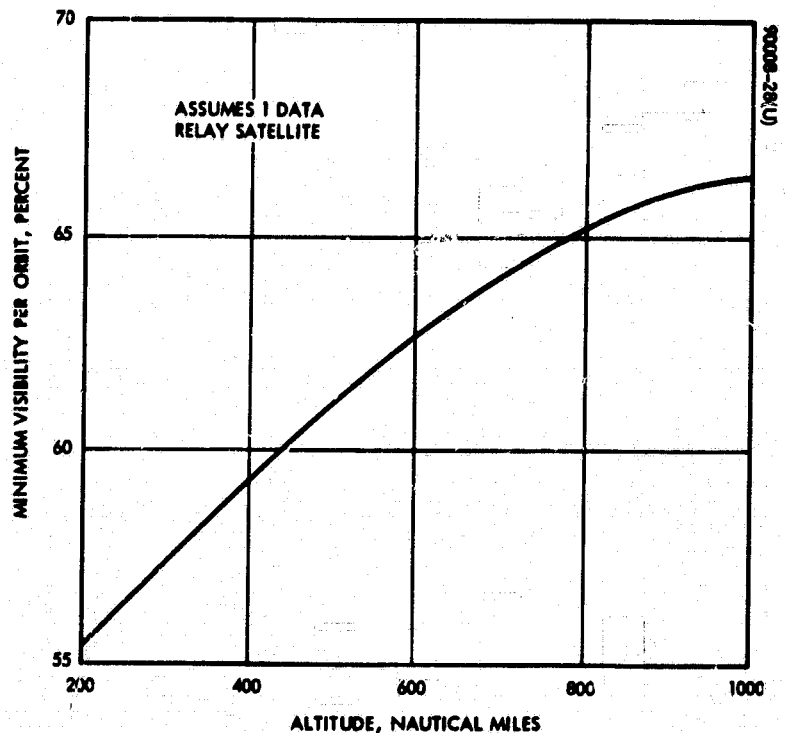
Figure 4-12. Minimum Visibility of LAS by DRS

Referring to Figure 4-6, if $P = N - 1$, then the swath on the $n + 1$ orbit will overlap the swath of the first. This is a slightly more desirable imaging sequence than most other possibilities, since contiguous swaths are 24 hours apart. But this swath sequence requires the satellite to be near an altitude which results in an integer number of orbits per day. If this is done, the nominal altitude is relatively independent of the swath width.

From Tables 4-1 and 4-2, if $P = N - 1$, then possible altitudes for a 68-mile effective swath width are 307 and 489 n.mi. and, for a 90-mile effective swath width, 308 and 487 n.mi. However, for this technique, the altitude must be maintained to within 1 n.mi.

If $P = 1$, then the nth orbit will fall just to the east of the first orbit and their swaths will overlap. Thus, for this case also, contiguous swaths occur 24 hours apart. But the advantage is that orbit injection and maintenance is not as critical. For a 68-mile effective swath width, there are ranges of altitudes (292 to 299 and 474 to 475 n.mi.) that result in the above type of coverage. For a 90-mile effective swath width, the ranges are 290 to 296 and 468 to 472 n.mi.

4.4 ALTITUDE SELECTION

The closer the LAS is to the earth, the better the potential quality of the picture. Thus, a low altitude is preferred from an image resolution standpoint. However, the disturbances on the satellite due to atmospheric drag increase as the altitude decreases. Analysis indicates that altitudes below 250 n.mi. will result in excessive disturbances. As just discussed, an altitude near 300 or 480 n.mi. has a desirable and convenient coverage pattern. Furthermore, altitudes just below these allow more tolerance in the correction of injection errors than those just above. Based upon all these considerations, an altitude of 293 n.mi. is chosen. This is in the center of the altitude range allowable for the camera with the 100-mile swath width and is also included in the 75-mile swath width range (see Tables 4-1 and 4-2).

4.5 ALTITUDE DEPENDENT PARAMETERS

A number of quantities of interest are functions of the satellite altitude. These include orbital inclination, i, altitude sensitivity to inclination, satellite velocity, orbital period, subsatellite velocity, maximum and minimum LAS-DRS range, and minimum LAS/DRS visibility.

The functional dependence is shown in Figures 4-1, 4-2, and 4-9 through 4-12.
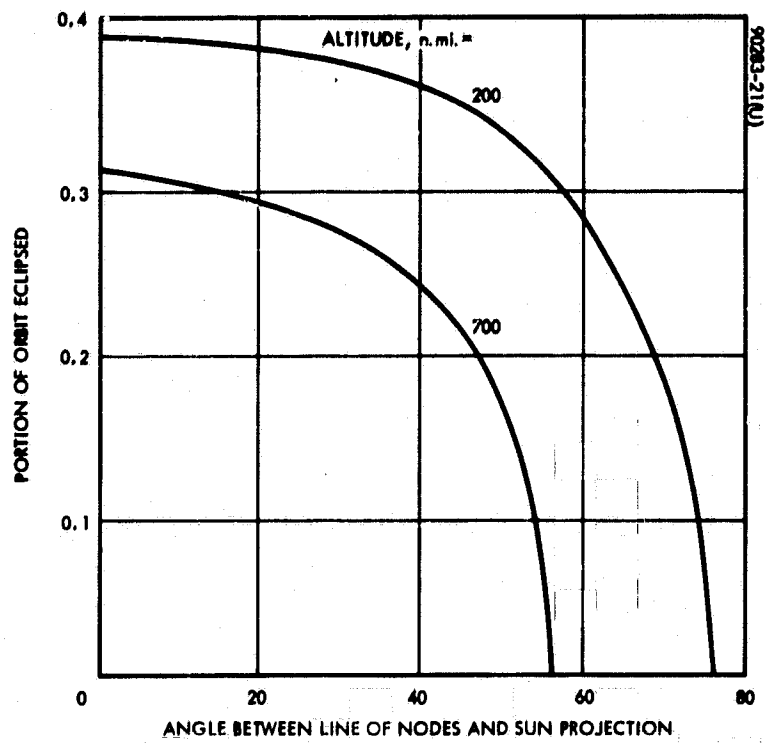
Figure 4-13. Portion of Orbit Eclipsed as Function of Angle, φ , Between Line of Nodes and Sun Projection

For an altitude of 293 n. mi., the values of these quantities are listed as follows:

Parameter

Orbital inclination	97.5 degrees
Altitude sensitivity to inclination	141.6 n. mi./degrees
Satellite velocity	24,898 fps
Orbital period	95.5 minutes
Subsatellite velocity	4.35 mi/second
Maximum LAS-DRS range	23,955 n. mi.
Minimum LAS-DRS range	19,015 n. mi.
Minimum LAS-DRS visibility	58 percent

4.6 ORBIT-SUN RELATIONSHIP

The angle, ϕ, between the line of nodes and the projection of the earth-sun line on the equatorial plane should be chosen to give the desired lighting conditions on the ground. For this study, an angle of 30 degrees was arbitrarily chosen. This value corresponds to a 2:00 p.m. orbit and will give shadowing effects deemed desirable by earth resources authorities.

The portion of the orbit eclipsed is a function of the angle between the line of nodes, the sun line projection, and the satellite altitude. This relationship is shown in Figure 4-13. For ϕ = 30 degrees and a 293 n. mi. altitude, the sun is not visible to the LAS for 35.5 percent of the time, or 33.9 minutes of the orbit.

5. COMMUNICATION SYSTEM

The design philosophy of the LAS communication system required two separate subsystems: one to have a broad coverage antenna with a relatively low baseband or data rate capability, and the other a wideband system capable of transmitting the optical imaging data along with other data as well.

The objective of this section is to present the rationale for choosing the basic system components and parameters and to discuss the capability of the system chosen. Since the payload is only representative, rather than analyze the details of multiplexing, the emphasis here is upon the basic system parameters. These include the following:

1) Antenna

2) Carrier frequency

3) Radiated RF power

4) Baseband and/or data rate

Modulation is considered only as to its influence on postdetection signal-to-noise ratios and, hence, the link capacity.

Consistent with the above mentioned design philosophy, there are two communication systems on the LAS, designated here as the VHF system and the data transmission system (DTS). The primary function of the VHF system is to provide telemetry and command communication, while the DTS is used for transmitting the payload sensor data. There is a reliability and convenience advantage in providing the capability to transmit and receive some data through both systems. The concept presented here has that capability.

The data to be received by the LAS includes spacecraft commands, data collection interrogation commands, and satellite tracking signals. Those data to be transmitted include housekeeping data, data collection messages, tracking signals, radar scatterometer data, and the camera data. Table 5-1 lists these data along with their baseband or bit rate and the system or systems handling each.

TABLE 5-1.   LAS DATA

Receive	Transmit	Baseband or Bit Rate	Communication Subsystem
Commands	Housekeeping	500 bits/sec	VHF and DTS
Data collection system	Data collection system	2560 bits/sec	VHF and DTS
Tracking	Tracking	5 kHz	DTS
	Radar scatterometer	200 Hz	DTS
	Multispectral scanning camera	8 MHz	DTS

5.1 VHF SYSTEM

The principal function of the VHF system, as mentioned above, is to provide command and housekeeping telemetry communication. Inasmuch as this communication is critical to the mission and operation of the spacecraft, it is desirable to have the VHF communication link operational for as much of the time as possible. Consistent with this objective is an omnidirectional antenna on the LAS and an earth-coverage antenna on the DRSs.

5.1.1 Antenna Selection

Omnidirectional radiation from the LAS is difficult to achieve because of the many appendages to the spacecraft, as well as its size. The most critical time for command capability is when the LAS is near the earth's poles. At this point, the DTS antenna must be commanded to change its transmission from one DRS to another. At other times, the commands and housekeeping data can be transmitted via the DTS system. Based upon this reasoning, a spiral dipole antenna was selected. This antenna, pictured in Figure 5-1, has the gain pattern illustrated in Figure 5-2. Since the DTS antenna must be located on the side of the spacecraft facing away from the earth, the VHF antenna must be located on the other side to prevent blockage of one by the other. Mounted, as shown in Figure 2-1 (see Section 2), the antenna gain toward the DRSs is maximum when the LAS is near the poles, and from Figure 5-2, it can be seen that the gain drops 3 dB at 45 degrees from the top or bottom of the orbit (nearest the north or south poles, respectively.) From Figure 5-2 and a brief analysis of the LAS/DRSS geometry, a gain of -1 dB is selected for link calculations.

Although the spacecraft will obstruct the radiation somewhat, if there are three or more DRSs one should be in view of the VHF antenna most of the time. Figure 5-3 shows several relative positions of the LAS and DRSs. A cursory analysis indicates that with this antenna satisfactory communication will be possible more than 75 percent of the time. This coverage capability may be increased by adding another antenna on the opposite side of the spacecraft. The way this may be done without interfering with the DTS antenna will be discussed later.

5.1.2 Link Analysis

The carrier frequency selected is 136 MHz, which is consistent with EARC frequency allocations for space use. An earth coverage antenna on the DRS with a 20-degree, half-power beamwidth would have a diameter of about 25 feet and a gain of about 18 dB, so that at the half-power points, the gain is 15 dB. However, 13 dB will be used for link calculations. If the DRS noise temperature is taken as 1000° K, the range equation yields the following result:

$$\text{LAS EIRP} = \frac{C}{\eta} \text{ (dB)} - 41.9$$

where $\frac{C}{\eta}$ is the carrier-to-noise density ratio. Assuming an RF power of 10 watts (10 dB) and a worst case transmit antenna gain of -1 dB,

90283-30(U)

H POL

V POL

45° POL

5
10
15
20
25
30
35
db
35
30
25
20
15
10
5

CIRCULARLY POLARIZED
VHF ANTENNA 135.15 MC/S
1. INCH DIAMETER
15 INCH HEIGHT
150 HELIX ANGLE
POLAR CUT
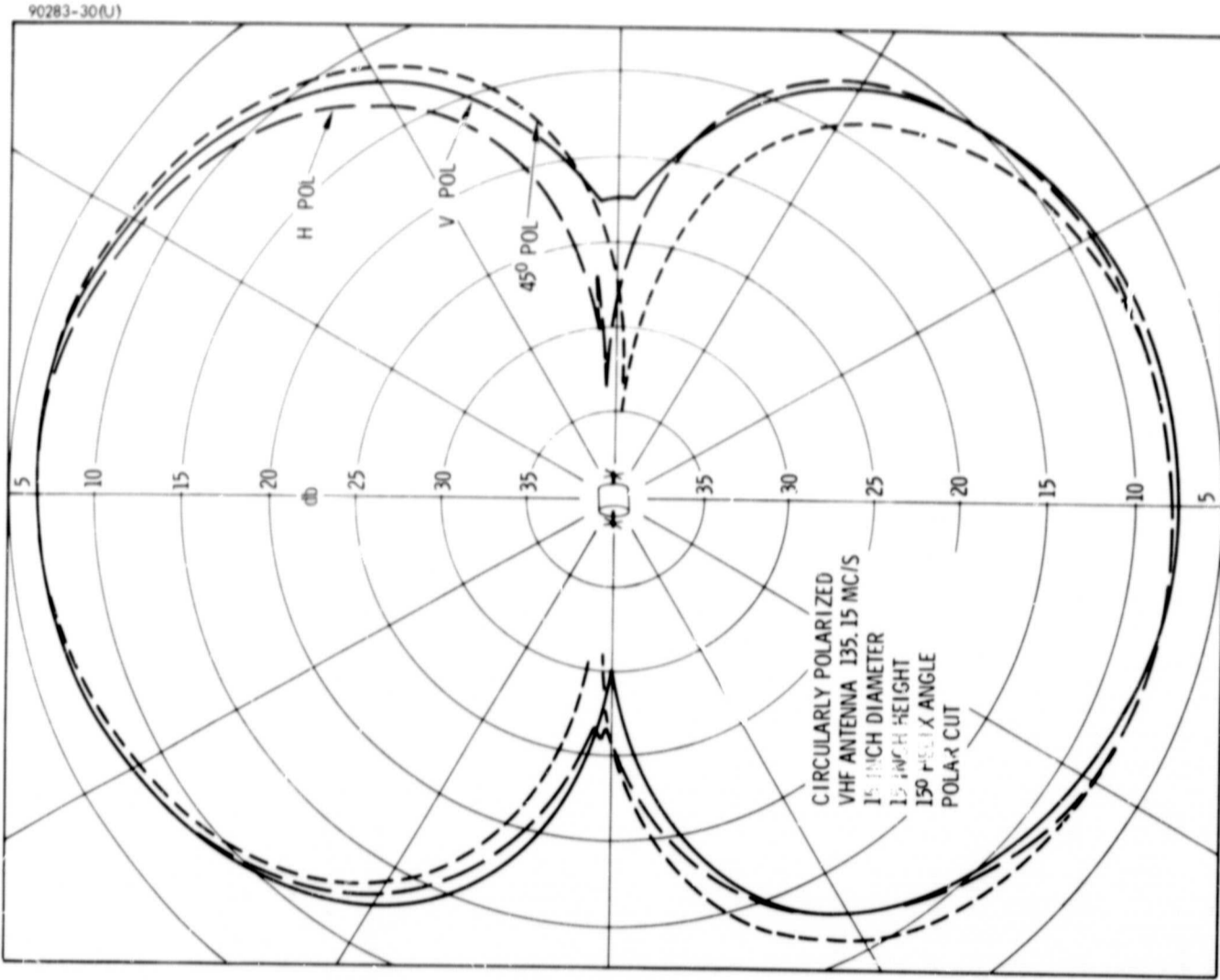
Figure 5-2.   Antenna Pattern

90283-29(U)
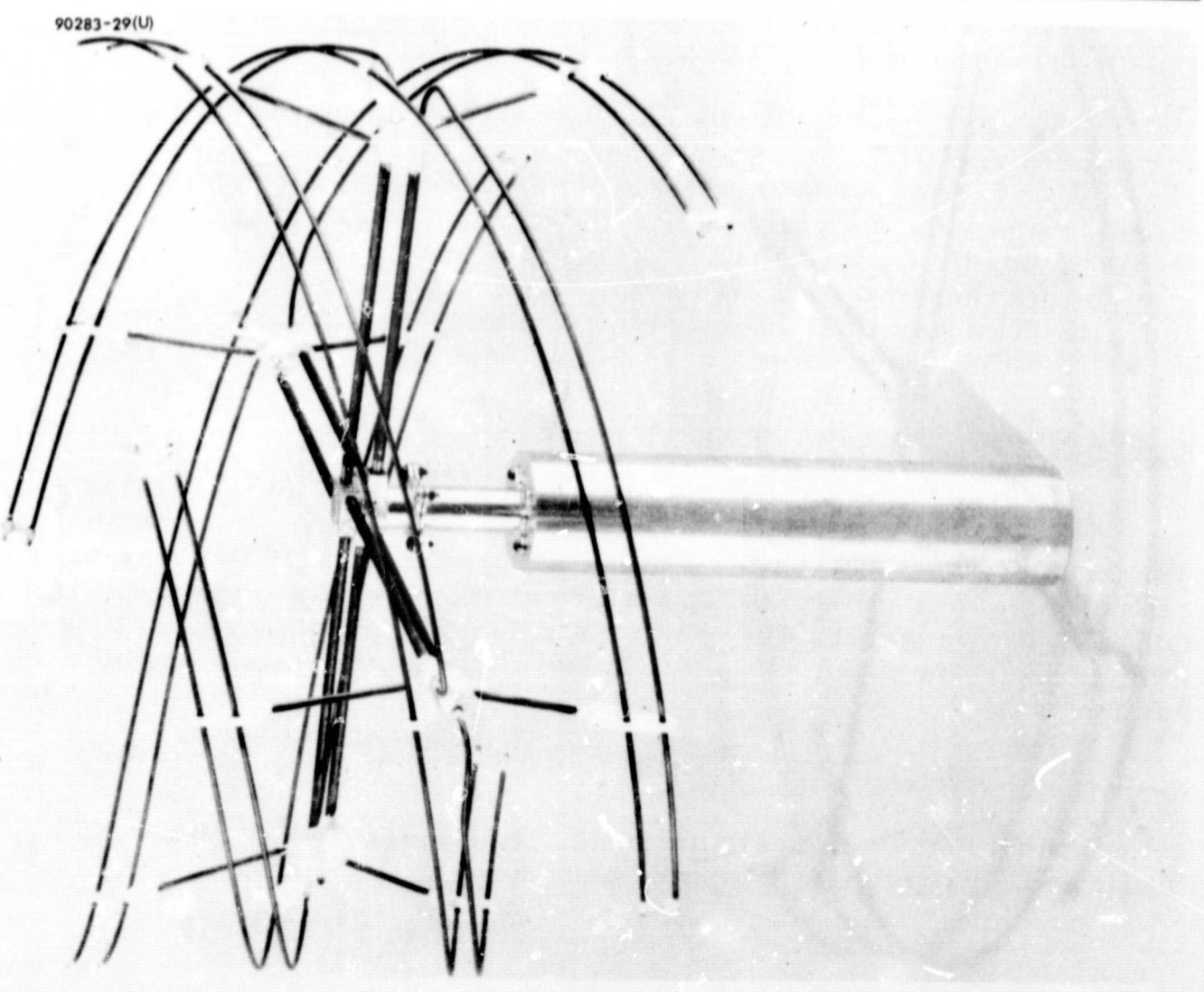
Figure 5-1.   VHF Antenna

5-4

$$\frac{C}{\eta} = 10.9 \text{ dB-Hz}$$

With a desired carrier-to-noise power ratio of 10 dB, the RF bandwidth may be 40.6 dB = 11.5 kHz. Such a bandwidth will support the data collection bit rate of 2560 bits/sec, as well as a housekeeping telemetry channel.

If the DRS transmitter power is also 10 watts, the above analysis applies for transmission to the LAS, and the data collection interrogation commands and the spacecraft commands can be supported by this link. Table 5-2 presents the detailed breakdown analysis of the VHF link, and Figure 5-4 illustrates the system.

5.2 DATA TRANSMISSION SYSTEM (DTS)

The DTS must transmit and receive all data, providing a redundant capability for housekeeping data, commands, and data collection messages. Table 5-1 shows that the camera provides the major bandwidth requirement. For optical resolution in the neighborhood of 150 feet, the baseband of a single spectral band signal will be less than 2 MHz, allowing for multiplexing efficiency. Thus, a four-band camera will have a baseband less than 8 MHz.

All of the other data have much smaller bandwidth requirements and can be multiplexed within a 2-MHz baseband. Thus, the requirement of the DTS are:

1) 10-MHz baseband

2) No storage

3) Good quality reception

The reception requirement is a constraint on the carrier-to-noise ratio and the test tone-to-noise ratio at the receiver for an FDM/FM system, or the error probability for digital transmission.

The system elements and parameters to be selected include the antenna, carrier frequency, and RF power.
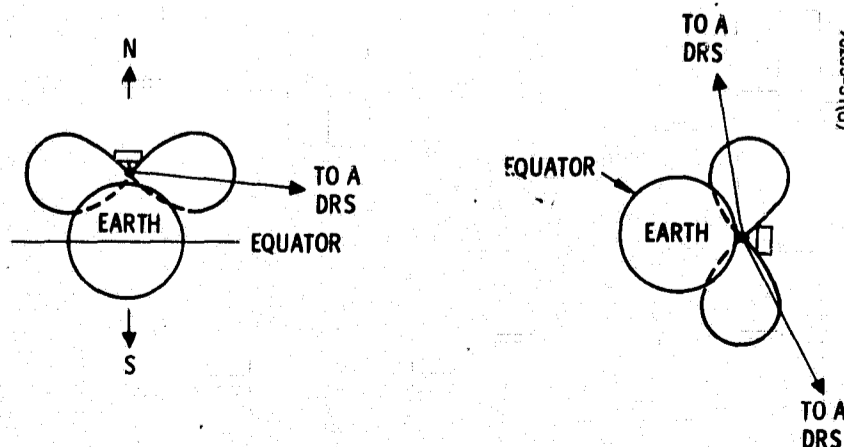
Figure 5-3. VHF Antenna Coverage

TABLE 5-2. VHF LINK ANALYSIS

Parameter	Value, dB	Digital Transmission
Transmit power	+10	Bit error rate - 10^{-5}
LAS antenna gain	-1	$\dfrac{E}{\eta} \approx 13$ dB
DRS antenna gain (worst case)	+13.	FSK incoherent
Path loss	-168.2	
Polarization loss	-0.5	$\dfrac{\text{Signal power}}{\text{Total RF power}} = 0.63 = -2$ dB
Miscellaneous losses	-1.0.	
Received power, P	-147.7	BIT rate = 3.9 kilobits/sec
Receiving system noise power density, η (1000° K system temperature)	-198.6	
Link capacity = P/η	50.9	

90283-32(U)
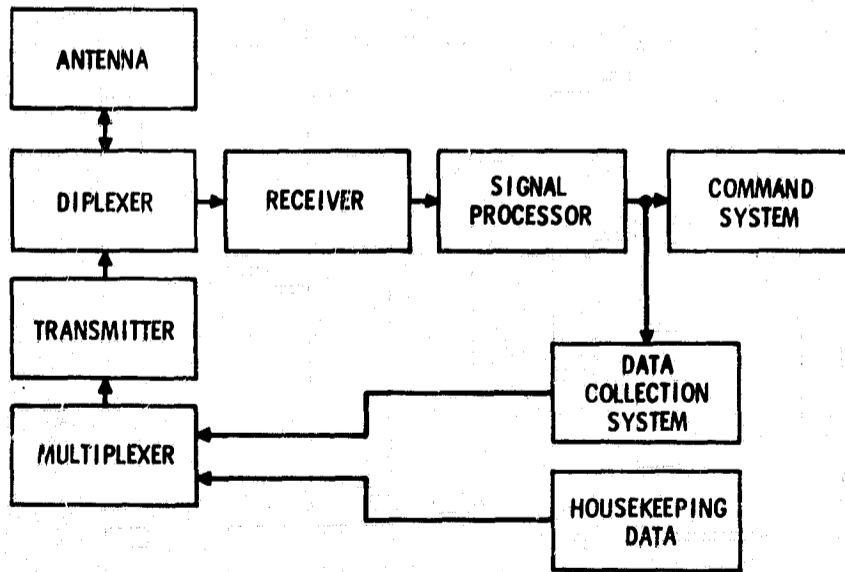
Figure 5-4. VHF Communication System

5.2.1 Antenna and Carrier Frequency Selection

The primary factors in choosing an antenna are:

1) Packaging constraints

2) Weight

3) Radiation pattern

As discussed in the Phase I report, packaging requirements are the major criteria for antenna selection. Figures 5-5 and 5-6 compare four types of antennas with respect to size and weight at 15 GHz.

Figure 5-5 shows that for gains greater than 36 dB, the side of a square planar array is smaller than the major dimension of the other three antenna types; this relationship is nearly independent of frequency. Figure 5-6, which compares the weight of these antennas, shows that a parabolic reflector weighs the least at higher gains. However, for gains less than 42 dB, the weights of the helical array, parabolic reflector, and planar array are all less than 12 pounds. Since the support and gimbaling system will probably weigh at least this much, weight is not a main consideration.

A limited comparison of the radiation pattern was presented in the Phase I report. Although it is difficult to make generalizations because of the specialized techniques available for certain antennas and frequencies, it appears that the planar array is the most efficient, but the parabolic reflector has lower sidelobes. Still, the pattern of a planar array is quite acceptable.

The rather strict limitations imposed by the Delta shroud limit the size of a rigid antenna to approximately 3 feet. Also, the spacecraft has flat sides, which makes a flat surface antenna attractive. The above considerations lead to the selection of a rigid, square planar array with a maximum side length of 3 feet.

A partial list of frequencies allocated for this type of mission is given in Table 5-3. The Phase I study considered the frequencies 2.25, 8, 15, and 35 GHz. The carrier frequency affects the other system parameters significantly. From an analysis of the communications link, if the gain of the DRS antenna is fixed, the required LAS effective isotropic radiated power (EIRP) increases with carrier frequency. For a fixed LAS antenna size, the gain increases and beamwidth decreases. The size of the DRS antenna decreases for a fixed gain. The trades involve antenna sizes, required RF power, and antenna pointing requirements. These are all interrelated and some of the relationships are presented and discussed below.

An analysis of the link, using frequency division multiplexing and frequency modulation, yields the curves of Figure 5-7. The 10-MHz baseband was assumed composed of 80 kHz analog channels with 20 kHz guard
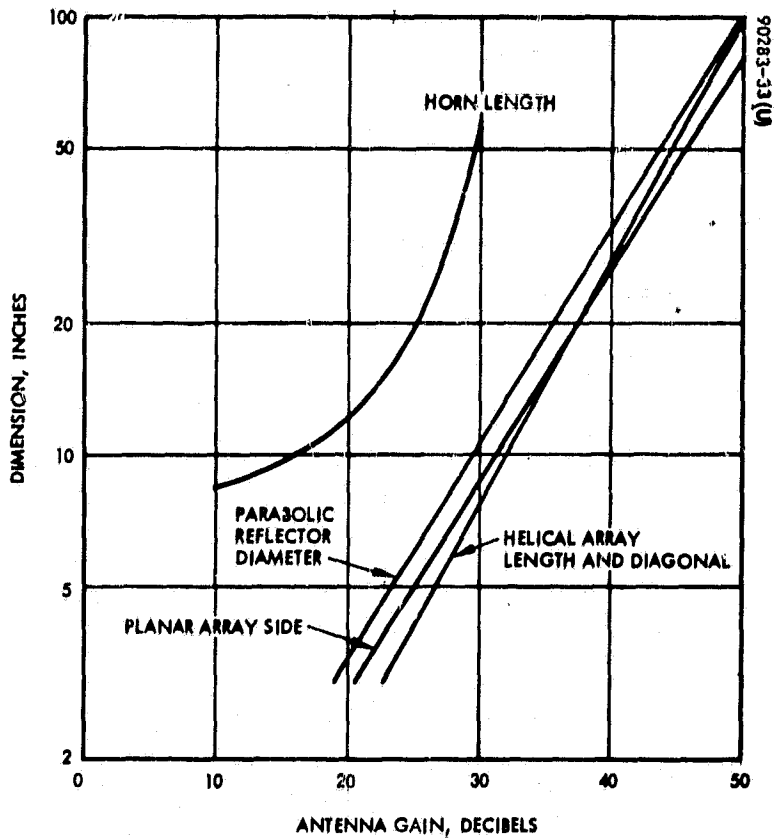
Figure 5-5. Antenna Size Comparison
at 15 GHz

Figure 5-6. Antenna Weight Comparison
at 15 GHz

TABLE 5-3. FREQUENCY
ALLOCATION IN ACCORDANCE
WITH EARC. GENEVA 1963

1750 to 1850 MHz
2200 to 2290 MHz
7300 to 7750 MHz
8400 to 8500 MHz
15.25 to 15.35 GHz
31.0 to 31.3 GHz
34.2 to 35.2 GHz
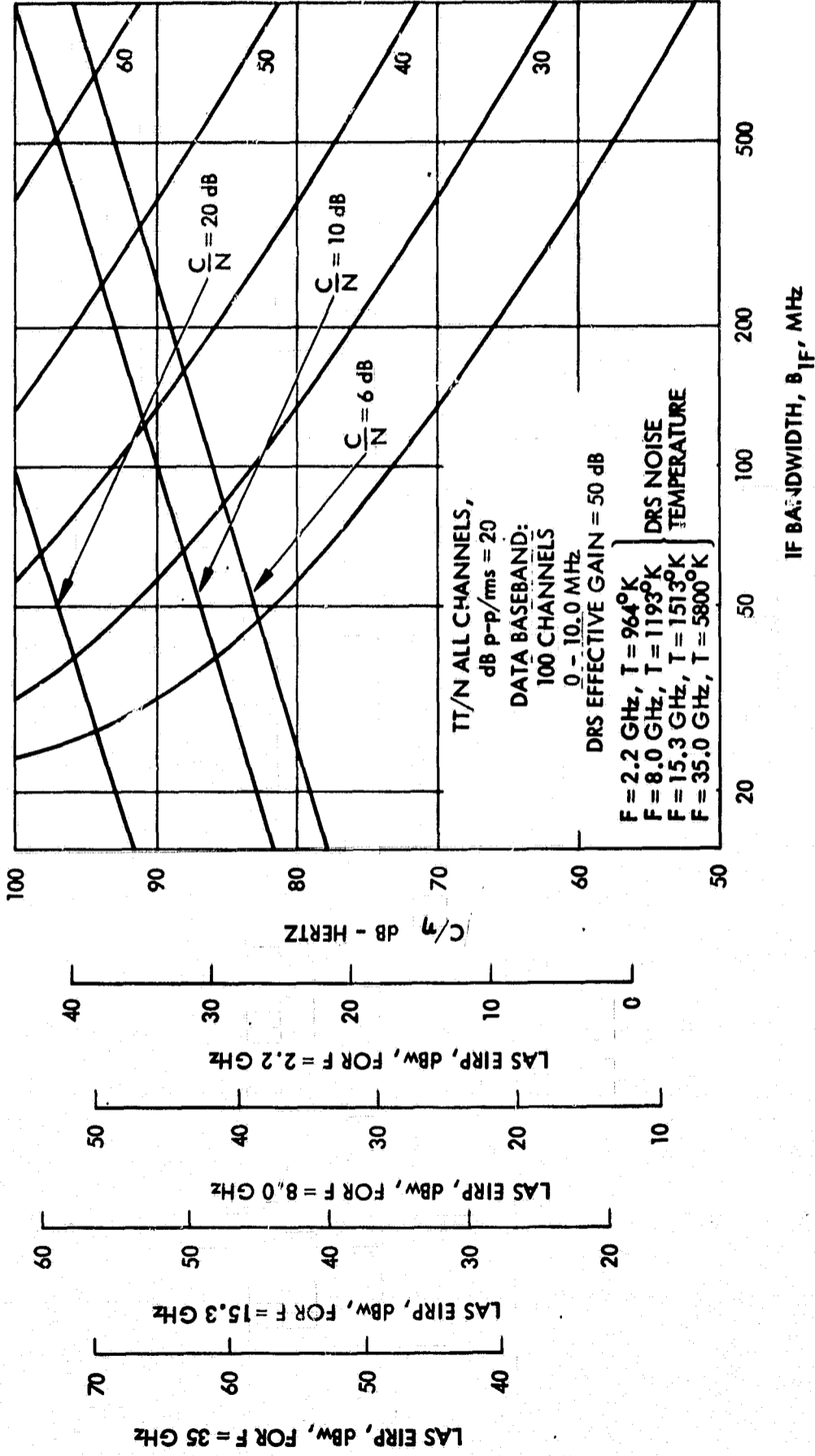
Figure 5-7. LAS-DRS Link FDM/FM Modulation 10 MHz Baseband
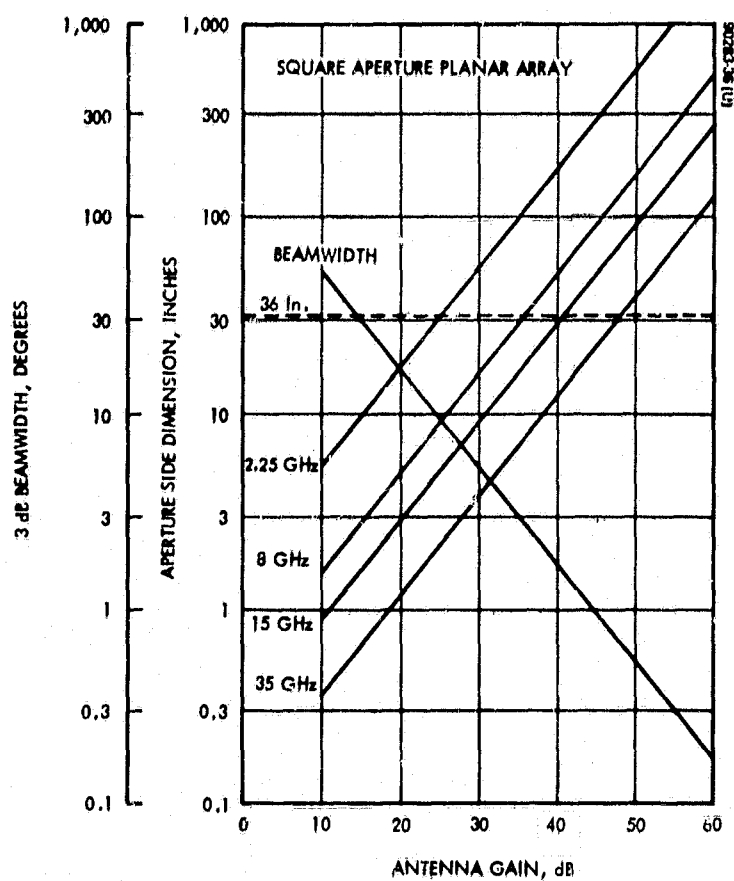
Figure 5-8.   Aperture Size versus Antenna Gain

bands. Each such channel can be represented by a test tone at its center, and the quality of reception is judged by the ratio of test tone power to noise power. A common modulation technique filters the baseband signal in such a way as to make all the postdetection test tone-to-noise ratios (TT/N) equal. These assumptions ensure that all signals of the baseband will be received with equal quality. In general, a TT/N greater than 40 dB is required for good quality reception, and a carrier-to-noise ratio of 10 dB is required.

Figure 5-8 shows the relationship between the side length of a square planar array and its gain for the frequencies of interest in this study. The beamwidth is also plotted as a function of gain. The coordinate corresponding to a 3-foot side is shown to aid in the analysis.

Using Figures 5-7 and 5-8, Table 5-4 was constructed to illustrate the effect of carrier frequency selection. Two cases were examined; in one the DRS antenna gain was assumed to be constant at 50 dB and the effect upon antenna size and LAS RF power was calculated, while in the other case, the diameter of the DRS antenna dish was set at 9 feet and the effect of carrier frequency upon the DRS antenna gain and LAS RF power was tabulated. The latter is the more realistic case, and 9 feet was chosen arbitrarily, but represents a size that could be packaged in a Titan booster shroud.

Note that for a carrier frequency of 2.2 GHz, a 50-dB antenna requires a 61-foot diameter dish, or for a 9-foot dish, 446 watts of RF power must be transmitted by the LAS. Another combination consists of a 30-foot diameter dish and 40 watts of LAS RF power. At 8 GHz, a 50-dB antenna has a diameter of 16.6 feet, and 12.6 watts of RF power are required; and a 9-foot DRS antenna requires 43.6 watts from the LAS. At 15 GHz, a 9-foot antenna has a gain of 50 dB and 15.8 watts and must be transmitted by the LAS; and from Figure 5-8 the beamwidth of a 50-dB antenna is 0.5 degree. Finally, at 35 GHz, a 50 dB antenna is only 3.9 feet in diameter, but 63 watts are required from the LAS. This large increase in required power is due to the much higher noise figure of a 35 GHz receiver (see Figure 5-7). A 9-foot dish allows the required power to drop to 11.2 watts.

However, a 9-foot diameter antenna at 35 GHz has a gain of 57.5 dB and a 3-dB beamwidth of about 0.22 degree; and a 3-foot square planar array has a beamwidth of 0.63 degree. Although the pointing accuracy required by these beamwidths is within the capability of current technology, the beamwidths necessary for 15-GHz transmission place less stringent requirements upon the tracking and acquisition system, thereby reducing cost and improving reliability.

The combination shown in Table 5-4 for 15 GHz of a 41-dB planar array and a 50-dB DRS antenna, requires 15.8 watts of LAS RF power. These antenna gains correspond to 3-dB beamwidths of about 1.5 and

TABLE 5-4. FREQUENCY SELECTION

FDM/FM Modulation

$$\frac{C}{N} \geq 10 \text{ dB}$$

$$\frac{TT}{N} \geq 40 \text{ dB}$$

Carrier Frequency, GHz	3-Foot Planar Array Gain, dB	DRS Antenna Gain = 50 dB		DRS Antenna Diameter = 9 ft		DRS Gain x LAS RF Power, dBw
		Dish Antenna Diameter, feet	LAS RF Power, watts	DRS Antenna Gain (55 percent efficiency), dB	LAS RF Power, watts	
2.2	25	61	10	33.5	446	60
8	36	16.6	12.6	44.6	43.6	61
15	41	9	15.8	50	15.8	62
35	48	3.9	63	57.5	11.2	68

0.5 degree, respectively. Since the DRS has a much smaller required coverage zone, the greater tracking burden is placed on that satellite. This is also consistent with the concept of the DRS being much larger than the LAS. Note, that at 35 GHz, due to the higher noise figure, the power is reduced 4.6 watts less than at 15 GHz, while the beamwidth is decreased 56 percent. Even if the LAS power at 35 GHz was set at 15.8 watts, the required DRS antenna gain is 56 dB, with a diameter of 7.6 feet and a 3 dB beamwidth of 0.26 degree.

Based upon all the above considerations, the carrier frequency was selected as 15.3 GHz. The LAS planar array antenna side was set at 3 feet, and the required DRS antenna gain is 50 dB.

5.3 TOTAL SYSTEM CONFIGURATION

The basic components and parameters of both the VHF and DTS systems are summarized in Table 5-5. An arbitrary decision, indicated in Table 5-1, was made to provide communication capability for the VHF data through the DTS also. Thus, the total LAS communication system in basic block diagram form can be represented as shown in Figure 5-9.
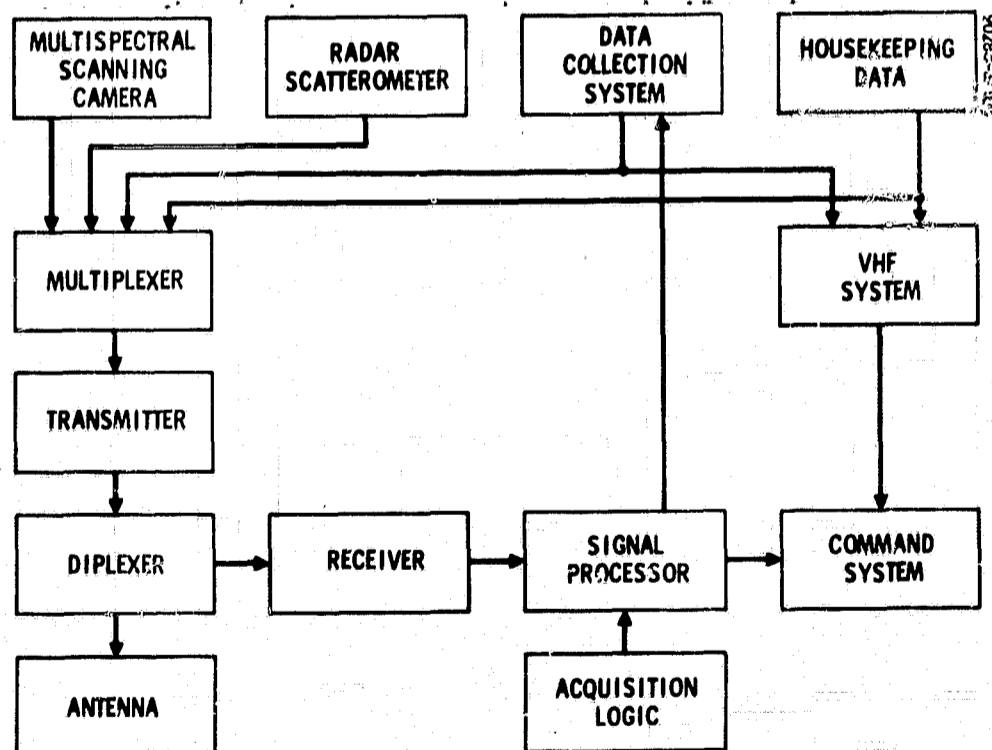
Figure 5-9. LAS Communication System Block Diagram

90283-38(U)

ADDITIONAL
VHF ANTENNA

ADAPTER RING

SOLAR
ARRAY

INCLINATION
CONTROL
THRUSTER

DATA
TRANSMISSION
ANTENNA

VELOCITY
CONTROL
THRUSTER

VHF
TELEMETRY AND
COMMAND ANTENNA
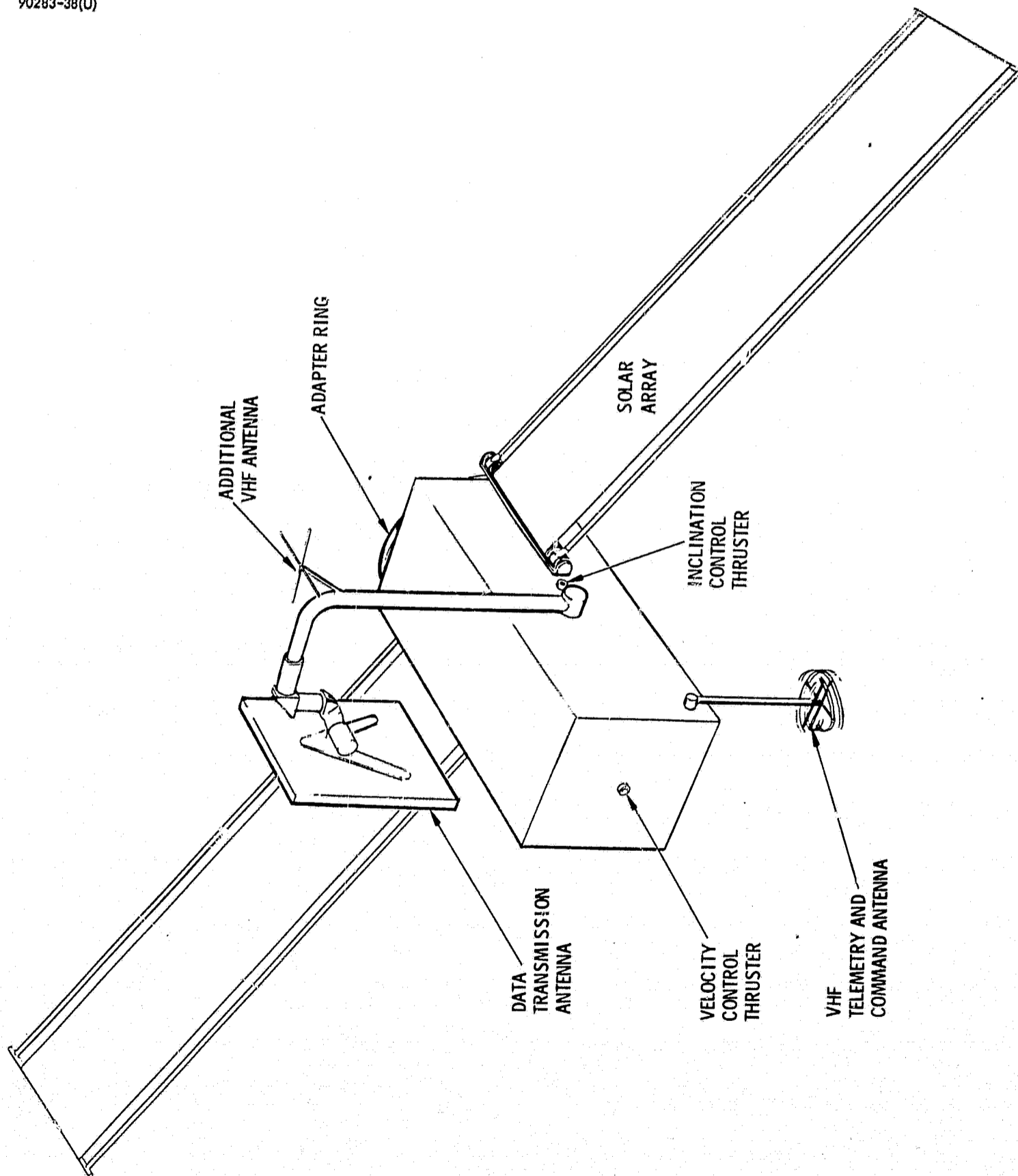
Figure 5-10. LAS With Additional VHF Antenna

TABLE 5-5.   COMMUNICATION SYSTEM SUMMARY

	VHF System	DTS
Antenna	Spiral dipole omnidirectional (See Figure 5-1)	Square planar array, 3-foot side
Gain	See Figure 5-2	41 dB
Beamwidth	— — —	1.6 degrees
Carrier frequency	136 MHz	15.3 GHz
RF power	10 watts	16 watts
Data rate or baseband capacity	10 kilobits/sec	10 MHz
Reception quality	C/N ≥ 10 dB	C/N ≥10 dB TT/N ≥40 dB

5.3.1   VHF Antenna Coverage Improvement

With the antenna discussed in section 5.1, there are times when a DRS will not lie in the antenna pattern. Although the loss of this link will occur less than 25 percent of the time, a nearly 100 percent or total coverage can be achieved by adding a crossed-dipole antenna on the "top" side of the spacecraft, i.e., on the side facing away from the earth. Such an antenna could be mounted near the surface, near one end, so as not to interfere with the DTS antenna coverage. This location, however, will result in some interference of the VHF radiation by the DTS antenna. A preferred location for the additional VHF antenna is on top of the DTS antenna boom near the first elbow. This concept is illustrated in Figure 5-10.

6. ANTENNA CONTROL

This section discusses the method for mechanically pointing the 3-foot square planar array data transmission system (DTS) antenna selected in Section 5. The rationale for design choices is presented in the most logical order of consideration. The number of DTS antennas to be employed must be determined and then the scheme for mechanical gimbaling must be selected. Following these choices, the method of tracking the DRS must be chosen and, finally, the problem of acquisition must be dealt with. Each of these topics is treated in the Phase I report, but here, definite choices are made, and the subjects of tracking and acquisition are discussed in greater detail.

6.1 NUMBER OF ANTENNAS AND MOUNTING CONSIDERATIONS

The number of antennas to be used on the LAS depends on the data transmission requirements. If continuous, uninterrupted communication is required, then two antennas are needed, whereas only one is needed if blackout periods during each orbit are acceptable.

Future LAS missions may require optical or infrared imaging of the entire earth, or relayed data from ground instrument packages may be desired on a global basis. The first and, possibly, the latter mission will require uninterrupted data transmission, if data storage is to be avoided.

On the other hand, for many earth observation missions, the polar regions may be ignored, which would allow time to steer an antenna from one DRS toward another. Some optical imaging missions may require data transmission only on the sunlit side of the earth, which would allow one-half of an orbit to reposition a single antenna.

6.1.1 Continuous Data — Two Antennas

The necessity for two antennas for continuous data is obvious from a consideration of the changeover problem. As the earth interrupts the line of sight (LOS) between an LAS antenna and a DRS, another antenna must be pointed at another DRS ready for changeover. This changeover situation is illustrated in Figure 6-1, where LOS 1 is about to be intercepted by the earth, while LOS 2 will be the transmission path after changeover.
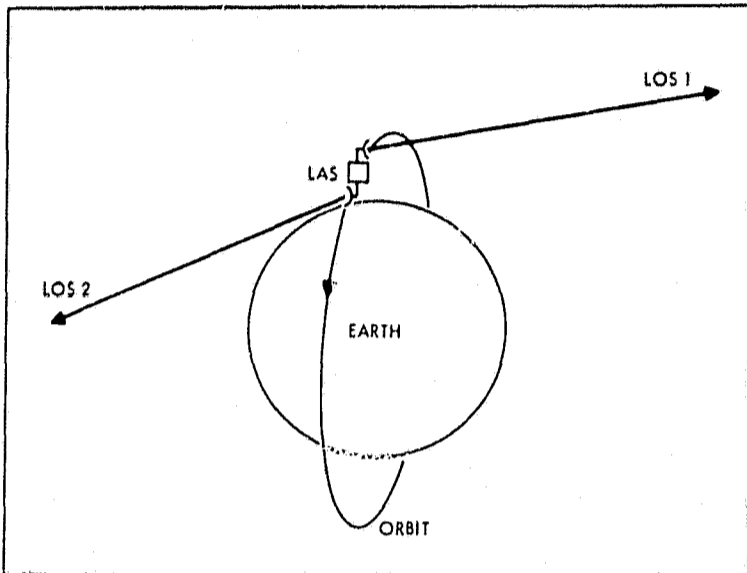
Figure 6-1. Necessity for Changeover LOS 1 about to be intercepted by Earth
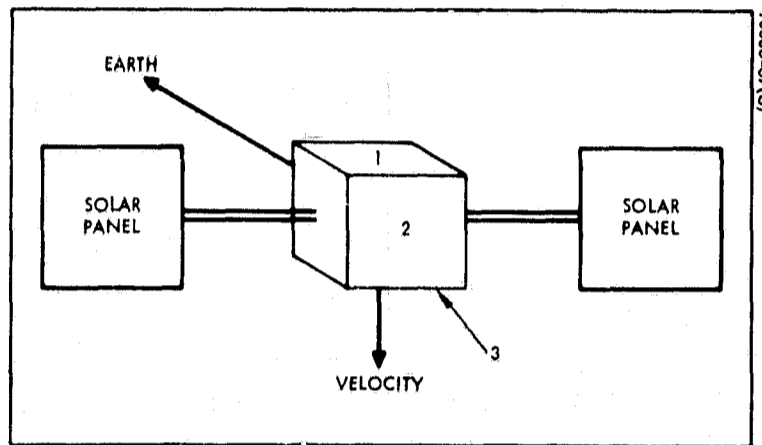
Figure 6-2. Sides of Earth-Oriented Body Available for Antenna Mounting
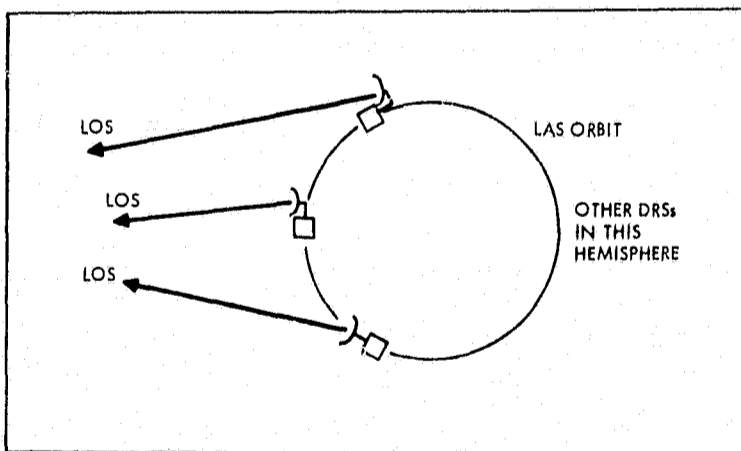
Figure 6-3. Spacecraft Interference Forcing Changeover at Undesirable Orbit Position for Mounting as Shown
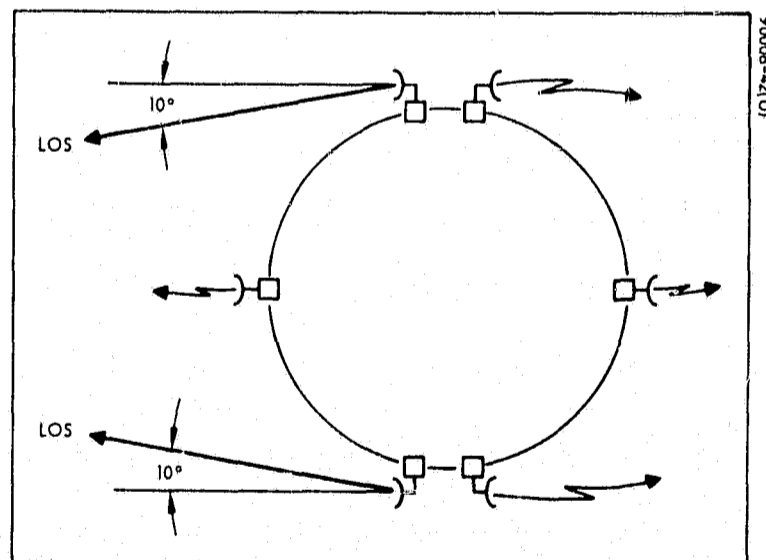
Figure 6-4. Pointing a Single Antenna

6.1.2 Noncontinuous Data — One Antenna

If an LAS mission will allow periods of data interruption, only one DTS antenna is necessary. For many optical imaging missions, the regions near the poles will be of less importance than lower latitude areas. This is due to poorer lighting conditions near the poles, as well as the fact that these regions are relatively uninhabited. Such a mission may only require high data quantity transmission on the sunlit side of the earth. In either case, time is allowed to steer the antenna from one DRS to another to provide communication during the required portions of the orbit.

Two DTS antennas present packaging difficulties which, although not insurmountable, require considerably more complex stowage and deployment schemes than a single antenna. Furthermore, for the primary optical imaging mission of the representative payload, it was felt that interruptions, such as mentioned above, are tolerable. Thus, it was decided to use only one DTS antenna. Because pictures of major interest will occur at the lower latitudes rather than at the poles, it was decided to have the changeover from one DRS to another occur near the poles. Mounting and tracking considerations are based upon this concept.

6.1.3 Antenna Mounting

Figure 6-2 shows the available sides for antenna mounting on a three-axis stabilized spacecraft. If a single antenna were mounted on sides 1 or 3, spacecraft interference would force changeover at an undesirable position; when this interference occurs, there may be no other DRS within view. This problem is illustrated in Figure 6-3.

If there are three DRSs spaced symmetrically, a DRS will always lie in the region which is slightly greater than the half-space defined by a plane parallel to side 2 of Figure 6-2, i.e., a plane perpendicular to the local vertical. This region can be pictured as a near-hemisphere with the bottom "drooping" 10 degrees from the plane described above. If the changeover begins at about 10 orbit degrees of the nearest point to the poles, during data transmission, a DRS will always lie in the hemisphere away from the earth whose "bottom" is parallel to side 2 of Figure 6-2. The conclusion from these geometrical considerations is that the single DTS antenna should be mounted and gimbaled so that it can be pointed anywhere in this hemisphere. In general, the antenna should be mounted on a structure extending away from side 2 of Figure 6-2 along the local vertical. The pointing geometry with implied changeover near the poles is shown in Figure 6-4.

6.2 GIMBALING

Gimbaling refers to the method of providing the required antenna rotational motion. In the Phase I report, this subject is treated in considerable detail. The fundamental choice is between two or three axes of rotation, i.e., between two gimbal axes or three gimbal axes. For the sun-synchronous orbit of this spacecraft, which requires an inclination of

97.5 degrees (see Section 4), the conclusion of the Phase I study was that a three-gimbal system be used. A brief summary of the reasoning behind this conclusion is presented below, followed by the description and attributes of the particular gimbaling scheme selected for the LAS.

6.2.1 Two-Gimbal Axes

Theoretically, an antenna can be pointed in any direction if it has two connected axes of rotation — one fixed to the spacecraft (the primary) and the other fixed to the antenna (the secondary). One heuristic argument supporting this statement is based on the fact that rotational motion about the axis defined by the LOS is unnecessary and/or unimportant; hence, only two other degrees of rotational motion are required. Practical considerations of structural design and mounting methods limit the antenna motion to less than the ideal. However, this limitation occurs for any antenna steering system. The major problem with a two-gimbal system is that the angular rate about the primary axis can be very large. To see how and why this occurs, consider the following heuristic discussion.

Denote the primary axis of an orthogonal two-gimbal system by g_1 and the secondary axis by g_2. Orthogonal means that g_1 is perpendicular to g_2. Let the antenna boresight axis be perpendicular to g_2. Such a configuration is shown in Figure 6-5. Since the boresight must coincide with the LOS to the target, g_2 lies in the plane normal to the LOS, but also must lie in the plane normal to g_1 because of the orthogonal design. Thus, the rotation of g_2 about g_1 must be such as to make g_2 coincide with the intersection of these two planes. But in addition to this positioning requirement about g_1, the relative angular rate of the LOS with respect to the body to which g_1 is fixed must be compensated.

It was mentioned previously that rotational motion about the LOS is unimportant. Thus, the angular rate $\dot{g}_1$ and $\dot{g}_2$ must compensate for the LOS angular rate, Ω. As just explained, g_2 is defined by g_1 and the LOS. And consistent with the above argument, $\dot{g}_1$ and $\dot{g}_2$ are defined by the projection of the Ω vector along the LOS onto the g_1 - g_2 plane. This geometric interpretation is illustrated in Figure 6-6. The gimbaling problem occurs when the LOS and g_1 coincide or nearly coincide. Figure 6-7 indicates geometrically why $\dot{g}_1$ becomes very large; namely, the projection of the LOS angular rate, Ω, along the LOS onto the g_1 - g_2 plane results in a large value of $\dot{g}_1$. Theoretically, when the LOS and g_1 coincide, $\dot{g}_1$ must be infinite in order to point the antenna at the target.

For the purposes of analysis, the gimbal rate is deemed undesirably large if it exceeds twice the maximum angular rate of the LOS which occurs when the DRS lies in the LAS orbit plane and the LAS is at the equator nearest the DRS, i.e., when both satellites lie on the line of nodes and are closest to each other. For a 300-n.mi. orbit, this maximum angular rate is 4.52 deg/min. The orbital angular rate is 3.77 deg/min. Consider now the two geometrical cases discussed below.

Case 1 - Primary Axis Coincides with the Local Vertical

From the analysis of the Phase I report, the primary gimbal rate becomes undesirably large if the angle between the LOS and the primary axis is less than 30 degrees. If, when the LAS crosses the equator, a DRS is within 30 degrees of the line of nodes, the gimbal rate will become excessive. This will occur about 60/180 = 33 percent of the time, i.e., 33 percent of the LAS orbits will require an excessive gimbal rate. A cone with a 30-degree half-angle centered about the line of nodes intersects 13.4 percent of the area of a unit hemisphere. Thus, the gimbal rate will be excessive about 13.4 percent of the total transmission time.

Case 2 - Primary Axis Normal to Orbit Plane

Again, following the analysis of the Phase I report, an excessive gimbal rate will occur if the primary axis and LOS are separated by less than 4 degrees. For this to occur, the DRS must lie more than 75 degrees from the line of nodes. Further, if the inclination of the orbit is less than about 76 degrees or greater than 104 degrees, the gimbal rate will not become excessive because the orbit normal and LOS will always be separated by more than 4 degrees. For the 293-n.mi., sun-synchronous orbit chosen in Section 4, the inclination is 97.5 degrees, and so excessive gimbal rates can occur.

If there are three DRSs spaced symmetrically about the earth, the gimbal rate problem can be avoided by transmitting to another DRS if tracking one would cause large gimbal rates. For this case, a DRS must lie near the orbit normal extending from the LAS. But, under these circumstances, two other DRSs will lie in such a position as to allow communication and yet not cause the occurrence of large gimbal rates.

If there are two DRSs, the gimbal rate problem may be avoided under certain DRSS geometrical configurations, but may not for others. If there is only one DRS, excessive gimbal rates cannot be avoided without terminating communication. Further, there may be other reasons, such as continuity of communication, for desiring to transmit to a DRS near the orbit normal.

Considering now the case of a single DRS in order to develop some numerical estimate of the problem, the particular inclination calculated in Section 4 will be used. Referring to Figure 6-8, a rather cursory analysis indicates that a worst case situation might arise during one quarter of an LAS orbit, where for 68.4 orbital degrees the LOS and primary gimbal axis may lie within 4 degrees of each other. This represents about 19 percent of an orbit. But, only about 15 percent of LAS orbits have this potential problem. Thus, excessive gimbal rates will occur less than 2.8 percent of the total communication time.

Comments

It can be seen from the above discussion that a two-gimbal, antenna steering system with the primary axis normal to the orbit plane can provide
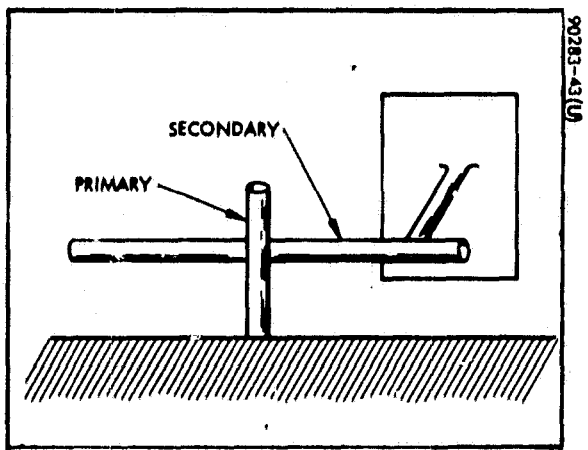
Figure 6-5. Two-Gimbal System
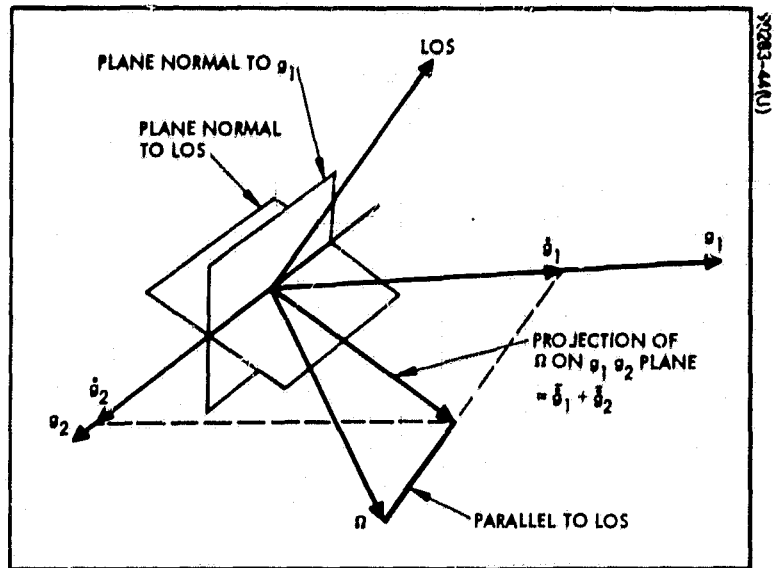
Figure 6-6. Geometric Determination
of Gimbal Rates
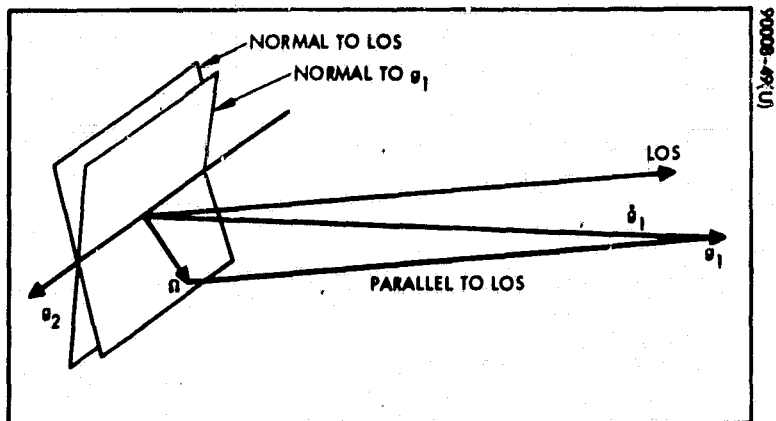
Figure 6-7. Primary Gimbal Axis Rate
Increase When LOS and Primary
Axis are in Close Proximity
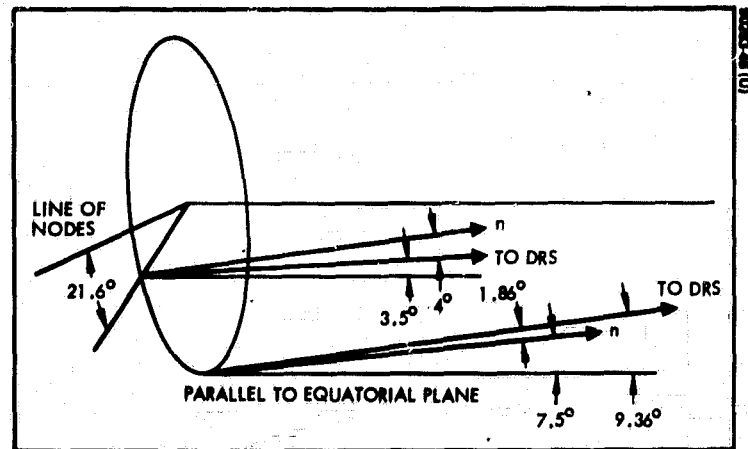
Figure 6-8. Geometry for Gimbal Rate
Problem With Primary Axis
Parallel to Orbit Normal

the required rotational motion, and that the gimbal rate problem can be avoided with certain DRSS configurations. However, with other DRS configurations or under some special communication requirements, the gimbal rate problem cannot be avoided. Further, as can be seen from the analysis of subsection 4.4.3 of the Phase I report, the relationship between the gimbal angles and the LAS and DRS orbital parameters is not simple. Thus, the changeover and acquisition is not as simple and easily conceived as is possible with the three-gimbal system to be described shortly. Since changeover will usually occur once or twice an orbit, this is an important consideration. Further, the complexity of computation in the control system is greater for a two-gimbal system than for the three-gimbal system described below. Thus, attention is now turned to capabilities of a three-gimbal system.

6.2.2 Three-Gimbal Axes

Providing an additional gimbal axis allows another degree of rotational freedom and eliminates the gimbal rate problem. In this case, the third axis keeps the "primary" axis always pointed away from the LOS, thereby precluding the gimbal rate problem.

Consider now the conceptual simplicity of the three-gimbal system represented in Figure 6-9. Gimbal axis 1 is the "outer" gimbal axis, i.e., is fixed rigidly to the spacecraft body and is parallel to the orbit normal. The second gimbal axis is mounted to the first with an angle between the two axes equal to the orbital inclination angle. The third, or innermost axis is mounted orthogonal to the second.

This configuration allows operation in the following manner: The gimbal drive about the first axis maintains a constant speed equal to the orbital angular velocity keeping the second gimbal axis always parallel to the earth's polar axis. Then, this second gimbal axis provides "azimuthal" motion and compensates for the motion of the DRS. The third gimbal axis provides "elevation" motion and compensates for angular movement of the LOS due to the translational motion of the LAS in its orbit. The motion about the third axis is relatively small — about ±9.4 degrees during one LAS orbit.

Since the second gimbal axis tracks the DRSs in the equatorial plane, 360-degree rotation is desirable. Since the first axis compensates for the rotation resulting from the LAS earth pointing requirement and is driven at constant speed, 360 degree rotation about this axis, is also desirable.

6.2.3 Gimbal System Selection

A three-gimbal system introduces additional mechanical and RF feed problems, which tend to offset its advantages. Table 6-1 lists the advantages and disadvantages of a three-gimbal system, as compared to a two-gimbal system. A quantitative comparison of each of these systems, with respect to cost, weight, reliability, and functional effectiveness, was not
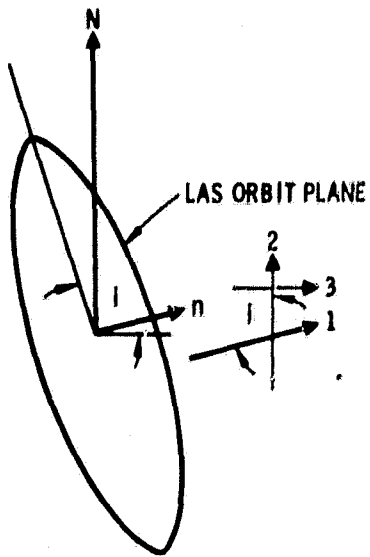
Figure 6-9.   Three-Gimbal
System
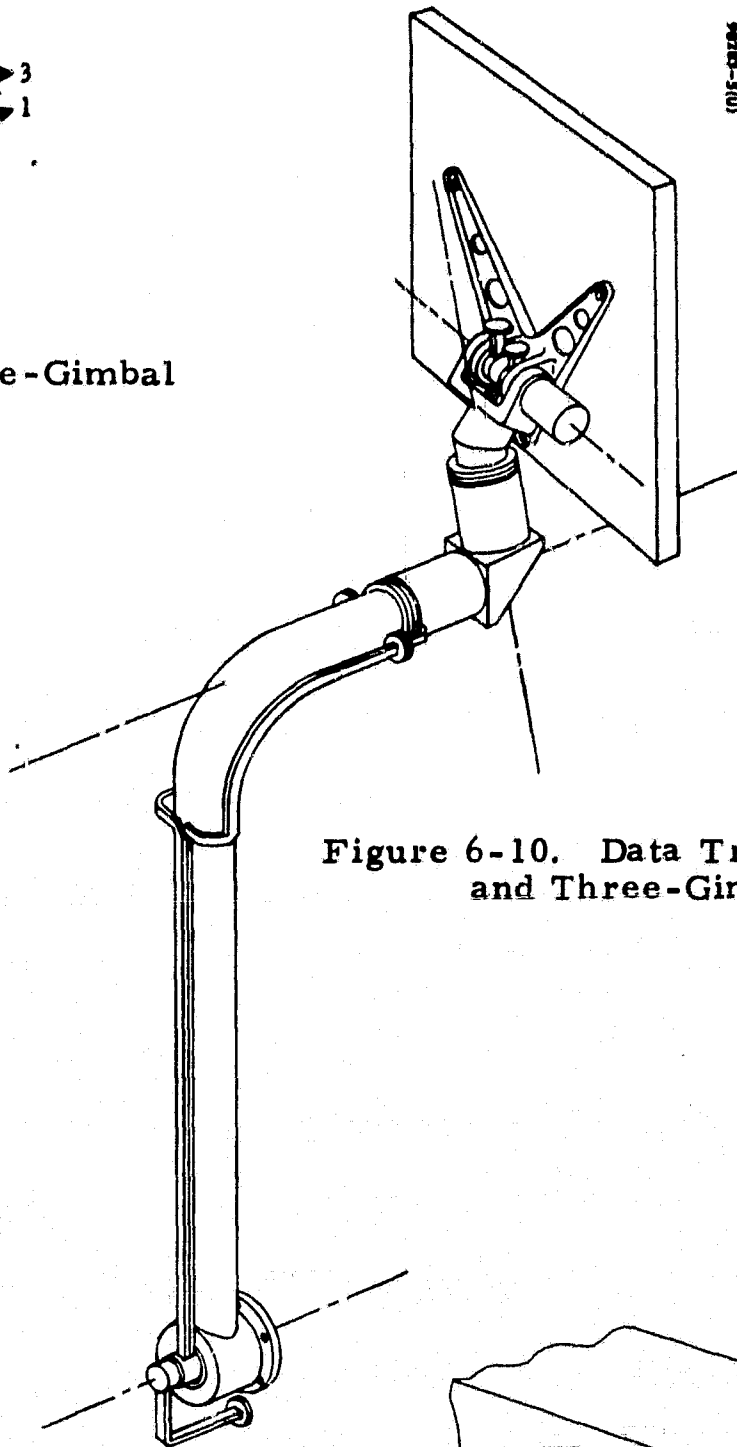
Figure 6-10.   Data Transmission Antenna
and Three-Gimbal System
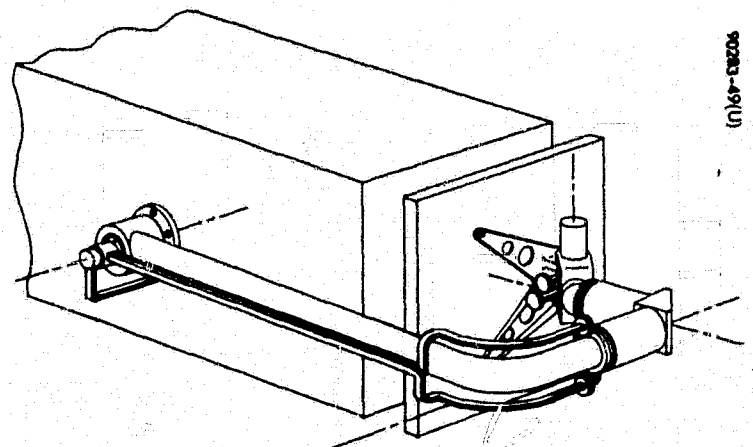
Figure 6-11.   DTS Antenna
in Stowed Position

TABLE 6-1. THREE-GIMBAL SYSTEM COMPARED WITH
TWO-GIMBAL SYSTEM

Advantages	Disadvantages
Gimbal rate problem eliminated	Additional mechanical complexity.
Simpler steering system computations	Additional RF feed problems.
Simpler changeover and acquisition	
Motions more easily understood	

possible with the limited effort devoted to this portion of study. But, a very limited comparison led to a decision that the advantages of the three-gimbal system outweighed its disadvantages; thus, a three-gimbal system was selected.

After this selection was made, a conceptual design effort was initiated to provide a workable concept consistent with packaging constraints and the desire that gimbal axes 1 and 2 be capable of 360-degree rotation. The result is shown in Figure 6-10. Figure 6-11 shows the antenna in its stowed position. Figure 6-12 is a more detailed drawing of a portion of the three-gimbal mechanical design and the internal RF feed associated with it.

6.3 ANTENNA STEERING

During data transmission there are two fundamental methods of steering the antenna so that its boresight axis coincides with the LOS to the DRS: open loop and automatic feedback control. The first can be accomplished either by relayed, continuous ground command, or by updated, on-board, programmed control. The automatic steering technique most amendable to the use of a planar array antenna is called monopulse.

6.3.1 Open Loop Control

The 3-dB beamwidth of the LAS antenna is about 1.6 degrees, and with currently available techniques, there is no great difficulty in mechanically pointing the antenna with this accuracy. However, open loop control cannot compensate for structural distortions due to thermal gradients. And, since the LAS attitude control system maintains the spacecraft to within 0.5 degree, attitude information on the ground would probably be required for steering the antenna. These reasons alone are sufficient for choosing

RF COAX

SLIP RING ASSY

POSITION PICKOFF

DRIVE ASSY

HOUSING

BEARING

MOUNTING FLANGE-
SHAFT ASSY

RF ROTARY JOINT
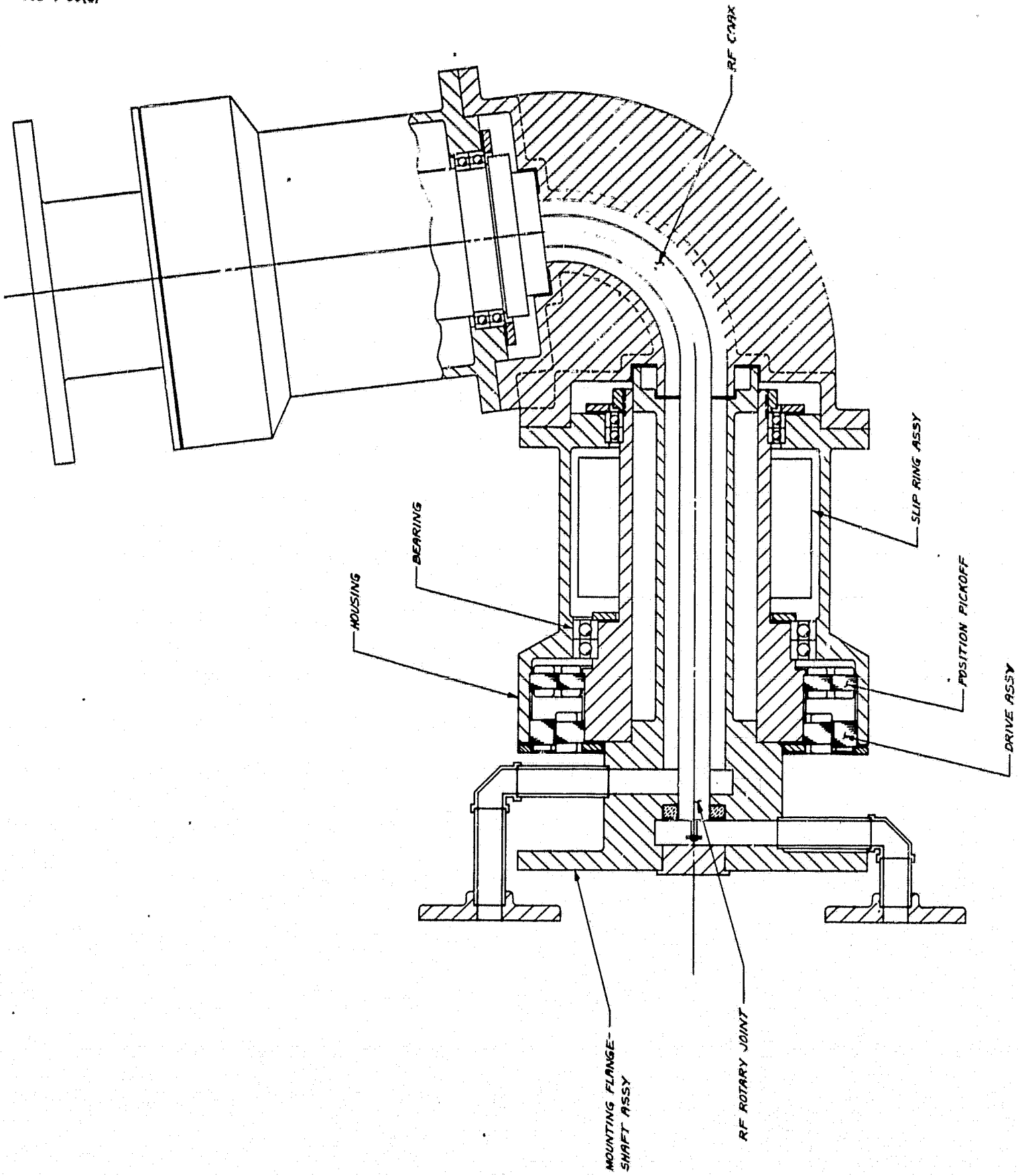
Figure 6-12. Concept for Two 360-Degree Gimbal Axes

monopulse tracking for automatic antenna steering, but, in addition, it was felt that future bandwidth and carrier frequency requirements may require higher antenna gains, with automatic tracking the only feasible choice.

6.3.2 Monopulse Tracking

When an incoming electromagnetic wave from a far-field radiation source is received on two different antenna patterns simultaneously, the absolute amplitudes and phases of the received signals may vary with the changing characteristics of the source or propagation medium, but their relative values are functions only of the angle of arrival. In its simplest form, the concept of monopulse involves a comparison of a single pair of signals, which is sufficient to determine the angle of arrival in a single plane. However, as discussed previously, for complete tracking, rotational motion and, hence, angle of arrival, information is required in two planes which are usually orthogonal. Thus, a monopulse system for use on the LAS will require comparisons of two pairs of signals. The signal processing is simplified if the gimbal axes controlled by the monopulse system are directly geometrically related to the antenna radiation patterns.

The square planar array chosen lends itself easily to monopulse tracking. The antenna is divided into four quadrants which, for the mono-pulse concept, can be thought of as four separate antennas. The received inputs are combined in RF circuits attached to the antenna to produce three signals. Two of these correspond to the pointing errors in azimuth and elevation and the third is the sum of the outputs from all four of the quad-rants. This monopulse signal generation is illustrated in Figure 6-13. The two difference signals are used in a control system to drive the second and third gimbal motors so as to make the antenna boresight axis and the LOS coincide.

The generation of the monopulse signals and the antenna control system techniques are well-established technology. The major problem with monopulse tracking is to get the monopulse signals to the receiver and signal processor. The two extreme methods are: 1) place the receiver and signal processor on the antenna structure and feed the resulting signals to the spacecraft through slip rings, or 2) send all three RF signals through rotary joints associated with the three gimbals. The latter method is very difficult because two of the gimbals have 360 degrees of rotation which require concentric, lossy feeds. Method 1 presents thermal control problems for the signal processing equipment, requires a large number of slip ring con-nections for each 360-degree rotary joint, and makes the structural and mechanical design more difficult. Also, with this method, one RF channel is needed between the antenna and the transmitter.

There are other alternatives which require either one or two RF feeds through the three-gimbal system. One possibility is to phase shift one of the difference signals and then combine them in a modulation process into one signal. This double difference channel is then combined with the sum channel to yield a single RF channel for transmission through the gimbal system. This concept is illustrated schematically in Figure 6-14.

MONOPULSE SIGNAL GENERATION
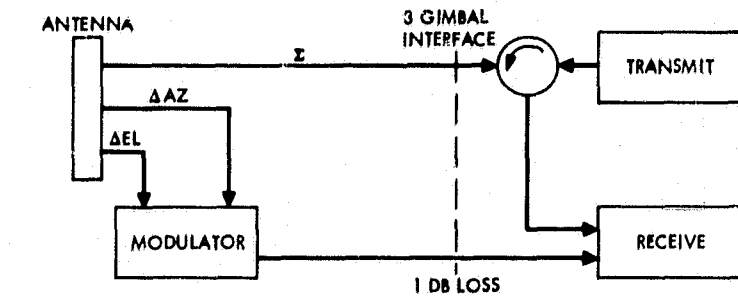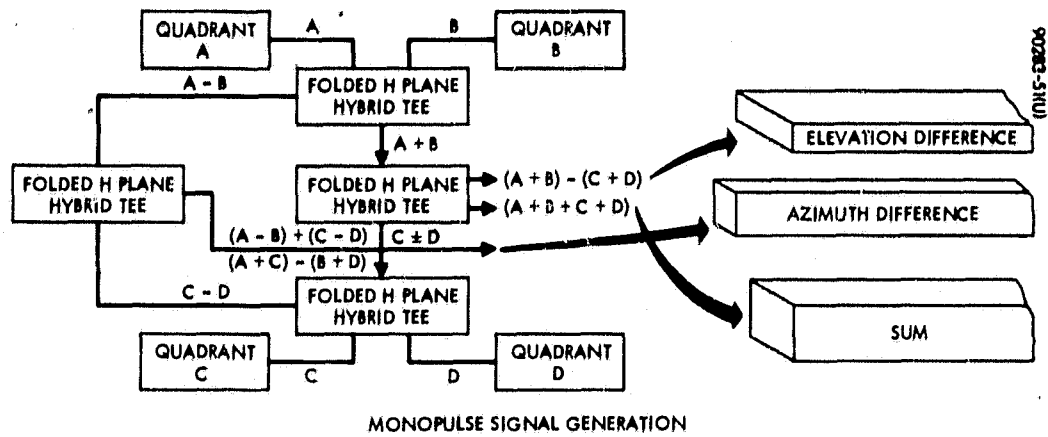
Figure 6-13.   Monopulse Signal Generation
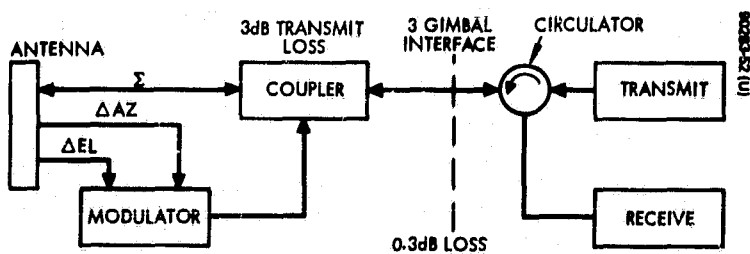
Figure 6-14.   Single RF Feed
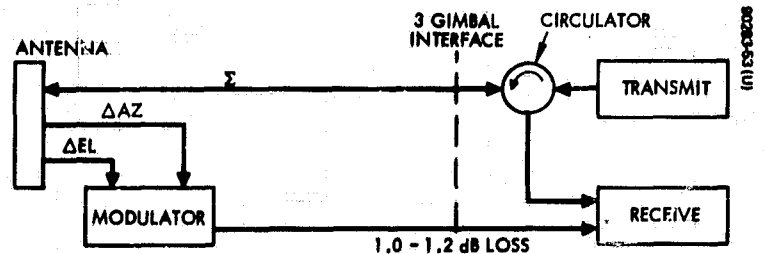
Figure 6-15.   Double RF Feed
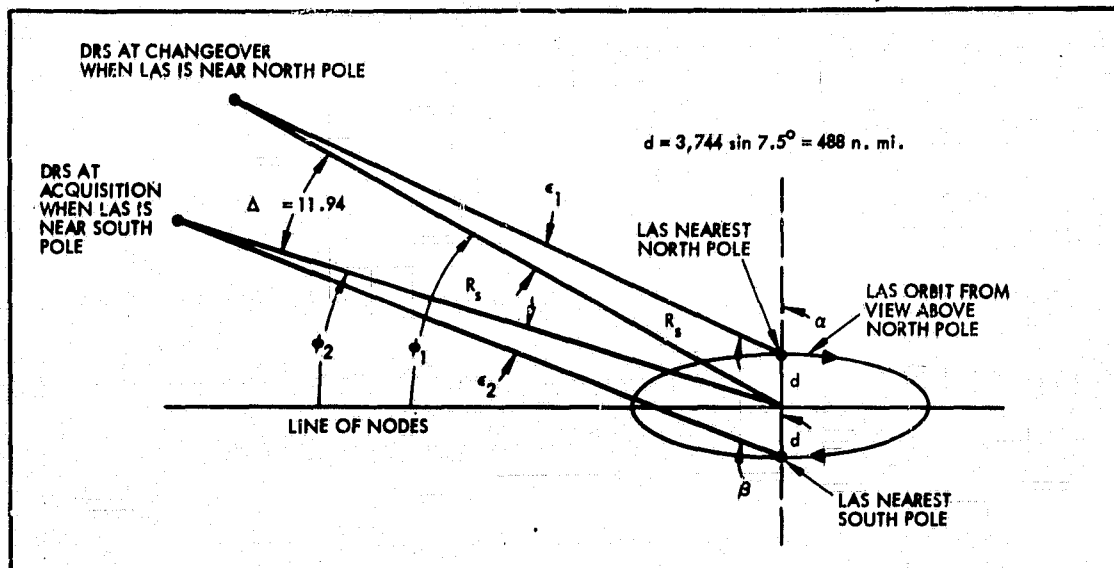
Figure 6-16.   Changeover Geometry, Looking Down on Equatorial Plane

Such a system has a serious drawback in that the coupler results in a 3-dB power loss of the transmitted signal. This concept has been used with three-gimbal antennas on aircraft, but considerably more transmitter power was available. This 3-dB loss would require a doubling of transmitted and load power to establish the link as stated in Section 5. This additional load power, approximately 50 watts, would place the total required power very near the capability of the power system, leaving very little for contingencies.

Another concept utilizes the modulation technique described above, but does not employ the coupler. Thus, two RF channels must be fed through the gimbal system. The rotary joints necessary for a two-channel feed have more loss than the single-feed joints, but the 3-dB transmit power loss is avoided. This scheme is illustrated in Figure 6-15. This method has 1.0 to 1.2 dB loss in the receive direction compared to 0.3 dB loss for the single-feed system, but the loss in the transmit direction is only 1.0 to 1.2 dB compared to 3.3 dB for the single-feed system. Since data transmission is the primary function of the communication system, the two-feed system was selected because the loss is smaller.

This choice is based on a rather limited analysis and has in no way been shown to be optimal. Further investigation of this problem is recommended. A more comprehensive study must consider feed power losses, cost of the gimbal and feed system, mechanical complexity, thermal control requirements for processing on the antenna, slip ring problems, and tracking accuracy. The choice made here was an attempt to arrive at a feasible and reasonable specific concept. But, it must be emphasized that further study is required to confirm this choice or to arrive at a more optimal one.

6.4 CHANGEOVER AND ACQUISITION

Changeover refers to the process of discontinuing data transmission to one DRS and repositioning the antenna in order to transmit to another. Acquisition follows this procedure and involves the re-establishment of the communication link and the automatic tracking system operation.

6.4.1 Changeover

If a DRS lies nearly 90 degrees from the LAS line of nodes, it is possible to transmit to this DRS for an entire orbit without interruption. However, this situation will occur infrequently, and for most LAS orbits, changeover will be required once per orbit if data transmission is desired on only one side of the earth and twice if transmission on both sides of the earth is desired. The LAS concept presented in this report does not have the power capability for data transmission on the dark side of the earth. During eclipse, the camera, radar scatterometer, and data transmission system must be turned off. Hence, DTS antenna tracking is required only on the sunlit side of the earth. For this case, the geometry of changeover with the three-gimbal system is particularly simple. This geometry is shown in Figure 6-16.

During one LAS orbit of 95.5 minutes duration, a DRS moves 23.9 degrees in the equatorial plane about the earth. During one-half of an orbit, the DRS angular movement is 11.94 degrees. The required LOS motion during changeover about the second gimbal axis, which is parallel to the polar axis, can be determined by referring to Figure 6-16. The required slewing angle, Δg_2, is given by $\beta - \alpha$, where

$$\alpha = 90 - \phi_1 + \epsilon_1$$

$$\beta = 90 - \phi_2 - \epsilon_2$$

$$\epsilon_1 \approx \frac{d}{R_s} \cos \phi_1$$

$$\epsilon_2 \approx \frac{d}{R_s} \cos \phi_2 = \frac{d}{R_s} \cos (\phi_1 - \Delta\phi)$$

Then

$$\Delta g_2 = \beta - \alpha = \phi_1 - \phi_2 - (\epsilon_1 + \epsilon_2) = \Delta\phi - \frac{d}{R_s} \left[\cos(\phi_1 - \Delta\phi) + \cos \phi_1 \right]$$

$$= \Delta\phi - \frac{d}{R_s} \left[\cos \phi_1 (1 + \cos \Delta\phi) + \sin \phi_1 \sin \Delta\phi \right]$$

$$\approx 11.94 - 2.42 \cos \phi_1 \text{ degrees}$$

The change in the third gimbal angle is due to the translational orbit motion over one-half of an orbit and requires a rotation of 9.3 degrees.

During each orbit as the LAS reaches the point nearest the north pole, the second-gimbal axis is rotated Δg_2 and the third gimbal axis is rotated 9.3 degrees, while the first axis continues its constant speed rotation at orbital angular velocity. This orients the antenna so that it is nominally pointing at the DRS when the LAS reaches the point of its orbit nearest the south pole. If there are three data relay satellites spaced 120 degrees apart, then approximately every ten orbits, the second gimbal axis must be rotated in the opposite direction by 120 - Δg_2 degrees to begin transmission to a different DRS. Since these changeover motions are simple and there are only three basic maneuvers, it is an easy matter to make the changeover procedure completely automatic.

6.4.2 Acquisition

With the antenna repositioned to point toward a DRS as the LAS reaches the southernmost point of its orbit, approaching the sunlit side of the earth, the tracking system must be reactivated and lock-on must be achieved. This can be accomplished by lowering the gain of the antenna

beam and thereby increasing its beamwidth. With the planar array, this is most easily done by dividing each of the four quadrants into four subquadrants as shown in Figure 6-17. During acquisition, only the portions of the antenna designated in Figure 6-17 as A_1, B_1, C_1 and D_1 are used for monopulse signal generation. The gain of this reduced antenna is approximately one-fourth of the entire antenna, which implies a gain of 35 dB and a 3-dB beamwidth of about 3 degrees, which is sufficient to achieve acquisition. Once lock-on has been accomplished with the reduced antenna, the other antenna modules are activated and the data link is re-established. A functional block diagram of the acquisition/antenna control system is shown in Figure 6-18.

It should be emphasized that the simplicity of the changeover antenna motions and the periodicity of changeover and acquisition will allow the entire procedure to be accomplished automatically, with no ground control required, except initialization after orbit injection and possible corrections to the procedure three or four times a year. It is this automatic changeover concept that is recommended.
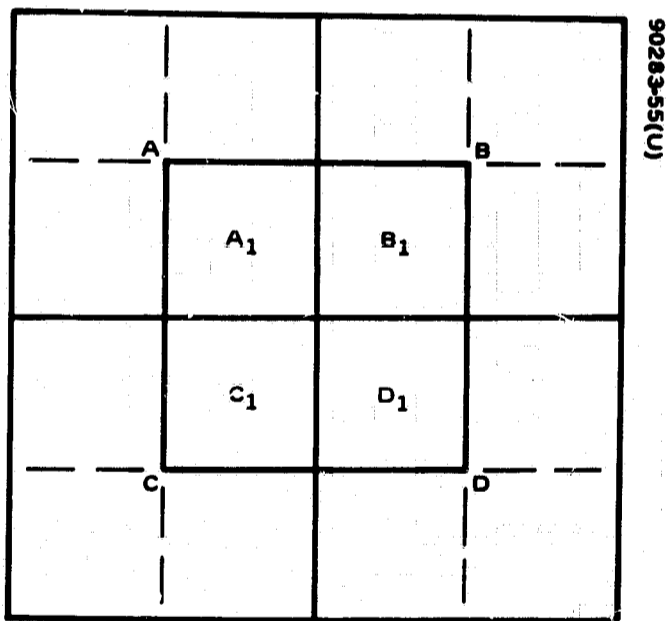
Figure 6-17. Antenna With 16 Modules
For Wide and Narrow Beams
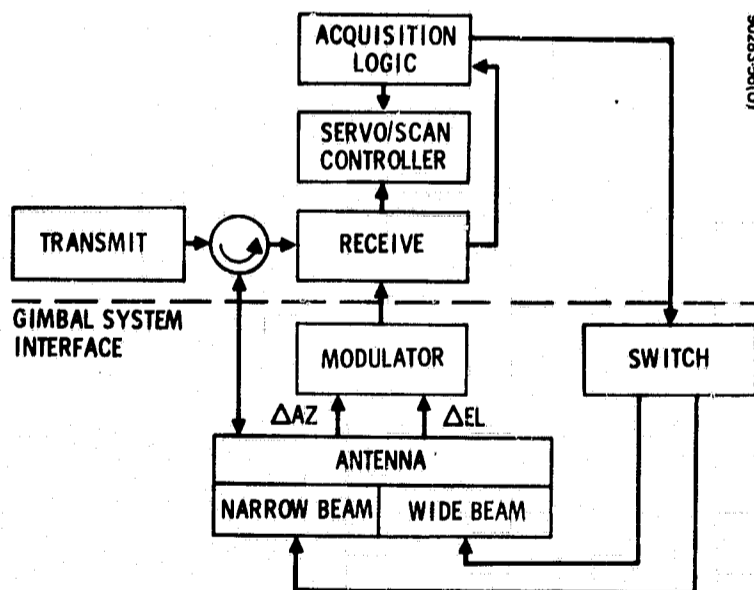
Figure 6-18. Acquisition/Antenna
Control System

6.5 SUMMARY

The following is a list of the basic concepts chosen here for antenna control:

1) One DTS antenna with coverage of hemisphere away from earth

2) Three gimbal axes

    a) First   - constant speed about the orbit normal

    b) Second   - maintained parallel to the earth's polar axis; provides azimuth motion

    c) Third   - provides elevation motion

3) Two RF feeds through the gimbal system with a combination of the difference signals required on the rear of the antenna

4) Automatic changeover and acquisition

5) Acquisition by antenna gain reduction

7. ATTITUDE AND VELOCITY CONTROL

The primary objective of the attitude control system is to provide a stable platform for earth oriented sensors. Sensor earth pointing accuracy and rate limitation requirements significantly influence the design of the attitude control system. Additionally, a velocity control (ΔV) capability is provided to reduce injection errors and to periodically control orbital parameters to ensure total earth coverage.

The design presented here minimizes on-board equipment complexity by placing the emphasis for control activation and execution on infrequent ground commands. A design lifetime exceeding 1 year was the objective.

7.1 SYSTEM DESCRIPTION, OPERATION, AND REQUIREMENTS

7.1.1 System Description

The system selected to control and stabilize the spacecraft employs a dual spin configuration; a high speed, rigid momentum wheel and an earth oriented, or despun, platform for the mission sensors. A large, angular momentum is generated by the wheel to provide sufficient gyroscopic stability so that spacecraft motion is reasonably insensitive to cyclical precession torques. Magnetic torquing is utilized to trim secular disturbance torques as well as the effects of ΔV thruster firings. The configuration of the spacecraft is illustrated in Figure 7-1, which also defines the coordinate axes of the body and shows the arrangement of system elements, including earth horizon scanner geometry. Mission sensors are aligned relative to the yaw (z_b) which is nominally earth pointed along the local geocentric vertical. Attitude errors (pitch and roll/yaw) are established by a horizon scanner that utilizes the momentum wheel to generate a conical scan pattern. The wheel spins about an axis that is parallel to the satellite's pitch (y_b) axis, nominally oriented normal to the orbit plane.

Attitude control of the satellite is effected by wheel speed control and by the interaction of current carrying coils, fixed to the body, and the earth's magnetic field. Multiturn coils are arranged so that their planes are normal to the pitch axis for precession control or parallel to the pitch axis for control of the angular momentum. These coils are attached to the inner structure of the spacecraft. A coil, designated as the orientation

PITCH (Y$_b$)
"NORMAL TO ORBIT PLANE"

SCAN CONE

30°

SOLAR ARRAY (2)

30°

MIRROR

HOLLOW SHAFT

BOLOMETER (2)

NUTATION DAMPER

YAW (Z$_b$) "TO EARTH"

MULTISPECTRAL CAMERA

ΔV THRUSTORS (4)

SPIN COIL

ROLL (-X$_b$)

BIAS COIL

ORIENTATION COIL

a) SPACECRAFT CONFIGURATION
(ANTENNA NOT SHOWN)

ORBIT PLANE

EARTH SCAN CHORDS

b) EARTH DISC AND SCAN PATTERN

90283-57 (U)
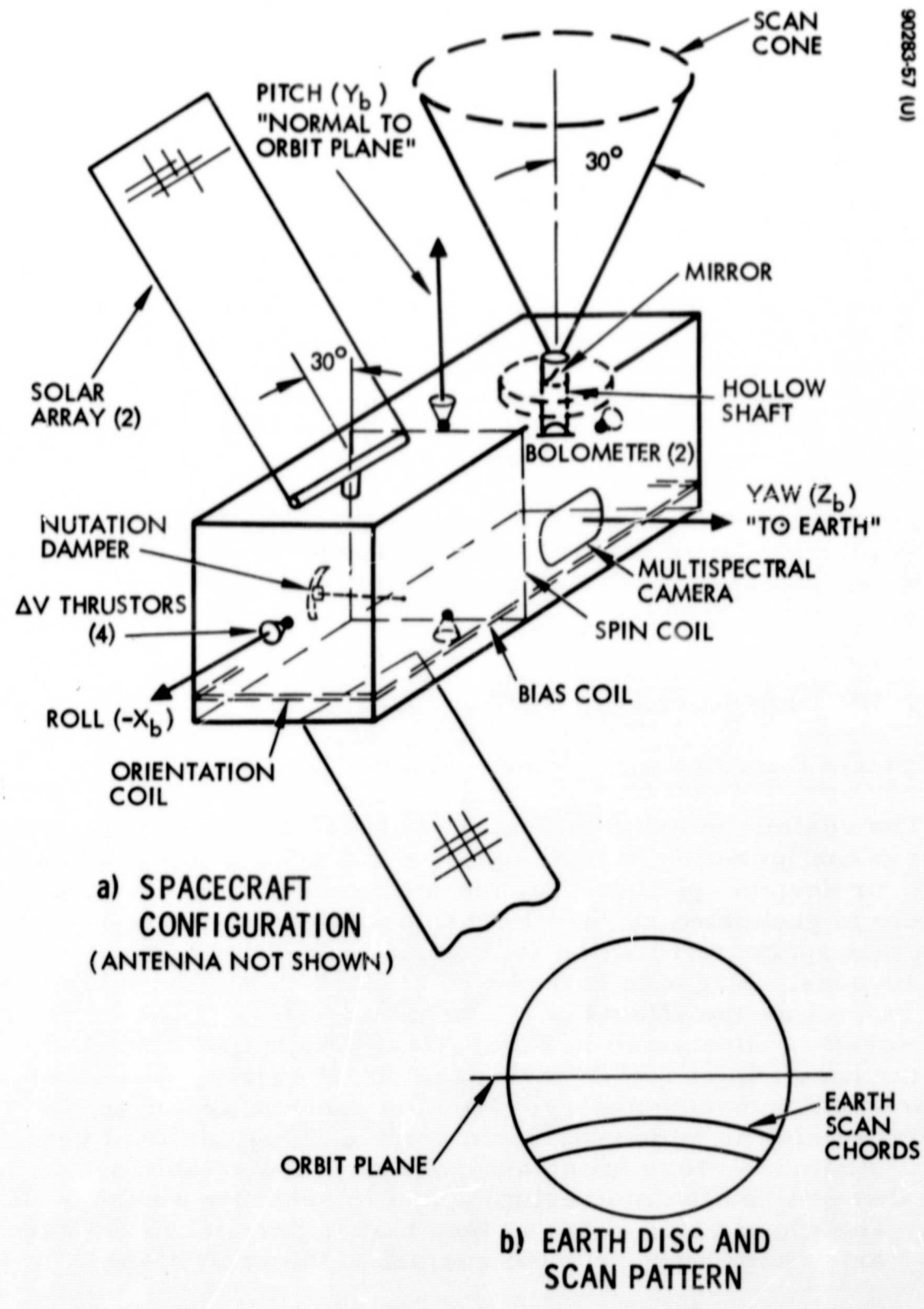
Figure 7-1. Spacecraft Configuration With Control Elements

coil, is utilized to precess the angular momentum vector for large reorientation maneuvers, as well as to provide for precession at regular prescribed intervals to achieve earth pointing. Additionally, the orientation coil is used to trim disturbance torques during ΔV maneuvering. A bias coil, arranged parallel to the orientation coil, provides for continuous precession of the momentum vector and compensates for the transverse components of solar disturbance torque. The spin control coil is cycled to compensate for pitch disturbances and thereby maintain the angular momentum of the wheel within prescribed limits. Pitch control is achieved by a wheel controller that very accurately controls pitch attitude.

A pair of opposed ΔV thrusters are aligned parallel to both the pitch and roll axes such that their thrust vectors nominally pass through the satellite's center of gravity. These thrusters are used to correct injection errors and to provide orbit control capability.

An eddy current nutation damper, which is free to oscillate about an axis of rotation parallel to the velocity vector, reduces transverse attitude rates following orbital injection and damps motion of the satellite's spin axis caused by disturbance and control impulses.

7.1.2 Modes of Operation

The operation of the LAS attitude and velocity control system may be divided into a number of modes or sequences, all of which are initiated by ground command. These modes are defined below.

Separation and Spinup

Prior to separation, the second stage will execute a roll maneuver to orient the satellite's pitch axis normal to the orbit plane.* With the pitch axis oriented close to the orbit normal, the Delta stage can then impart an initial pitch rate. As the momentum wheel is spun up, it will reduce this initial spin rate to near orbital rate. The wheel controller is operating in its rate mode. To attenuate wobbling motion of the spin axis, due to initial transverse rates, the nutation damper is uncaged at the initiation of spinup. At the conclusion of this mode, the satellite will be rotating about its pitch axis at a near orbital rate.

Initial Reorientation

Orientation of the satellite's spin axis relative to an earth referenced coordinate frame is determined by processing horizon scanner pitch and pointing error signals. The wheel controller utilizes scanner derived pitch attitude error to close its position loop and reduce pitch error by necessary changes in wheel speed. With the satellite's yaw axis in a plane which includes the local vertical and orbit normal, horizon scanner outputs representing pointing error are sensed over a quarter orbit interval to determine

---

*When mounted on the booster, the satellite's roll (x_b) axis coincides with the longitudinal axis of the booster.

two orthogonal components of pointing error in inertial space. Corresponding-
ly, magnetic torquing is used to null these two components by proper
cycling of coil current. Following earth lock, the solar arrays are unreeled
to their deployed configuration and continually track the sun.

Normal Attitude Control

Normal mode is characterized by continual wheel controller opera-
tion to maintain earth lock about the pitch axis. Roll/yaw attitude correc-
tions are performed about once per week by appropriate cycling of the
orientation coil. Magnetic control to precess the satellite's momentum
vector approximately 1 degree/day and compensate for secular disturbances,
are provided for by sending appropriate signals to the bias coil. All control
functions, except for control of pitch attitude, are performed upon receipt
of ground commands.

ΔV Mode

ΔV maneuvers are effected by commanding a series of thruster
firing pulses to the appropriate thruster. The orientation coil receives
cyclical commands to trim disturbances.

7.1.3 System Requirements

To guide the design of the attitude and velocity control system and
ensure that mission requirements are satisfied, a set of preliminary
specifications was established. Table 7-1 lists important performance
parameters along with maximum allowable errors.

TABLE 7-1. SUMMARY OF ATTITUDE AND VELOCITY
CONTROL SYSTEM PARAMETERS

Item	Requirement
Attitude control	
Pointing accuracy	$\leq \pm 0.5$ degree (3σ) about all three earth referenced coordinate axes
Pointing stability	$\leq \pm 0.03$ deg/sec (3σ) about body pitch and roll axes
Precess satellite momentum vector	≈ 1 deg/day about line of nodes (continually)
Period between altitude corrections (normal mode)	≥ 1 week
System lifetime	> 1 year
Velocity control	
Correct injection errors	$\Delta V \leq 200$ fps (3σ)
Control orbital period error	$\leq \pm 1$ second

7.1.4 Pointing Accuracy Budget

To demonstrate that pointing accuracy requirements can be satisfied, a reasonable allocation of error contributions was made. Table 7-2 summarizes the pitch error budget representing error along the orbital track. Cross track or roll/yaw attitude error components are listed in Table 7-3.

TABLE 7-2. PITCH ATTITUDE, OR ALONG ORBITAL TRACK, ERROR BUDGET

Source	Random (3σ), degree	Static (3σ), degree	Remarks
Earth sensor errors	±0.02	±0.20	Filtering provided by wheel controller electronics
Wheel control loop errors	±0.02	±0.10	Loop noise and steady-state error
Earth sensor alignments		±0.05	
Tach pulse accuracy		±0.05	
RSS total	±0.03	±0.23	
RSS total, random and static (3σ)	±0.23		

TABLE 7-3. ROLL/YAW ATTITUDE (CROSS TRACK) ERROR BUDGET*

Source	Error (3σ), degree	Comments
Attitude determination error	±0.20	Derived from ground smoothing of earth sensor outputs
Earth sensor alignment	±0.05	
Cyclical disturbance torque	±0.20	Established by pitch momentum and disturbance torque environment
Wheel unbalance	±0.05	
Residual nutation error	±0.02	
RSS total	±0.29	
Allowable error due to uncompensated disturbance	±0.10	
Total cross track error (3σ)	±0.39	

*Payload sensor alignment errors are not included.
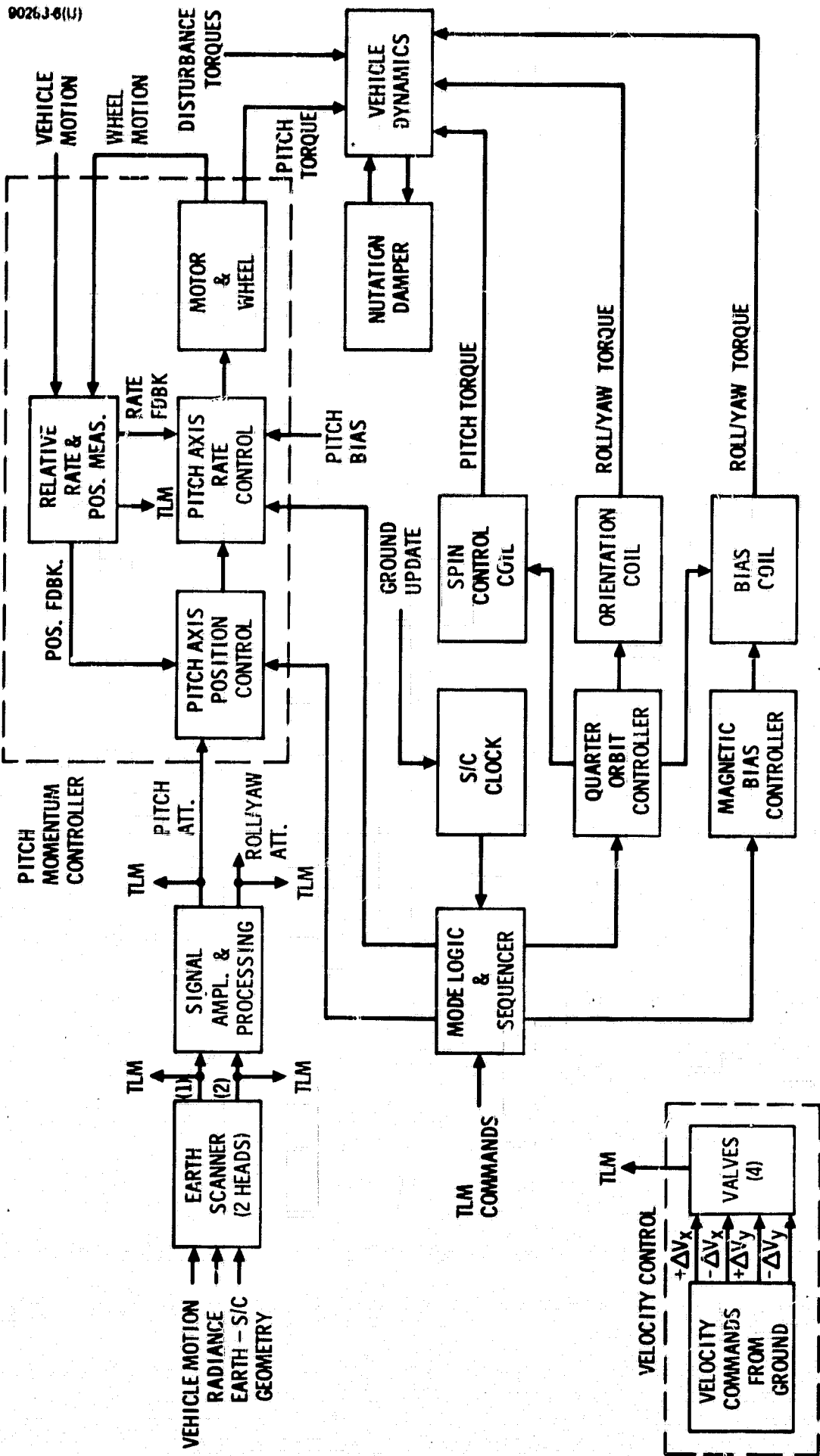
Figure 7-2. Attitude and Velocity Control System

7.1.5 System Design

A summary of the elements comprising the baseline attitude stabilization and velocity control system, as well as their function and salient characteristics, are reviewed in Table 7-4. The pitch momentum wheel and its controller has been specified such that sufficient spacecraft gyroscopic stability is provided to limit the effects of cyclical environmental disturbances to a maximum precession angle of ±0.2 degree. Substantial weight, power, and complexity savings are realized by integrating the earth sensor with the momentum wheel. A mirror, mounted to the wheel, scans the earth at wheel speed and reflects energy through the hollow wheel shaft to two pairs of identical bolometers that indicate the earth's leading and trailing edges at two different latitudes of the same hemisphere, once each wheel revolution. The sensor outputs are used to provide pitch attitude information for the wheel control loop and are telemetered via a DRS to the ground for attitude determination. The three electromagnetic coils, fixed to the satellite and oriented both normal and perpendicular to the spin axis, are used to adjust momentum along and normal to the spin axis. The operation of these coils is controlled by ground command with control logic dependent on the mode of operation and knowledge of the vehicle's attitude and orbital position relative to the earth's magnetic field. The coils are used to precess the angular momentum vector for pointing control, compensate for orbital regression and secular disturbance torques, and trim disturbances during and following ΔV maneuvers. The attitude of the spacecraft relative to the sun line during initial maneuvers is determined by a single sun sensor with its null axis normal to the spin axis. An eddy current nutation damper, consisting of a pendulous magnetic mass and conductive ring, is used to damp nutational motion during all modes of operation. A ΔV maneuver capability to effect orbital adjustments is provided by four thrusters aligned in opposed pairs along the velocity vector and normal to the orbit plane.

In addition to the elements of the on-board system described above, there is a requirement for ground data processing equipment. Such equipment must provide for processing of sensor data, implementation of an attitude determination algorithm, attitude error computation, mode control and attitude command routines, and logic for backup control, if required.

A functional block diagram of the attitude and velocity control system, illustrating the interrelationship between the various system elements, is shown in Figure 7-2. System operation is summarized in the paragraphs below.

Pulse outputs from the earth sensors and sun sensor are telemetered to the ground station and are processed for attitude determination purposes. Upon the establishment that attitude error has attained its untolerable limit, ground commands are provided to activate appropriate coils and initiate the required logic for coil current modulation. Outputs from the two earth sensor heads and the pitch wheel encoder are processed on-board by digital electronics to generate torque commands to the motor. Nutation, induced by separation transients and control maneuvers, is damped out by the eddy current nutation damper. Based on establishment of orbital errors by ground

TABLE 7-4. ATTITUDE AND VELOCITY CONTROL SYSTEM DESIGN

Element	Function	Characteristics
Momentum wheel (1)	Establishes pitch momentum bias	Pitch momentum: 43 ft-lb/sec
	Provides scan motion for earth sensor	Wheel speed: 500 rpm
		Wheel weight: 12 pounds
		Rotor shaft hollow
		Controller: rate plus position feedback
Earth sensor (two sensor elements)	Integral part of wheel	Scan period: 120 milliseconds
	Provides pitch and roll/yaw attitude errors	Nominal earth pulse: 27 milliseconds
		Scan cone: $\sigma = 30$ degrees
		Each sensor provides both pitch and roll/yaw errors
Magnetic control coils (3)	Precess angular momentum vector	Orientation: 350 amp-ft^2
	Trim disturbances	Bias: ≥ 15 amp-ft^2
		Spin control: ≥ 670 amp-ft^2
Sun sensor (1)	Attitude determination error and spin rate indication	Digital solar aspect sensor or double fan beam
Nutation damper (1)	Reduce nutational motion following separation and during attitude and velocity maneuvers	Eddy current damper
		$\tau = 10$ minutes
ΔV thrusters (4)	Maneuver along velocity	Thrust level: 5 pounds
	Manuever normal to orbit plane	Propellant: monopropellant hydrazine

tracking, required velocity corrections are implemented by sending command pulse trains to appropriate thruster valves. Because of the insensitivity of spacecraft pointing to environmental disturbances, provided by a sufficient level of pitch momentum bias and compensation torques by the magnetic torquers, the resultant slow attitude drift requires infrequent attitude commands from the ground station (approximately once per week).

7.2 ATTITUDE CONTROL SYSTEM ANALYSES

The purpose of this subsection is to analyze the disturbance torque environment, since the level and characteristics of these torques dictate the size of the momentum wheel and, correspondingly, the control torque levels which must be provided by the magnetic coils. Pertinent coordinate axes frames are related, and the magnetic torque equations are developed.

7.2.1 Definition of Coordinate Axes Systems

Orbital Reference Coordinate System

The orthogonal coordinate system necessary to fully describe the orbital position of the satellite, as well as its attitude relative to an earth referenced coordinate frame, is shown in Figure 7-3. The (x_e, y_e, z_e) system is an inertial coordinate set in the equatorial plane with its origin at the earth's center. The z_e axis is directed toward the autumnal equinox with y_e oriented normal to the equatorial plane. Defining the orbital plane in the (x_n, y_n, z_n) coordinate system, which is referenced to the inertial frame by the ordered rotations λ and i about the y_e and z_n axes, respectively, z_n is directed along the line of nodes with y_n normal to the orbit plane. The angle i defines the inclination of the orbit plane. The transformation relating the inertial coordinate frame to the orbital plane coordinate system is

$$
\begin{bmatrix} x_n \\ y_n \\ z_n \end{bmatrix} = \begin{bmatrix} \cos i & \sin i & 0 \\ -\sin i & \cos i & 0 \\ 0 & 0 & 1 \end{bmatrix} \begin{bmatrix} \cos \lambda & 0 & -\sin \lambda \\ 0 & 1 & 0 \\ \sin \lambda & 0 & \cos \lambda \end{bmatrix} \begin{bmatrix} x_e \\ y_e \\ z_e \end{bmatrix}
$$

$$
= \begin{bmatrix} (\cos i \cos \lambda) & \sin i & -(\cos i \sin \lambda) \\ -(\sin i \cos \lambda) & \cos i & \sin i \sin \lambda \\ \sin \lambda & 0 & \cos \lambda \end{bmatrix} \begin{bmatrix} x_e \\ y_e \\ z_e \end{bmatrix} \quad (1)
$$

where $\lambda = \lambda_o + \dot{\lambda} t$. The nodal regression rate of the orbit plane is $\dot{\lambda}$, and the initial angle between z_e and the line of nodes is λ_o. For the reference sun-synchronous orbit, i = 97.5 degrees at an altitude of 300 n.mi., and assuming z_ϵ represents the projection of the sun line in the orbit plane, $\dot{\lambda} = 0$ since both z_e and the line of nodes rotate at the earth's angular velocity about the sun. The angle λ is selected to ensure favorable lighting conditions on earth for surveillance purposes while orbital regression allows full coverage of the earth's surface.
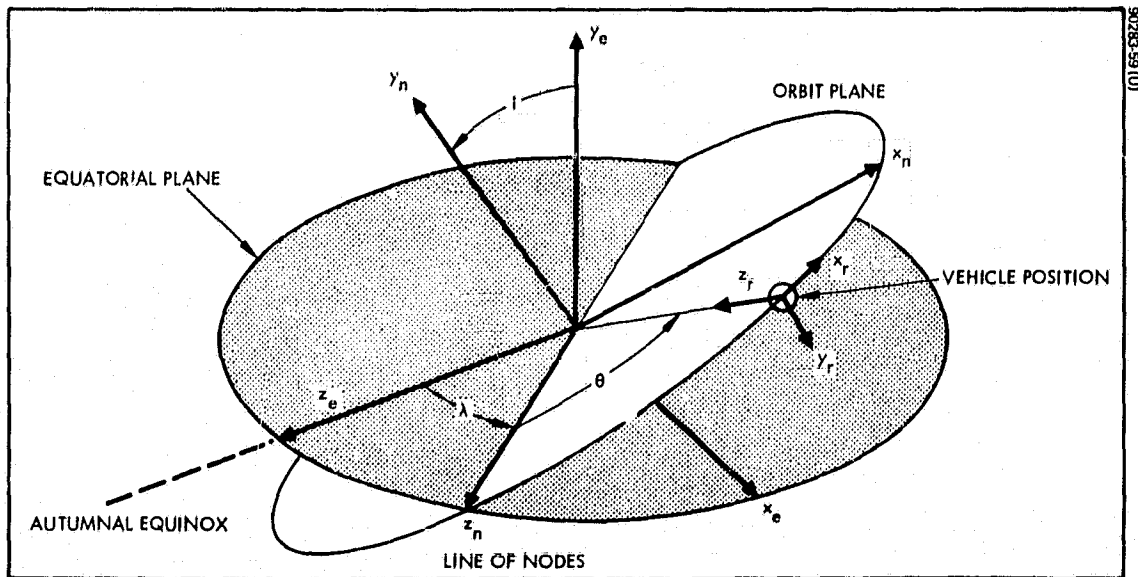
Figure 7-3. Coordinate Systems

Earth Reference Coordinate System

Again referring to Figure 7-3, the (x_r, y_r, z_r) coordinate system has as its origin the orbital position of the vehicle. The (x_r, z_r) plane is the plane of the orbit and z_r is directed toward the center of the earth. y_r is oriented normal to the orbit plane to complete the right hand triad. Orbital position of the satellite is measured by the angle θ. The relationship between the earth referenced coordinate frame and the orbital coordinate system is

$$
\begin{bmatrix} x_r \\ y_r \\ z_r \end{bmatrix} = \begin{bmatrix} \cos\theta & 0 & -\sin\theta \\ 0 & -1 & 0 \\ -\sin\theta & 0 & -\cos\theta \end{bmatrix} \begin{bmatrix} x_n \\ y_n \\ z_n \end{bmatrix} \tag{2}
$$

where $\theta = \theta_o + \dot{\theta}t$. Defining $\omega = \dot{\theta}$ for a circular orbit, at 300 n. mi, ω possesses a constant value approximately equal to $2\pi/0.96$ minutes or 1.05×10^{-3} rad/sec. Also, it can be noted that x_r and z_r are 90 degrees out of phase, i.e., they interchange orientation whenever θ advances 90 degrees.

The transformation of vectors from the x_e, y_e, z_e system to the x_r, y_r, z_r system is given by

$$
\begin{bmatrix} x_r \\ y_r \\ z_r \end{bmatrix} = A \begin{bmatrix} x_e \\ y_e \\ z_e \end{bmatrix} \tag{3}
$$

where

$$a_{11} = \cos\theta \cos i \cos\lambda - \sin\theta \sin\lambda$$

$$a_{12} = \sin i \cos\lambda$$

$$a_{13} = -(\sin\theta \cos i \cos\lambda + \cos\theta \sin\lambda)$$

$$a_{21} = \cos\theta \sin i$$

$$a_{22} = -\cos i$$

$$a_{23} = -\sin\theta \sin i$$

$$a_{31} = -(\cos\theta \cos i \sin\lambda + \sin\theta \cos\lambda)$$

$$a_{32} = -\sin i \sin\lambda$$

$$a_{33} = (\sin\theta \cos i \sin\lambda - \cos\theta \cos\lambda)$$

Body Reference Coordinate System

The desired satellite orientation is that where the individual body axes (x_b, y_b, z_b) are aligned parallel to their respective earth referenced axes (x_r, y_r, z_r) (see Figures 7-1 and 7-3). Such an alignment ensures that the z_b axis is pointed toward the earth's center with y_b oriented normal to the orbit plane. Since there will exist a large net angular momentum along the y_b axis, displacement of this axis from the orbit plane normal can be described by yaw and roll component errors which are relatively slowly varying in inertial space. Thus, a yaw error at one point in orbit becomes a roll error when the orbit position has moved 90 degrees (see Figure 7-4). As a consequence of this interchange of roll/yaw errors which occurs every quarter of an orbit period, only two measurements of attitude error are necessary each time a determination is made. The attitude sensor determines pitch error (angle between the z_b and z_r axes measured about the satellite's y_b axis) and bank angle or roll/yaw error, i.e., the angle which the satellite's y_r axis makes with the local horizontal plane.

The above described attitude errors may be defined by the two Euler rotations illustrated in Figure 7-5. The transformation from one coordinate system to the other takes the form

$$\begin{bmatrix} x_b \\ y_b \\ z_b \end{bmatrix} = \begin{bmatrix} \cos \alpha & 0 & -\sin \alpha \\ \sin \beta \, \sin \alpha & \cos \beta & \sin \beta \, \cos \alpha \\ \sin \alpha \, \cos \beta & -\sin \beta & \cos \beta \, \cos \alpha \end{bmatrix} \begin{bmatrix} x_r \\ y_r \\ z_r \end{bmatrix} \qquad (4)$$

or for small angles

$$\begin{bmatrix} x_b \\ y_b \\ z_b \end{bmatrix} \approx \begin{bmatrix} 1 & 0 & -\alpha \\ 0 & 1 & \beta \\ \alpha & -\beta & 1 \end{bmatrix} \begin{bmatrix} x_r \\ y_r \\ z_r \end{bmatrix} \qquad (5)$$

Therefore, for normal attitude control, attitude error is defined by the angles α and β, each of which must be limited to 0.5 degree (3σ).

Geomagnetic Coordinate System

Although reasonable estimates of the interaction between the earth's magnetic field and the satellite can be obtained assuming that the magnetic pole is aligned with the north pole, precise evaluation requires actual relationships. Figure 7-6 shows the geometrical relationship between the inertial coordinate set (x_e, y_e, z_e) and the magnetic coordinate set (x_m, y_m, z_m), both with their origins at the earth's center. The y_m axis is directed along the magnetic north pole, while the x_m-z_m axes define the magnetic equatorial plane. The angle between the z_m axis (axis which is coincident with the intersection of the magnetic equatorial and equatorial
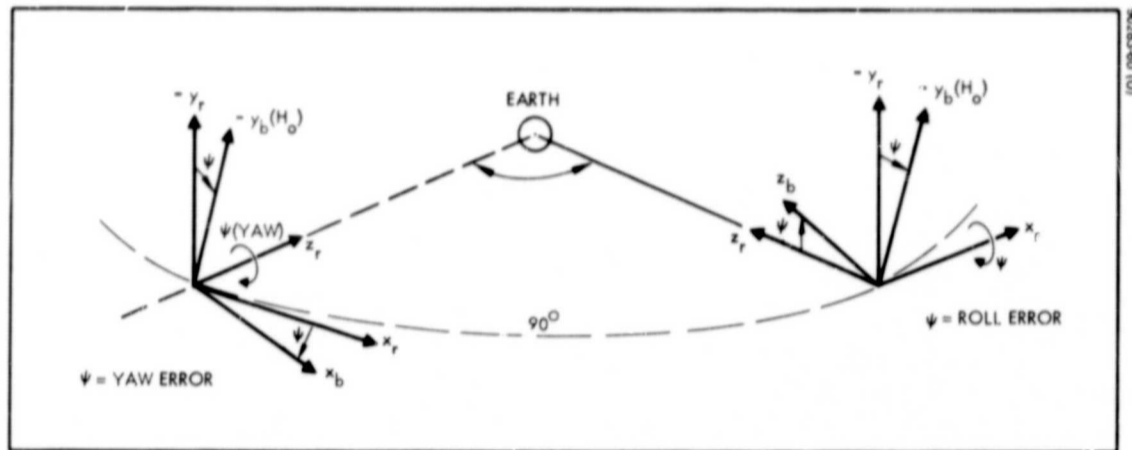
Figure 7-4.   Interchange of Roll and Yaw Pointing Errors
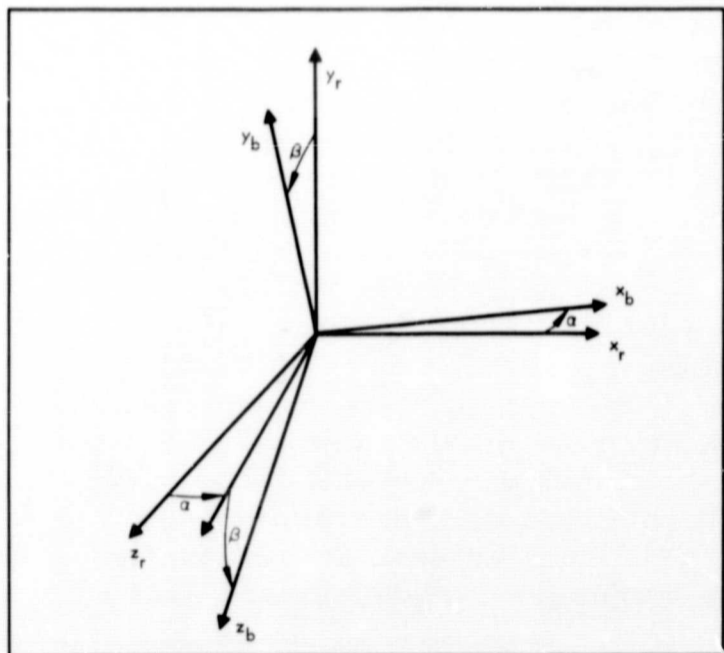
Figure 7-5.   Relation Between Body and
Earth Reference Coordinate Systems
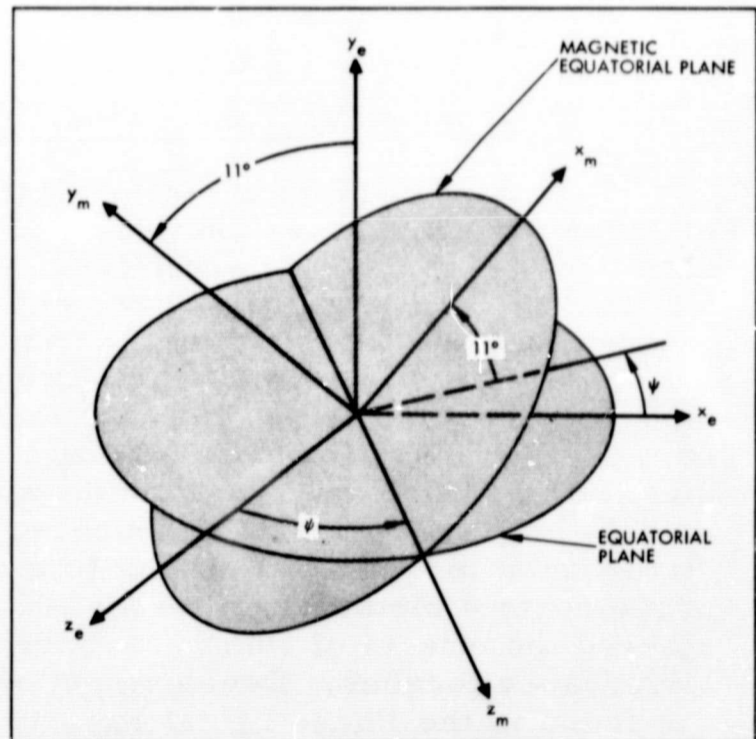
Figure 7-6.   Magnetic and Inertial
Reference Coordinate Systems

planes) and the z_e axis is given by $\psi = \psi_o + \Omega t$, where Ω is the earth's rotational rate. The angle between the y_m and y_e axes is approximately 11 degrees.

The transformation between the magnetic axis and inertial coordinate systems takes the form

$$\begin{bmatrix} x_m \\ y_m \\ z_m \end{bmatrix} = \begin{bmatrix} C_m \cos\psi & Sm & -C_m \sin\psi \\ -S_m \cos\psi & C_m & S_m \sin\psi \\ \sin\psi & 0 & \cos\psi \end{bmatrix} \begin{bmatrix} x_e \\ y_e \\ z_e \end{bmatrix} \qquad (6)$$

where $C_m = \cos 11$ degrees and $S_m = \sin 11$ degrees and, taking the transpose,

$$\begin{bmatrix} x_e \\ y_e \\ z_e \end{bmatrix} = \begin{bmatrix} C_m \cos\psi & -S_m \cos\psi & \sin\psi \\ S_m & C_m & 0 \\ -C_m \sin\psi & S_m \sin\psi & \cos\psi \end{bmatrix} \begin{bmatrix} x_m \\ y_m \\ z_m \end{bmatrix} \qquad (7)$$

7.2.2 Environmental Disturbance Torque Analysis

There exists an inherent relationship between the amount of pitch momentum required to ensure that pointing accuracy requirements are satisfied, frequency of corrections, and the level of disturbance torques. Furthermore, particular attitude control system techniques and control torque levels are dictated by the characteristics (level, frequency, distribution) of individual disturbance torques. The characteristics of the disturbance torques are, in turn, influenced by orbital parameters and the satellite configuration, i.e., inertia distribution, surface area and material, and cg location. To expedite a preliminary design, certain simplified models based on prior experience were used to reasonably estimate the disturbance torque environment to sufficient accuracy to establish the size of the control elements. The disturbance torque analysis performed considered the effects of solar, aerodynamic, gravity gradient, and magnetic disturbance torques. Development of the disturbance torque models used are found in the Phase I final report.

Summary of the Effects of External Disturbance Torques

The magnitudes of the above described disturbance torque components are influenced by satellite configuration parameters. Pertinent parameters and their maximum expected values are summarized in Table 7-5. To ensure a conservative design, expected worst case values are utilized.

TABLE 7-5.   ESTIMATES OF SATELLITE CONFIGURATION PARAMETERS THAT INFLUENCE DISTURBANCE TORQUE LEVELS

Reference Parameters	Estimated Value (3σ)	
CP - cg displacement; $\ell_x = \ell_y$	0.5	feet
Average effective surface area; A_i where i = x, y, or z	100	square feet
A_i x d_i	50	cubic feet
$\Delta I = I_y - I_z$	200	slug-ft^2
Principal axes displacement from local vertical; α_p	2.5 degrees	

From these estimates of configuration parameters, analysis and computation yield the disturbance torque estimates of Table 7-6.   Values for the x, y, and z components of magnetic dipole moment are not included, since these are established by the magnetic control coils and are based on tradeoff considerations to be discussed later in this report.

A review of the analysis results indicates that aerodynamic forces are the major contributor to cyclical transverse disturbances.   Also, the predominant secular disturbance torque is contributed by aerodynamic effects and is directed along the satellite's pitch axis.

7.2.3 Magnetic Torque Control

Due to the nature of the orbit — a low altitude, circular near-polar orbit — it is advantageous to utilize the interaction of the earth's magnetic field and current carrying coils onboard the satellite for attitude control purposes. The benefits of this control technique becomes apparent when the magnetic control equations are analyzed.

Development of Magnetic Torque Equations

The earth's magnetic field may be modelled by a simple magnetic dipole at the center of the earth with the dipole axis inclined from the earth's polar axis approximately 11 degrees.   Referring to Figure 7-7, the earth's magnetic field ($\vec{B}$) expressed in a spherical coordinate set is

$$\begin{bmatrix} B_r \\ B_\gamma \\ B_\eta \end{bmatrix} = - \frac{M_e}{r^3} \begin{bmatrix} 2 \sin \gamma \\ - \cos \gamma \\ 0 \end{bmatrix} \qquad (8)$$

TABLE 7-6. ESTIMATES OF COMPONENT DISTURBANCE TORQUE LEVELS

Disturbance Torque Source	Component Magnitudes, ft-lb					
	Secular			Cyclical		
	N_{x_n}	N_{y_n}	N_{z_n}	N_{x_n}	N_{y_n}	N_{z_n}
Magnetic moment*	0	0	$-8.57 \times 10^{-7} M_y$	$2.57 \times 10^{-6} M_y \sin 2\theta$**	1.73×10^{-6} $[2M_x \sin \theta -M_z \cos \theta]$	$2.57 \times 10^{-6} M_y \cos 2\theta$
Aerodynamic	0	(7×10^{-4})	0	$0.7 \times 10^{-4} \sin \theta$	0	$0.7 \times 10^{-4} \cos \theta$
Solar	0.39×10^{-6}	6.75×10^{-6}	1.05×10^{-6}	0	0	0
Gravity gradient	0	0	0	$-3.13 \times 10^{-5} \cos \theta$	0	$3.13 \times 10^{-5} \sin \theta$

*M_y is the pitch component of the spacecraft's magnetic dipole moment.
**θ is the angle in the orbit plane, referenced to the line of nodes, which defines the orbital position of the spacecraft.

90283-63(U)
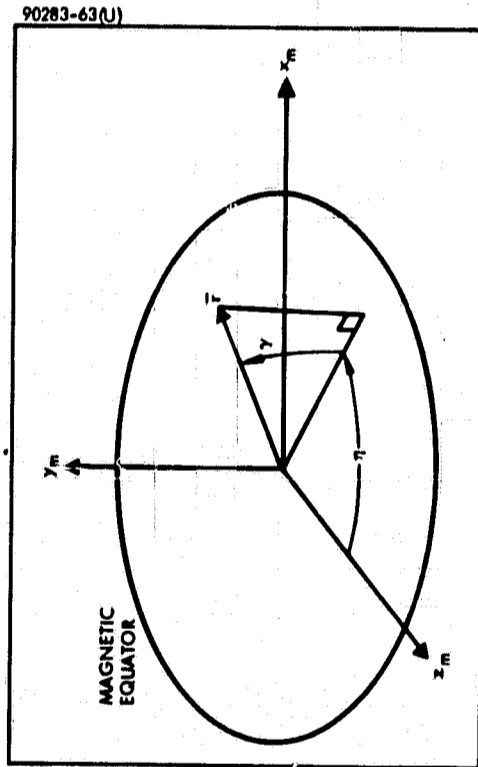
Figure 7-7. Magnetic Cartesian and Spherical Coordinates

where M_e is the geomagnetic dipole moment, r is the magnitude from the dipole to the satellite's center of mass, and γ is the latitudinal position relative to the magnetic equator. The position of a satellite relative to the (x_m, y_m, z_m) set may be defined in terms of the geomagnetic latitude γ and the geomagnetic longitude η, (See Figure 7-6). Then the transformation of vectors from the (x_m, y_m, z_m) set to the geomagnetic spherical set (η, γ, r) is given by:

$$
\begin{bmatrix} e_\eta \\ e_\gamma \\ e_r \end{bmatrix} = \begin{bmatrix} \cos\eta & 0 & -\sin\eta \\ -\sin\gamma\sin\eta & \cos\gamma & -\sin\gamma\cos\eta \\ \cos\gamma\sin\eta & \sin\gamma & \cos\gamma\cos\eta \end{bmatrix} \begin{bmatrix} x_m \\ y_m \\ z_m \end{bmatrix} \tag{9}
$$

where e_η, e_γ, e_r, x_m, y_m and z_m are unit vectors with the inverse transformation characterized by the transpose of the above matrix. Transforming the expression for $\bar{B}$ in Equation (8) into the x_m, y_m, z_m coordinate system yields

$$
\begin{bmatrix} B_{x_m} \\ B_{y_m} \\ B_{z_m} \end{bmatrix} = -\frac{M_e}{r^3} \begin{bmatrix} 3\sin\gamma & \cos\gamma & \sin\eta \\ 3\sin^2\gamma - 1 & & \\ 3\sin\gamma & \cos\gamma & \cos\eta \end{bmatrix} \tag{10}
$$

The magnetic spherical coordinates can be expressed as functions of the parameters in the transformation matrix relating the (x_r, y_r, z_r) and (x_m, y_m, z_m) coordinate systems. Further manipulation yields the following expressions for the components of $\bar{B}$ in the earth reference system.

$$
B_{x_r} = \frac{M}{r^3}\left[C_m \sin i \cos\theta - S_m(\cos i \cos\theta \cos\Omega + \sin\theta \sin\Omega) \right]
$$

$$
B_{y_r} = \frac{M}{r^3}\left[C_m \cos i + S_m \sin i \cos\Omega \right]
$$

$$
B_{z_r} = \frac{2M}{r^3}\left[C_m \sin i \sin\theta + S_m (\cos\theta \sin\Omega - \cos i \sin\theta \cos\Omega) \right] \tag{11}
$$

where

$$
C_m = \cos 11 \text{ degrees}, \quad S_m = \sin 11 \text{ degrees}, \text{ and } \Omega = \psi - \lambda.
$$

Since i = 97.5 degrees for the sun-synchronous orbit chosen, an assumption that the earth's magnetic pole and axis of rotation are coincident

and that the orbit is polar yields simplified expressions for components of $\bar{B}$. These assumptions amount to setting $C_m = 1$, $S_m = 0$, and $i = 90$ degrees. Then

$$\begin{bmatrix} B_{x_r} \\ B_{y_r} \\ B_{z_r} \end{bmatrix} = \frac{M_e}{r^3} \begin{bmatrix} \cos \theta \\ 0 \\ 2 \sin \theta \end{bmatrix} \tag{12}$$

The earth's magnetic field, $\bar{B}$, interacts with the magnetic dipole moment, $\bar{M}$, generated by currents and/or magnetized material on the satellite, to produce a torque $\bar{N}$, on the satellite,

$$\bar{N} = \bar{M} \times \bar{B}$$

The components of magnetic torque acting on the spacecraft in the earth referenced coordinate frame are

$$N = \bar{M} \times \bar{B} = \begin{vmatrix} i & j & k \\ M_x & M_y & M_z \\ B_{x_r} & B_{y_r} & B_{z_r} \end{vmatrix}$$

Evaluating the determinant,

$$\begin{bmatrix} N_{x_r} \\ N_{y_r} \\ N_{z_r} \end{bmatrix} = \begin{bmatrix} (M_y B_{z_r} - M_z B_{y_r}) \\ (M_z B_{x_r} - M_x B_{z_r}) \\ (M_x B_{y_r} - M_y B_{x_r}) \end{bmatrix}$$

Transforming from earth referenced coordinates to orbital coordinates:

$$N_{x_n} = (M_y B_{z_r} - M_z B_{y_r}) \cos \theta + (M_y B_{x_r} - M_x B_{y_r}) \sin \theta$$

$$N_{y_n} = (M_x B_{z_r} - M_z B_{x_r})$$

$$N_{z_n} = (M_z B_{y_r} - M_y B_{z_r}) \sin \theta + (M_y B_{x_r} - M_y B_{y_r}) \cos \theta \tag{13}$$

and substituting the results of Equation 12 and simplifying terms, yields

$$
\begin{bmatrix} N_{x_n} \\ N_{y_n} \\ N_{z_n} \end{bmatrix} = \frac{M_e}{r^3} \begin{bmatrix} (\frac{3}{2} M_y \sin 2\theta) \\ (2M_x \sin \theta - M_z \cos \theta) \\ (\frac{1}{2} \left[3 \cos 2\theta - 1 \right]) \end{bmatrix} \tag{14}
$$

At an altitude of 300 n. mi., $M_e/r^3 = 0.25$ gauss. Using this unit (gauss) and expressing $\overline{M}$ in amp-ft^2, a conversion factor of 6.86×10^{-6} must be used to express N in ft-lb. It should be noted that the component of magnetic torque along the line of nodes (z_n) has a secular component.

7.2.4 Attitude Control System Sizing Considerations

Wheel Momentum

A momentum wheel bias of 43 ft-lb/sec was selected based on an analysis of the environmental disturbance torques acting on the spacecraft, as well as pointing accuracy considerations. Estimates of both the secular and cyclical components of disturbance torques acting along a set of orbital-fixed coordinate axes were presented in Table 7-6. It is noted that a constant level of pitch magnetic dipole moment, M_y, can be used to effect the desired 1 deg/day precission of the spacecraft's pitch momentum vector about the x_n axis (see Figure 7-2). The gyroscopic interaction between the angular momentum vector along the y_n axis, and a torque along the z_n axis, causes the momentum vector to precess about the axis which is closely aligned to the earth's spin axis.

To limit the frequency at which the earth pointing controller need be activated, a decision was made to limit the displacement of the pitch momentum vector to ±0.2 degree of nominal (40 percent of the tolerable earth pointing error) due to cyclical disturbance torques. The nominal value of pitch momentum and the related magnetic dipole moment required to precess the spacecraft's angular momentum vector to compensate for orbital regression were selected as a result of the tradeoff illustrated in Figure 7-8. Curve (a) indicates the level of M_y required to precess the spacecraft's angular momentum 1 degree/day as a function of the magnitude of angular momentum. The minimum level of angular momentum required to ensure that cyclical disturbances do not precess the angular momentum vector more than ±0.2 degree, with M_y allowed to vary, is represented by curve (b). This latter curve is derived from the relationship

$$
H_{y_n} = \frac{\left[(N_{x_{nM}}^2 + N_{z_{nM}}^2)^{1/2} + (N_{x_{n_1}}^2 + N_{z_{n_1}}^2)^{1/2} \right] \Delta t}{\Delta \alpha}
$$
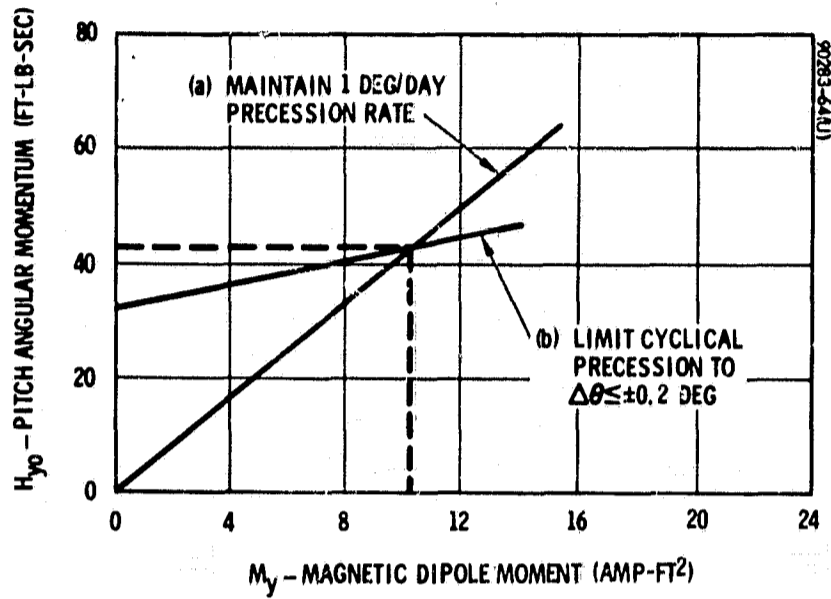
Figure 7-8. Momentum Wheel Sizing
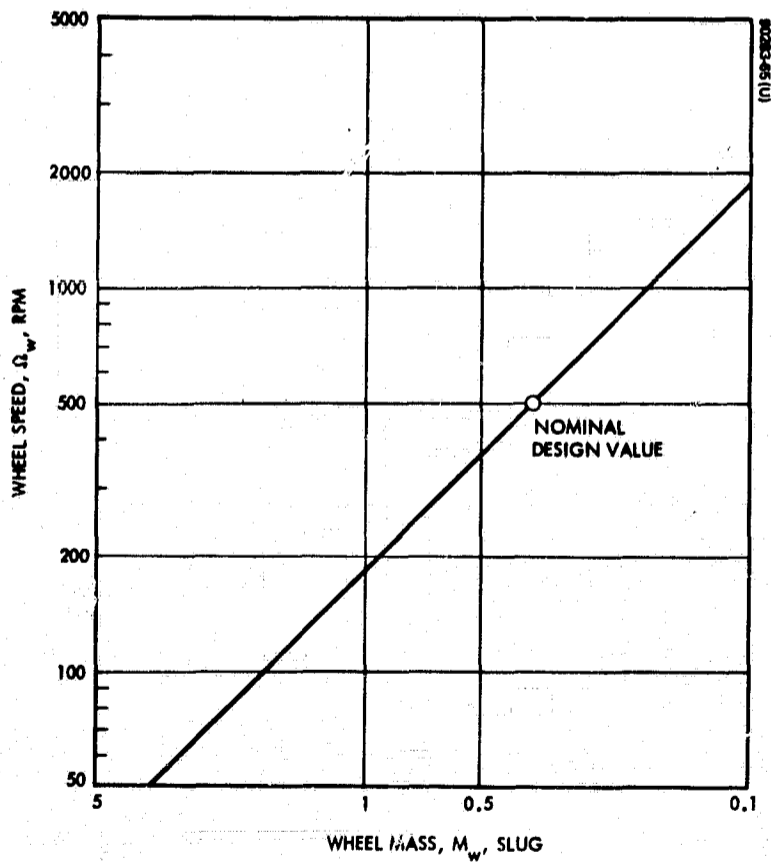
Figure 7-9. Tradeoff Between Design
Parameters Affecting Wheel Size

Radius of gyration: 1.5 feet

where

$\Delta \alpha$ = allowable precessional angle; ±0.2 degree

Δt = period over which disturbance torques are applied; 1.44×10^3 seconds

$N_{x_{nM}}$ = cyclical disturbance torque along x_n axis due to magnetic dipole; $2.57 \times 10^{-6} M_y \sin 2\theta$.

$N_{x_{n_1}}$ = cyclical disturbance torque along x_n axis due to aerodynamic and gravity gradient effects; $(0.7 \times 10^{-4} \sin \theta = 3.13 \times 10^{-5} \cos \theta)$

$N_{z_{nM}}$ = cyclical disturbance torque along z_n axis due to magnetic dipole; $2.57 \times 10^{-6} \cos 2\theta$.

$N_{z_{n_1}}$ = cyclical disturbance torque along z_n axis due to aerodynamic and gravity gradient effects; $(0.7 \times 10^{-4} \cos \theta + 3.13 \times 10^{-5} \sin \theta)$

The intersection of the two curves represents the minimum level of pitch angular momentum and M_y, which ensure that the cyclical and long-term precession requirements are satisified. The results are $H_{yo} \approx 43$ ft-lb/sec and $M_y = 10.2$ amp-ft^2.

Wheel Speed and Mass

There are a number of factors which affect selection of the nominal wheel speed for the pitch momentum wheel. Since the wheel is to be utilized to provide the scanning function for the earth sensor, wheel speed must be compatible with acceptable earth sensor scan rates. Also, reliability considerations, the physical constraints imposed by the spacecraft configuration, and the wheel mass required to achieve the desired level of angular momentum are important considerations. Spacecraft dimensions limit the wheel's radius of gyration to about 1.5 feet. Figure 7-9 illustrates the relationship between wheel speed and mass, which, in combination, provide the desired level of pitch momentum. Although increasing wheel speed reduces the required weight of the rotor, an upper limit is imposed by the response of the earth sensing element and wheel reliability. A nominal wheel speed of 500 rpm, corresponding to a rotor weighing approximately 12 pounds (assuming the mass is concentrated at the rim) and an inertia of 0.82 slug-ft^2, was selected as a reasonable value satisfying the conflicting constraints. The nominal value of wheel speed selected produces a scan rate for the earth sensor of 8.4 Hz (120 millisecond period). This rate will provide earth sensor pulse widths which are an order of magnitude greater than the sensor element's time constant.

TABLE 7-7. CHARACTERISTICS OF THE MAGNETIC CONTROL SYSTEM

Coil Designation	Magnetic Dipole Moment Orientation	Function	Magnitude of Dipole Moment Required, amp-ft^2	Mode of Operation	Maneuver Capability
Orientation coil	M_y; parallel to pitch axis	Precession for large reorientation maneuvers.	≤ 350 or larger	Quarter orbit phasing	≤ 4 deg/orbit or larger.
		Trim disturbance torques during ΔV maneuvers.	≤ 350	Continuous quarter orbit phasing of coil current.	Allows injection errors to be reduced in less than 2.5 days.
		Normal mode precession	≤ 70	Quarter orbit phasing	≤ 0.8 deg/orbit
Bias control	M_y; parallel to pitch axis	Compensate for orbital regression	10.2	Bias	1 deg/day
		Compensate for solar disturbance torque.	≤ 2	Quarter orbit phasing	0.2 deg/day
Spin control	M_x; parallel to roll axis	Trim large pitch disturbance torque during ΔV maneuvers.	≤ 350	Quarter orbit phasing	0.02 ft-lb/sec per orbit.
		Compensate for pitch aerodynamic disturbance torques.	≤ 320	Continuous quarter orbit phasing	$7 \times 10^{-4} \, \Delta t$ ft-lb/sec
		Adjust initial spin rate	≈ 10	Quarter orbit phasing	3.7×10^{-4} rad/sec/orbit

Magnetic Coils

The sizing requirements for the magnetic coils used to provide attitude control torques are determined by the functions provided by each coil, as well as the modes of operation or control logic associated with individual coils. Magnetic coils have been designated by function; vis., orientation coil, bias coil, and spin control coils. By investigating the character of cyclical and secular components of magnetic and disturbance torques in orbital coordinates (see Table 7-6), the following points are evident.

1) The momentum vector may be precessed in any arbitrary direction by reversing the polarity of the current every quarter orbit to the coil producing a magnetic dipole moment parallel to the spacecraft's pitch axis. Phase modulation of a square wave, referenced to the line of ascending nodes, varies the orientation of the precessional change, while amplitude and/or pulse modulation controls the amplitude of the amplified transverse torque or angular impulse bit. The basic logic will be referred to a quarter orbit phasing. This technique is used for both large re-orientation maneuvers and normal mode precession, as well as to trim transverse components of disturbance torques during ΔV maneuvers and to null the effects of solar disturbance torques.

2) The required precession to compensate for orbital regression can be achieved by commanding a constant current to a coil aligned parallel to the orientation control coil; i.e., the plane of the coil is normal to the spacecraft's spin axis, causing a dipole moment along the y_b-axis, M_y. This causes the generation of a constant control torque along the z_n-axis, resulting in precession of the spacecraft about the x_n-axis.*

3) Control torque along the pitch axis is realized most efficiently by orienting a coil to produce a dipole moment parallel to the x_b-axis, with the plane of the coil aligned parallel to the spacecraft's pitch axis. Quarter orbit phasing of coil current is required to produce a net torque that is nominally parallel to the y_n-axis.

A summary of the characteristics of the magnetic control system, including required coil sizes, is given in Table 7-7.

---

*It is noted (refer to Table 7-6) that a constant M_y can be used to cancel the major transverse component of solar disturbance torque. However, the uncompensated component will cause the spacecraft's angular momentum vector to drift about the z_n-axis at a rate of about 0.05 deg/day.

Orientation Coil

The maximum control capability required of the orientation coil is based either on the need to trim disturbance torques, resulting from the offset of the ΔV thrust vector from the spacecraft's center of gravity, or the maximum precession rate desired for large reorientation maneuvers. If the ΔV thrusters are sized to 5 pounds, a coil generated magnetic dipole moment of 350 amp-ft^2 allows for the reduction of ΔV injection errors of 200 fps and/or resulting attitude errors in approximately 3 days. Specific details can be found in Section 7.3. A coil of this size provides for a maximum momentum vector reorientation capability of approximately 4 deg/orbit, assuming continuous quarter orbit cycling of coil current. The relationship between pitch magnetic dipole moment and resultant precessional change of the spacecraft's angular momentum vector is

$$\Delta = 57.3 \frac{\left(\frac{2}{\pi}\right) \cdot \left(N_T\right) \cdot \left(\Delta t\right)}{H_{yo}} \text{ degrees}$$

where

N_T = transverse magnetic control moment = $2.57 \times 10^{-6} M_y$

H_{yo} = pitch angular momentum = 43 ft-lb/sec

Δt = time interval that current is applied = 5.76×10^3 sec/orbit

The factor $2/\pi$ represents the average value of a full-rectified sine wave.

During normal mode control, it is desirable to provide limited precessional torque capability. The control function in this mode is to reorient the satellite's pitch axis from time to time to reduce the buildup of attitude error. A maximum 70 amp-ft^2 requirement has been established which corresponds to a precession maneuver capability of 0.8 deg/orbit. Further reduction of coil current, or the application of coil current pulses of limited duration, reduces the resolution of precessional commands during normal mode operation. A reduced level of transverse angular momentum impulse will enhance attitude determination accuracy and provide for smaller nutation angles.

Bias Coil

Another coil oriented parallel to the orientation coil, but sized to 70 amp-ft^2, is used to compensate for orbital regression, solar disturbance torques, and to provide a limited backup capability for the orientation coil. A magnetic dipole moment, M_y, results in constant precession of the spacecraft about the x_n-axis of

$$\Delta\beta \approx 57.3 \frac{9.57 \times 10^{-7} M_y}{H_{yo}} \ \text{deg/sec}$$

To produce a constant precessional rate of 1 deg/day, a magnetic dipole moment of $M_y = 10.2$ amp-ft^2 is required. Of course, the bias controller must be able to adjust the current level to account for the residual magnetic dipole moment of the spacecraft.

Additionally, it is expected that the precessional rate due to solar disturbance torques is about 0.2 deg/day at a sun angle of 30 degrees. The quarter orbit controller, feeding the bias coil, can be designed to compensate for this effect by providing an average magnetic dipole moment of 2 amp-ft^2. This could be accomplished by: 1) reducing the current amplitude provided to the coil, 2) skipping a number of orbits between each cycle of coil current, or 3) providing an unidirectional current pulse every one-half orbit.

Spin Control Coil

The spin control coil is utilized to maintain the wheel speed and, hence, angular momentum, within the design limits, while the function of the pitch wheel controller is to correct for pitch pointing errors. Maximum coil size is dictated by the requirement to compensate for pitch environmental disturbance torques. Aerodynamic drag causes a secular pitch disturbance torque which has been estimated to be 7×10^{-4} ft-lb. If this torque were not compensated for, it would tend to increase or decrease pitch angular momentum at a rate of approximately 4 ft-lb/sec per orbit. Therefore, it is necessary to continuously command current to the spin control coils, using a quarter orbit cycling, to prevent a rapid change in pitch angular momentum. A magnetic dipole moment of 320 amp-ft^2 is required. Again, to allow for the reduction of ΔV injection errors within a 3-day period, using 5-pound thrusters, an additional magnetic dipole moment of 350 amp-ft^2 is required. Therefore, the maximum capability of the spin control coils should be approximately 670 amp-ft^2. This could be provided by two coils sized to 350 amp-ft^2, which would provide redundancy.

Following spinup of the spacecraft by the Delta stage and subsequent despin during wheel spinup, it will be necessary to use the spin control coil to adjust the final spin rate of the spacecraft to conform to orbital rate. This could be accomplished with a dipole moment in the order of 10 amp-ft^2, which could be used to change pitch rate by as much as 3.7×10^{-4} rad/sec per orbit.

The dipole moment requirements presented above are transformed to coil design parameters in subsection 7.4.

7.3 VELOCITY CONTROL SYSTEM ANALYSIS

7.3.1 Velocity Control Requirements

The velocity control system, consisting of four ΔV thrusters which are mounted in opposed pairs, provide for orbital correction of injection errors and control of orbital period. Injection errors are corrected by thrusting normal to the orbit plane to compensate for inclination errors, and along the orbit track to adjust orbital velocity. To completely cover the earth's surface in a minimum time period, it is necessary to control orbital period.

Reduction of Injection Errors

To provide a sun-synchronous orbit for optimum earth imaging, it is necessary to provide a ΔV capability to perform orbit trim maneuvers to eliminate nonsynchronistic behavior in orbital precession rate ($\dot{\Omega}$) resulting from injection errors. Since orbital precession rate is a function of altitude and orbit inclination, it is possible, in theory, to attain a sun-synchronous orbit by changing altitude to conform to the actual orbital inclination following injection. However, the disadvantage of this approach is that the payload imaging sensor is extremely sensitive to altitude changes relative to the nominal design altitude. Thus, it is necessary to adjust orbit inclination and velocity to obtain a sun-synchronous orbit which must precess at an average rate of 0.985 deg/day.

The precession rate of the nodes, $\dot{\Omega}$, is given by

$$\dot{\Omega} = -\frac{3}{2} \sqrt{\frac{K^2}{a^3}} \; J_2 \left[\frac{R_e}{a} \right]^2 \cos i \; \text{rad/hr} \tag{15}$$

where

a = semimajor axis = $R_E + \bar{h}$ for a circular orbit, $\bar{h}$ = 300 n. mi.

J_2 = 1.08219 x 10^{-3}, polar oblateness coefficient

K^2 = 8.155 x 10^{11} (n. mi.)^3/hr^2

R_E = radius of earth, $\approx$ 3442 n. mi.

i = inclination of orbit, i = 97.6 degrees

Information provided by McDonald-Douglas relative to the anticipated Improved Thor-Delta injection errors (3σ) for a 300 n. mi. sun-synchronous orbit is shown in Table 7-8.

The injection errors contributed by the Improved Thor-Delta in altitude (h) and orbit inclination (i) produce deviations in nodal rate ($\dot{\Omega}$) from the required sun-synchronous rate. This deviation in $\dot{\Omega}$ can be written as

$$\Delta\dot{\Omega} = \frac{\partial\dot{\Omega}}{\partial I} \Delta I + \frac{\partial\dot{\Omega}}{\partial a} \Delta a \qquad (16)$$

TABLE 7-8. LAUNCH VEHICLE INJECTION ERRORS*

Error	3σ Estimate
Altitude, n. mi.	±15
Velocity, fps	±30
Inclination, degree	±0.25

*Assumes a payload weight of 1300 pounds injected into a 90-degree inclined orbit and launched from the Western Test Range.

where a = 3742 n.mi. is the average altitude of the targeted orbit. The partial derivatives are obtained by differentiating Equation 15; viz.,

$$\frac{\partial \dot{\Omega}}{\partial i} = \frac{3}{2} \sqrt{\frac{K^2}{a^3}} \; J_2 \; \left(\frac{R_E}{a}\right)^2 \sin i \; \frac{rad/hr}{rad} \tag{17}$$

and

$$\frac{\partial \dot{\Omega}}{\partial a} = 5.25 \sqrt{\frac{K^2}{a^3}} \; J_2 \; \left(\frac{R_E}{a}\right)^2 \frac{1}{a} \cos i \; \frac{rad/hr}{n.mi.} \tag{18}$$

Making the necessary substitutions,

$$\frac{\partial \dot{\Omega}}{\partial i} \approx 0.131 \; deg/day$$

and

$$\frac{\partial \dot{\Omega}}{\partial a} \approx 0$$

Therefore, the resulting 3σ estimate in nodal rate variation is about 0.033 deg/day. If this error were allowed to accumulate over a 1-year mission, the total nodal shift would be ±11.7 degrees (3σ).

The velocity required to correct inclination errors may be considered independent of the velocity required to correct in-plane errors due to injection velocity and altitude. Assuming that velocity corrections are made near the line of nodes, that component of ΔV required to correct an inclination error is

$$\Delta V_i \approx V_o \sin (\Delta i) \approx \frac{V_o}{57.3} \Delta i \tag{19}$$

where

Δi = inclination error, degrees

ΔV_i = velocity required to correct inclination errors, fps

V_o = orbital velocity, 24,874 fps

Substituting the expected Δi = 0.25 degree (3σ) into Equation 19, a $\Delta V_i \approx 109$ fps is required for a 300 n.mi. orbit. If ΔV firings are distributed uniformly throughout the orbit, the ΔV_i requirement is increased by a factor of $\pi/2$ increasing the requirement to about 172 fps.

Errors in injection altitude and velocity will result in a period and eccentricity error in the final orbit. For small errors in injection flight path angle, the resulting period and eccentricity errors are approximately

$$\frac{\Delta \tau}{\tau} = 3 \left(\frac{\Delta V}{V_o} + \frac{\Delta r}{r} \right) \tag{20}$$

and

$$\Delta e = \frac{2 \Delta V}{V_o} + \frac{\Delta r}{r} \tag{21}$$

where

τ = Nominal orbit period

$\Delta \tau$ = Orbit period error

V_o = Nominal injection velocity

ΔV = Error in injection velocity

r = Nominal injection radius

Δr = Error in injection radius

Δe = Eccentricity error due to ΔV and Δr

The expected values of ΔV and Δr, as listed in Table 7-7, are ±30 fps (3σ) and ±15 n.mi. (3σ), respectively. Therefore, $\Delta V / V_o \approx 1.2 \times 10^{-3}$ and $\Delta r / r = 4.0 \times 10^{-3}$. These values will result in a worst case $\Delta \tau / \tau$ of approximately 0.01 and maximum Δe of about 0.005. Rearranging Equations 20 and 21, the maximum velocities required to remove errors in eccentricity and period are approximately:

$$\Delta V_e = \frac{(V + \Delta V)}{3} \frac{\Delta \tau}{\tau} \approx 86.3 \text{ fps} \tag{22}$$

and

$$\Delta V_\tau = \frac{(V + \Delta V)}{2} \Delta e = 62.2 \text{ fps} \tag{23}$$

To estimate propellant usage conservatively, the ΔV requirement to correct injection errors is obtained by taking the RSS of the two components of in-plane errors and adding the result to the out-of-plane component. The resulting 3σ estimate of the ΔV required to reduce injection errors is about 216 fps.

Orbital Period Control

In addition to providing an in-plane and out-of-plane ΔV correction capability to correct orbit injection errors, there is an in-plane ΔV requirement to control orbital period. To ensure complete coverage of the earth's surface in minimum time, it is required to control orbital period accuracy to about 1 second. Resultant requirements for the ΔV control system (propellant required and frequency of corrections) are developed below.

The relationship between orbital period, T, orbital velocity, V_o and the orbital radius, R, takes the form

$$T = \frac{2\pi R}{V_o} \tag{24}$$

Also, from the law of gravitation,

$$R = \frac{G}{V_o^2} \tag{25}$$

where G is the universal gravitational constant; 8.32×10^4 n.mi./sec^2. Substituting Equation 24 into Equation 25 results in a explicit relationship between orbital period and velocity; viz.,

$$T = \frac{2\pi G}{V_o^3}$$

Now, the sensitivity of changes in satellite velocity to corresponding changes in orbital period is

$$\frac{\partial T}{\partial V} = -\frac{6\pi G}{V_o^4} \tag{26}$$

Thus, the relation between a change in velocity and the resultant change in orbital period can be expressed as

$$\Delta T \approx -0.073 \, \Delta V \tag{27}$$

where ΔT has units of seconds and the units for ΔV are feet per second.

The factor causing orbital velocity changes is atmospheric drag, the value of which can be computed from the equation

$$F_D = \left(\frac{1}{2}\rho V_o^2\right) C_D \cdot A$$

where

ρ = atmospheric density, slugs/ft^3

V_o = spacecraft velocity, fps

A = spacecraft area exposed to aerodynamic flow (effective area)

C_D = drag coefficient
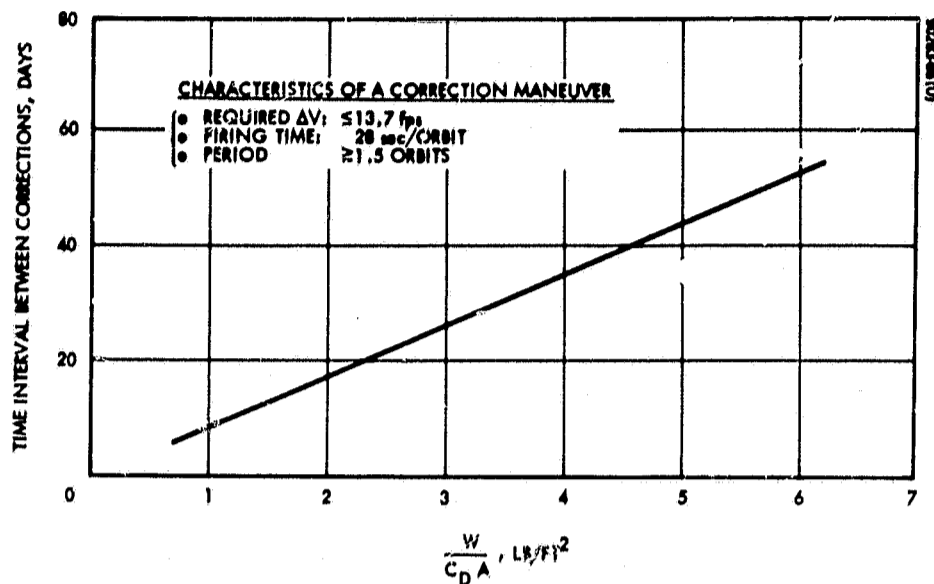
Figure 7-10. Orbit Control Characteristics

$|\Delta T| \leq 1$ second, 5-pound thruster

Utilizing a value for ρ of 1.8×10^{-15}, representing mean-to-high solar activity for a 10-hour orbit at 300 n. mi.[*] at $V_0 = 24,874$ fps, yields

$$F_D \approx 5.54 \times 10^{-7} C_D \cdot A$$

The resultant change of velocity over time is

$$\Delta V = 32.2 \frac{F_D}{W} \Delta t = 1.8 \times 10^{-5} \left[\frac{C_D \cdot A}{W} \right] \Delta t \text{ fps} \tag{28}$$

Substituting this expression for ΔV into Equation 27 yields

$$\Delta T = -1.32 \times 10^{-6} \left[\frac{C_D \cdot A}{W} \right] \Delta t \text{ sec}$$

The time interval, Δt, corresponding to a 1-second reduction in orbital period caused by aerodynamic drag is

$$\Delta T = 0.76 \times 10^6 \frac{W}{C_D \cdot A} \quad \text{seconds} \tag{29}$$

or

$$\Delta t = 8.8 \frac{W}{C_D \cdot A} \quad \text{days}$$

The above relationship is plotted in Figure 7-10. For a reference 1000-pound spacecraft with $C_D = 3$ and $A = 100$ ft^2, $(W/C_D A) = 3.3$ lb/ft^2 and orbit control corrections are required every 29 days. Substitution of Equation 29 into Equation 28 indicates that each correction requires a $\Delta V = 13.7$ fps to adjust orbital velocity to its nominal value.

[*]"The Upper Atmosphere in the Range from 120 to 800 km," I. Harris and W. Priester, Goddard Space Flight Center, Greenbelt, Maryland.

TABLE 7-9. SUMMARY OF ΔV AND PROPULSION SYSTEM REQUIREMENTS

ΔV Requirements for 1000-pound Spacecraft

Correction	ΔV, fps	Impulse, lb-sec
Injection errors	216 (3σ)	6,700
Orbit period	165	5,220
Totals	380	11,920

Thruster Characteristics (Baseline System)

Number: 4

Thrust Level: 5 pounds

Propellant: Monopropellant hydrazine - 75 pounds

$I_{sp} = 160$ seconds

Assuming a 0.2-inch offset of the ΔV thruster relative to the c.g., the orientation coil permits a maximum firing time of 140/F seconds per orbit when F = thrust level. Also, the total duration of thruster impulses for each orbit control ΔV sequence using the baseline 5-pound thruster is

$$t_o = \frac{m}{F} \Delta V = 42.5 \text{ seconds} \tag{30}$$

Limited by the 28-second maximum firing time per orbit, each maneuver sequence requires a minimum of 1.5 orbits.

In contrast, if resistojets sized to 0.005 pound were utilized, the maximum size of the orientation control coil allows these thrusters to fire continuously. If they could be fired continuously, 42.5×10^3 seconds or 7.3 orbits would be required to effect the necessary ΔV maneuver. However, in reality, they are duty-cycle limited, so that each ΔV sequence might require a number of days. For either case, at least 12 maneuvers are required for a year's operation for a total ΔV expenditure of 165 fps.

ΔV Impulse Requirements

Based on the foregoing analysis, a maneuver requirement of 216 fps is necessary to compensate for injection errors, while 165 fps (per year) has been estimated to maintain orbital period to within 1 second of nominal. Corresponding propulsion system requirements are summarized in Table 7-9.

7.3.2 ΔV Thruster Firing Characteristics

Since the ΔV thrusters cannot be perfectly aligned so that their thrust vector passes through the vehicle's cg, a disturbance torque is applied to the spacecraft each time they fire. The magnitude of this disturbance torque is proportional to the thrust level and thruster misalignment. Also, to preserve the pointing accuracy, the cumulative firing time must be restricted based on the limited torque capability of the magnetic control system.

As a result of equating disturbance and control transverse angular momentums, the maximum firing time per orbit which maintains satellite orientation, on the average is

$$\Delta t \leq \frac{\frac{2}{\pi} |N_t|}{a\,F} \cdot T \tag{31}$$

where

N_t = transverse magnetic control torque = $2.57 \times 10^{-6} M_y$, ft-lb

T = orbit period $\approx$ 5760 seconds

F = thrust level (pounds)

a = thrust vector offset (feet)

The factor $2|N_y|/\pi$ represents the average value of the applied magnetic torque that takes the form of a full rectified sine wave. For a 5-pound thruster, and $|N_T| = 9 \times 10^{-4}$ ft-lbs ($M_y = 350$ amp-ft^2), application of Equation 31 results in a maximum firing time of $\Delta t = (5.65/a)$ where a now has the dimension of inches. This relation is plotted as curve (a) in Figure 7-11. For a 0.2-inch offset, the maximum allowable firing time per orbit is 28 seconds.

From Equation 31, the total firing time to provide a velocity change of 216 fps, which would be required for the worst expected injection errors, is 1340 seconds. However, such a correction must be accomplished in a series of limited jet firings, no firing time per orbit exceeding that indicated by curve (a) of Figure 7-11. The maximum allowable firing time per orbit is a function of the thrust vector offset, a. Thus, for a = 0.2 inch, the time to perform the above injection error correction, while maintaining pointing accuracy requires 1,340/28 ≈ 48 orbits.

If thruster firing is performed continuously and pointing error is allowed to increase, 48 orbits will also be required (a = 0.2 inch) to reduce the pointing error. The torque capability of the magnetic control system establishes this time interval, and for either alternative, the initialization time is indicated as a function of thrust vector offset by curve (b) of Figure 7-11. If 0.005-pound resistojets were utilized, about 233 orbits, or nearly 16 days, are required to correct the reference injection error. This longer correction time is due merely to the lower thrust of the resistojets, whereas, for the 5-pound thrusters, the correction time is limited by the magnetic attitude control system capability.

7.4 SYSTEM MECHANIZATION

7.4.1 Magnetic Control

Magnetic moments for pointing and spin control purposes are provided by passing current through appropriately oriented coils. The analysis provided in subsection 7.2.4 and summarized in Table 7-7 indicated the requirements for coil design, in terms of magnetic moment and the requisite control logic required to modulate coil current. The following paragraphs discuss typical design characteristics coils which will meet these requirements.

Coil Design

The magnetic torque producing device consists of a coil of wire fitted against the interior walls of the spacecraft. This, in effect, is a core coil. For such a coil, the most efficient configuration is a planar winding with maximum dimensions consistent with spacecraft integration requirements. The magnetic moment produced by passing current through the wire is normal

to the plane of the coil. The relationship between the power-weight (PW) product and the magnetic dipole moment generated is

$$PW = \beta \left(\frac{S}{A}\right)^2 M^2 \qquad (32)$$

where β is a quantity involving the resistivity — density product and insulation factor of the wire and S/A is the ratio of perimeter of the coil to the area it encloses. If aluminum wire is utilized, the minimum value of $\beta = 8 \times 10^{-5}$ ohm-kg/m. Corresponding to the spacecraft's configuration, the orientation and bias coils have a rectangular configuration (3 by 81 feet) while the spin coil is 3 feet square. Table 7-7 shows that the dipole moment required from: 1) the orientation coil is 350 amp-ft^2 (32.2 amp-m^2), 2) the bias coil is 70 amp-ft^2 (6.5 amp-m^2), and 3) the spin coil is 670 amp-ft^2 (61.8 amp-m^2). The coil characteristics are summarized in Table 7-10. Additionally, the cross-sectional diameter, d, of a bundled wire coil is given by

$$P d^2 \approx \frac{1.4 \, \rho \, S \, M^2}{A^2} \qquad (33)$$

where the resistivity of aluminum, $\rho \approx 0.94 \times 10^{-7}$ ohm-ft. Considering a 0.75-inch diameter for the bundle of wire and utilizing Equation 33 yields the maximum power allocations and corresponding weights for each coil, as is indicated in Table 7-10.

7.4.2 Momentum Wheel and Controller

The pitch momentum wheel is required to produce 43 ft-lb/sec of angular momentum and rotate at a speed of 500 rpm to provide a reasonable mirror scan rate for an earth sensor assembly integrated with the wheel. A preliminary design of the combination momentum wheel and earth sensor is illustrated in Figure 7-12. The wheel's rotor weighs approximately 12 pounds and is 30 inches in diameter. Mass of the wheel is placed at its major diameter and the rim of the wheel is supported by spikes. Two earth sensor heads, are mounted on the despun hub of the momentum wheel, are tilted relative to the wheel's spin axis to effect two scan chords of the earth with a single mirror.

Motor

Several Hughes dual-spin satellites have used dc brushless motors and they have demonstrated a high power-to-weight ratio. For this motor, life is not limited by any factors in the motor. However, the electronic drive unit is about twice as complex and heavy as the conventional dc motor. The conventional dc motor has the lowest system weight, highest power efficiency, and a good record of performance in space where brush friction and life can be tolerated. The present state of the art on brush design for space applications and commutator lubrication allows a brush life of 10^9 revolutions. For the 500 rpm motor (0.24×10^9 revolutions per year), a factor of four in brush life will exist.
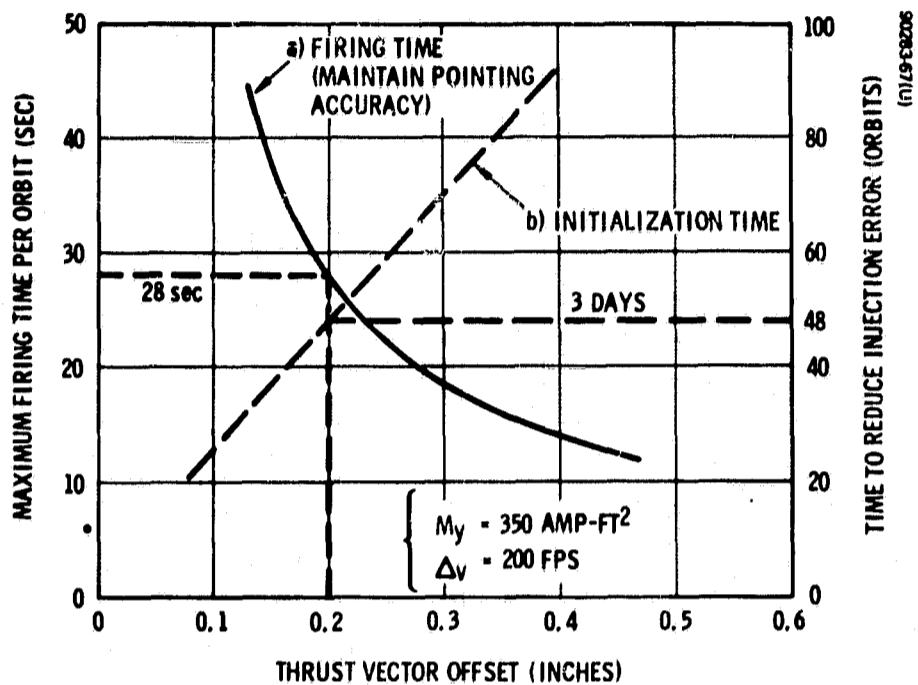
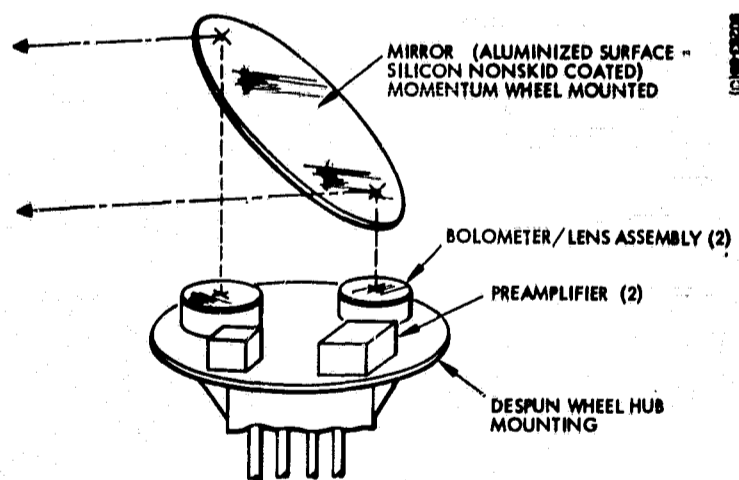Figure 7-11. Thruster Firing Characteristics
to Correct Injection Error

Figure 7-12. Geometry or Wheel Scan
Mirrors and Earth Sensors

## TABLE 7-10. TORQUER COIL CHARACTERISTICS

d = 0.75 inch

Coil	(S/A)	Magnetic Moment, (M) (amp-m^2)	PW, watt-lb	Pd^2 watt-ft^2	P, watt	W, pound
Orientation	0.917	<32.2	0.061	0.62×10^{-3}	0.160	0.38
Bias	0.917	< 6.5	<0.003	0.25×10^{-4}	0.006	0.50
Spin	0.750	<61.8	<0.258	2.1×10^{-3}	0.540	0.48

An encoder, consisting of a permanent magnet mounted to the rotor and pickoff device mounted to the stator, generates a master index pulse used to provide phase information on the spinning rotor relative to the despun platform.

Control Electronics

The momentum wheel control electronics and attitude sensor data processing electronics are very similar in function to those used in several existing Hughes dual-spin satellites. With the exception of the digital shaping network, the total electronics could be implemented with existing flight circuits. This approach would be somewhat inefficient in terms of power, weight, and component cost, since the requirements of this system are somewhat less stringent than existing dual-spin control systems. The approach proposed is to tie together simplified versions of existing circuits to provide a minimum risk design optimized for all aspects of performance.

The inputs to the control electronics are the mirror-scan earth sensor leading (LE) and trailing (TE) edge output pulses and the master index pulse (MIP) from the encoder, as shown in Figure 7-13. The LE pulse starts a counter, the MIP reverses the direction of the count, and TE stops the count and gates it out. The deviation of this count from zero is proportional to the error from the boresight to the center of the earth. This error number is processed by the shaping to provide the desired torque command. The motor torque is controlled by varying the duty cycle of the current applied to the motor. In addition to the pointing loop, there is a rate loop with the capability of overriding the position loop, keeping the rate of the satellite below a specified value at all times. This loop is used for acquisition and for open loop rate commands during the satellite spinning mode following injection. It also provides additional lead shaping for faster response under nominal conditions. The frequency lock loop locks up to the sensor pulse frequency. When sensor pulses are lost or erratic, the lock logic prevents change of this output frequency. The output frequency is compared with the MIP frequency and a torque proportional to this rate error is computed and summed with the position loop torque. Approximately 90 percent of the circuitry is identical or nearly so to working hardware actually in space or tested for space use.
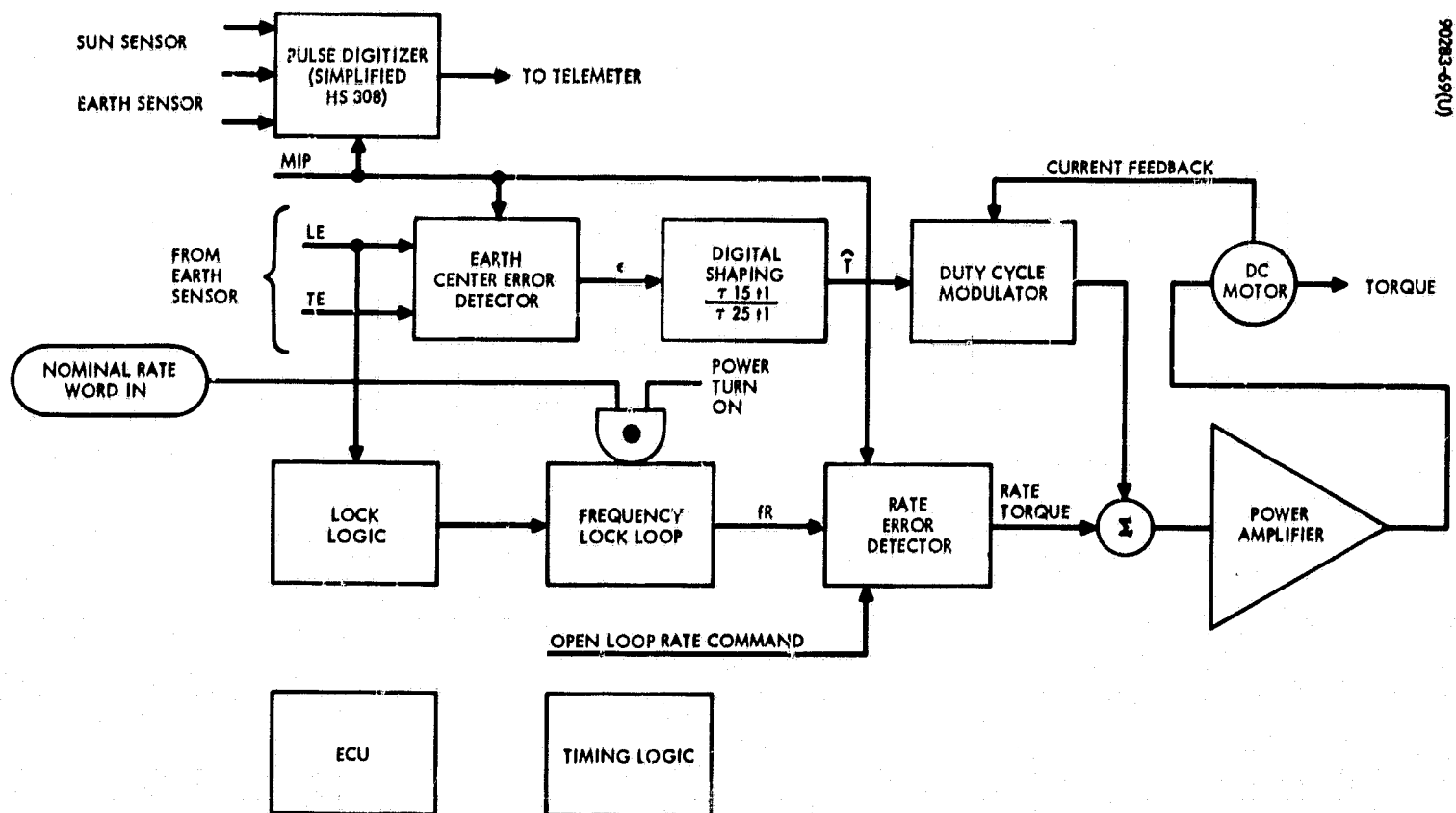
Figure 7-13. Control Electronics Mechanization

7.4.3 Earth Sensors

Alternative Systems Considered

Alternative earth sensor configurations, compatible with a low altitude circular orbit, considered were: 1) horizon scanner function incorporated with the momentum wheel assembly (conical scanner), and 2) edge tracking horizon scanners. The latter sensor system requires two independent dual tracker heads which track four points on the earth's horizon limb. Each tracking head incorporates a motor-mirror combination to provide scanning. A dual tracker unit (two required) weighs approximately 17 pounds, including the electronic unit, and requires less than 10 watts (average) of power. Thus, based on reliability considerations (additional moving parts) as well as weight and power requirements, the approach where the earth sensor is integrated with a momentum wheel (an approach which is similar to that used for NIMBUS and TIROS M) was selected.

Baseline Approach

For both pitch and roll/yaw error sensing, two identical infrared horizon scanners are used to produce uniform output pulses indicating earth horizon crossings. These signals are telemetered to establish spin rate, spin phase, and altitude error determination. Each sensor consists of a germanium lens system, germanium-immersed bolometer, and preamplifier which are mounted to the despun hub of the momentum wheel (see Figure 7-12). They view the earth through a spinning, wheel mounted mirror. The sensors are mounted symmetrically about and canted to the wheel's rotational axis (nominally parallel to y_b). To preclude possible field of view obstruction by the solar arrays, the one-half cone angle (symmetrical about the pitch axis) for the scanner field of view must be less than 30 degrees. Since the half earth angle from the satellite subpoint to the earth's horizon is 67 degrees, the one-half cone angle must be greater than 23 degrees. If the mirror is canted 15 degrees relative to the pitch axis, an earth scan 60 degrees above the spacecraft's local horizon, for a head aligned parallel to the pitch axis, is achieved. By tilting one of the heads 3 to 4 degrees, two earth scan chords are provided using a single mirror. The selection of the optimum alignment angle between the two sensor heads, within the allowable cone angles, is based on a compromise involving: 1) no sun interference, 2) optimum horizon crossing angles, and 3) large lengths and rate of change of the scanned earth chord; i.e., large sensitivity. Sun and moon interference can be eliminated by special circuitry. A sun detector can be used to disable the sensor output when the sun is within the field of view. Additional circuitry delays all output pulses by a fixed time, eliminating moon pulses which are narrower than the minimum earth-horizon pulse.

7.4.4 Nutation Damper

The nutation damper, which is attached to the main body, senses nutation frequency in spacecraft coordinates. Since the angular momentum (H_{yo}) of the spacecraft is maintained constant, but the spin rate varies during wheel spinup, the frequency sensed by the damper is

$$(\lambda_o - \omega_s)$$

where

$$\lambda_o = \sqrt{\frac{H_{yo}}{I_x I_z}} \approx 0.52 \text{ rad/sec is the inertial nutation frequency}$$

$$(H_{yo} = 43 \text{ ft-lb/sec}, \ I_x \approx 50 \text{ slug-ft}^2 \text{ and } I_z \approx 140 \text{ slug-ft}^2)$$

ω_s = spacecraft spin rate, which varies from 0.3 rad/sec to orbit rate (the latter is negligible compared to λ_o).

Over the course of operations, from separation through spinup to normal mode, the damper will sense nutation frequency over the range from 0.22 to 0.52 rad/sec. Furthermore, due to the expenditure of propellant, the maximum nutation rate sensed by the damper may increase to 0.65 rad/sec at the end of life. However, since the spacecraft possesses a nutationally stable configuration ($I_y > I_z > I_x$), reduction of the initial nutation angle can await wheel spinup.

Alternative Dampers

Alternative nutation dampers considered included a viscous ring and eddy current dampers. For the viscous fluid ring damper, the required fluid mass is:

$$m = \frac{I_T}{K r_o^2 \lambda \tau} \tag{34}$$

where

K = constant associated with the ring damper design; typically about 0.16

I_T = minimum transverse inertia; 50 slug-ft^2

r_o = radius of the ring damper; 1.5 feet

τ = time constant associated with rate nutational motion is damped (seconds)

To achieve a 10-minute time constant for nominal operation ($\lambda = 0.52$ rad/sec) requires a fluid mass of approximately 0.45 slugs, or 14.5 pounds. increasing the time will decrease the fluid weight requirement by a proportionate amount.

The baseline design utilizes a tuned eddy current damper that was selected because it maximizes the rate of energy dissipation per unit damper weight and is reasonably insensitive to environmental changes. Furthermore, the eddy current damper can be designed to accommodate the possible 3:1 ratio of maximum to minimum nutation frequency that it is capable of sensing. The weight of magnetic mass required of this pendulum-type damper can be expressed as

$$m = \frac{4\,I_T\,\zeta}{\lambda\,r_o^{\,2}\,\tau} \tag{35}$$

where ζ is the damping coefficient and r_o is the distance from the spacecraft's cg. For $\zeta = 0.1$, the required magnetic tip mass required for a $\tau = 10$-minute time constant at normal nutation frequency is approximately 0.03 slug or about 1 pound. Additionally, the parasitic weight should not exceed the tip mass by more than 50 percent.

Figure 7-14 illustrates how the eddy current damper might be designed to provide the required damping time constant over a wide range of nutation frequencies. Here, in addition to the nominal curve, reflecting an operating temperature of 77°F, curves illustrating the changes in time constant due to temperature variations from -150° to 250°F are shown. To ensure no worse than a 10-minute time constant over the operating range, the damper is tuned for $\tau = 5$ minutes, with a damper natural frequency of about 0.16 rad/sec. This approach will increase the magnetic tip mass to 6 pounds, based on Equation 35, where $\lambda = 0.16$ rad/sec and $\tau = 300$ seconds. However, for this type damper, the distance to the cg can be increased to 3 feet, reducing the tip mass to 1.5 pounds. Additionally, for comparison with the fluid ring damper, the latter damper would be designed to provide a $\tau = 10$ minutes, corresponding to $\lambda = 0.22$ rad/sec, which requires almost 34 pounds of fluid.

Description of Eddy Current Damper

The eddy current nutation damper is basically a pendulum-type device with a magnetic mass mounted on the end of an arm, the other end of which is attached to a flexure pivot. Nutation-induced motion of the magnetic tip mass relative to a conductive plate induces eddy currents, thereby introducing the desired energy dissipation.

Based upon previous comparisons with other types of dampers (e.g., pendulum fluid damper as used on TACSAT and OSO), the eddy current damper possess several distinct advantages: 1) it is a simple passive device that can be tested in a 1-g environment, 2) it has very few environmental
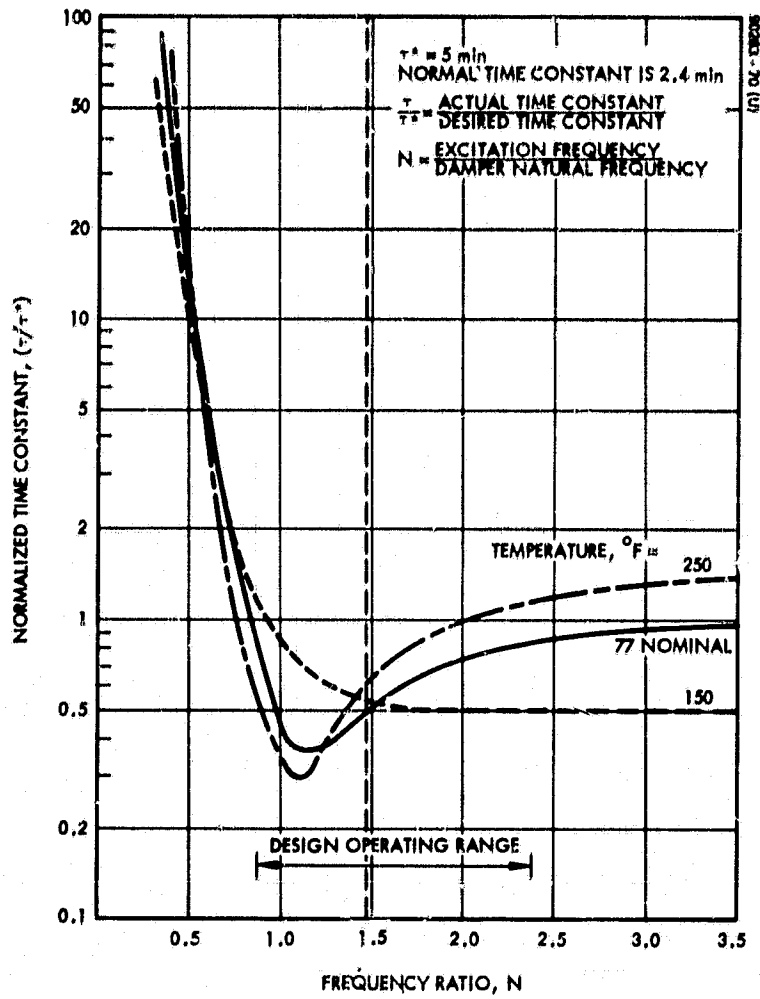
Figure 7-14. Performance Characteristics of
Eddy Current Damper

constraints (the temperature range of -150° to +250°F is tolerable), 3) it will tolerate large oscillations (limited by flexure pivot capability; ±20 degrees achievable), and 4) it is extremely rugged. The performance of the eddy current damper is optimized by maximizing the energy dissipation rate (E) over the operating range; the achieved energy dissipation rate per unit damper weight is substantially greater than for other damper candidates.

7.4.5 Sun Sensor

The sun sensor assembly is required to establish spacecraft attitude relative to the sun line and indicate spin rate during the initial spacecraft spin mode of operation. This assembly will be mounted so that a pulse output occurs whenever the sun is in the y_b - z_b plane with ±64 degrees of the z_b-axis. Such a pulse, occurring once per spacecraft revolution, provides an internal signal for spin reference control and is telemetered to the ground station for initial satellite attitude determination. Two candidate sun sensors are discussed briefly: 1) a Hughes sun sensor and 2) Adcole Corporation's digital solar aspect sensor.

Hughes Sun Sensor

An existing, highly reliable sun sensor design has been used on various Hughes satellite programs such as the ATS, TACSAT, and INTELSAT programs. The sensor is to be modified slightly to provide a ±64-degree (128 degrees total) field of view as compared to the present 90 degrees total field of view. The assembly serves two functions: spin rate detection, and spacecraft attitude sensing. The sun sensor assembly consists of two identical sensor units mounted on a precision bracket. Each sensor consists of a n/p silicon photovoltaic cell and a load resistor and two clam-like aluminum shells.

Sun sensor geometry is illustrated in Figure 7-15. A fan beam slit sensor parallel to the y_b-axis provides the desired sun gate. A second fan beam (ψ_2), inclined to the primary slit (ψ), is utilized to provide sun aspect angle for attitude determination purposes. The ψ and ψ_2 pulses are telemetered to the ground after appropriate shaping. With both prelaunch and in-flight calibration of the unit, and by smoothing the data over a number of measurements, the sun aspect (ϕ) angle uncertainty can be reduced to 0.3 degree.

Adcole Sensor

Adcole Corporation manufactures a digital solar aspect sensor that satisfies system requirements. A sensor consists of detector head and electronics with a 128 by 1 degree field of view. The detector head consists of a Gray-coded reticle, silicon photocells, and a housing.

The Gray-coded reticle is a small oblong block of fused quartz with a slit centered along the top surface and a 7-bit Gray-coded pattern on the bottom surface. Sunlight passing through the slit is screened by the pattern to either illuminate or not illuminate the photocells below. The outputs of

$$\cot \phi = \sin \left[(\psi - \psi_2) - 35^{\circ} \right] \cot 35^{\circ}$$

where $(\psi - \psi_2)$ — ANGLE IN DEGREES ABOUT
SPIN AXIS BETWEEN
ψ OUTPUT PULSE AND
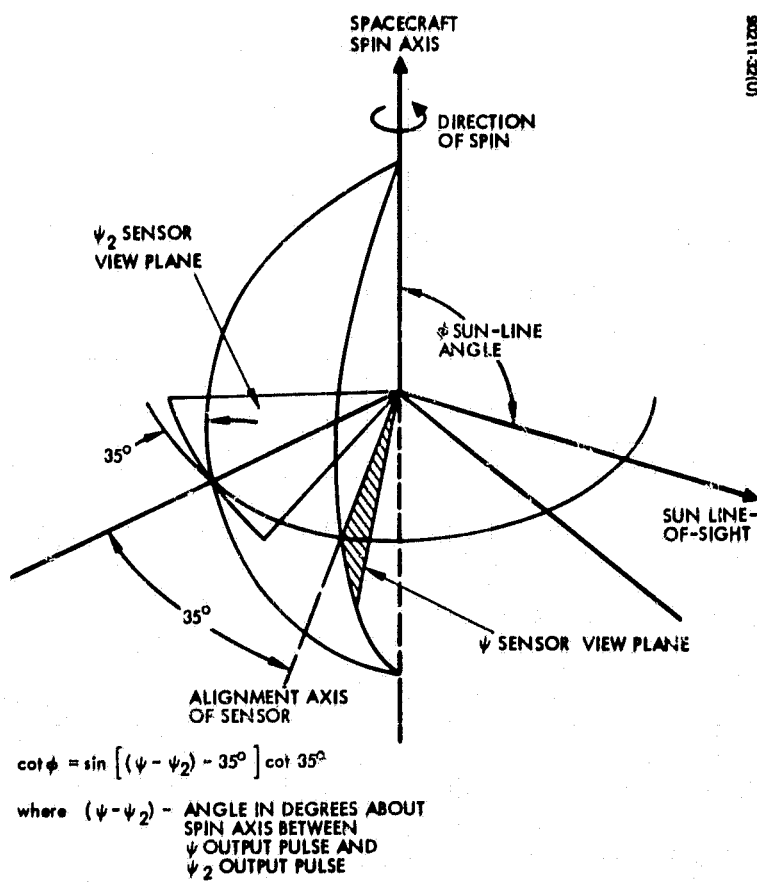ψ_2 OUTPUT PULSE

Figure 7-15. Sun Sensor Geometry

the photocells comprise a digital word representative of the solar aspect angle about one axis. An additional photocell is usually included which is always "ON" when the sun is within a field of view of the detector head. The output of this cell is used as an AGC signal to compensate for the photocell outputs as a function of solar angle. This permits accurate angular determination of the transition between resolution elements. This sensor possesses a 1-degree resolution and can provide angle determination accuracy at the transition between resolution elements of 0.25 degree.

7.5 DYNAMIC EFFECTS ON THE SPACECRAFT DUE TO ANTENNA MOTION

The data transmission antenna with its required large gimbal angles raises concern for the effect its motion may have on the pointing accuracy and angular rates of the spacecraft. A detailed development of the equations of motion was performed, * but only the principal results and a summary of the analysis development is presented here.
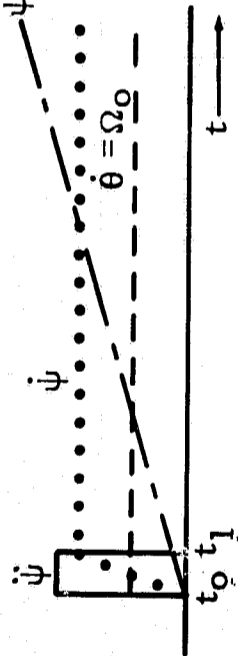
7.5.1 Principal Results

The analysis revealed that worst case motions of the antenna result in perturbations which are negligible relative to the pointing requirements of the payload described in Section 3. The most severe maneuver involving antenna positioning is dictated by the requirements for slewing from one DRS to another. For analysis purposes, it is assumed that this requires a 180-degree azimuth maneuver within a 5-minute interval. During this maneuver, pitch motion of the satellite is constrained to lie within ±10 degrees of the earth's north pole.

The model developed evaluates the impact of antenna slewing, about two of three gimbal axes, on spacecraft motion. Due to the complexity of the nonlinear, time-varying differential equations developed for the rigorous model, the large slewing maneuver was divided into segments so that small angle approximations could be utilized to expedite an analytical solution. The characteristic equations of motion, where motions of the antenna serve as forcing functions, were solved for the case where the antenna rotates at orbital rate about the pitch axis and is slewed at a maximum rate (180 degrees in 5 minutes) in antenna azimuth from on DRS to another. Resulting spacecraft maximum rates are typically less than 10^{-3} deg/sec, while corresponding spacecraft displacements are less than 10^{-2} degrees (36 arc seconds) at the end of a 5-minute time interval. Antenna slewing modes and corresponding motion of the spacecraft's angular velocity vector are summarized in Table 7-11.

---

* "Analysis of LAS Antenna-Spacecraft Interaction," Hughes Aircraft Co., IDC No. 2292/707, 18 July 1969.

TABLE 7-11. ANTENNA SLEWING MODES AND RESULTING SPACECRAFT MOTION

A. ANTENNA SLEWING MODES

B. SOLUTION TO "SMALL ANGLE" EQUATIONS $(\lambda = \lambda_1 \ \lambda_2 = 0.52$ rad/sec$)$

Mode	Transverse Rate, deg/sec	Transverse Displacement, degrees
$t_o \leq t \leq t_1$ $(t_o = 0; \ t_1 = 1$ second$)$	$\omega_x(t) \approx 3.5 \times 10^{-3} \left[1 - \cos \lambda t \right]$ $\omega_z(t) \approx 3.9 \times 10^{-6} \, t$ $\quad -2.1 \times 10^{-3} \sin \lambda t$	$\theta_x < 7 \times 10^{-3}$ $\theta_z < 4.2 \times 10^{-3}$
$t \geq t_1$ $(t - t_1) =$ $18 \cdot \Delta t = 300$ seconds	$\omega_x(t) \approx 3 \times 10^{-9}$ $\quad -6.2 \times 10^{-6}$ $\quad \cos (\lambda t - 90°)$ $\omega_z(t) \approx -9.2 \times 10^{-10} t^2$ $\quad + 3.8 \times 10^{-6} (t - \cos \lambda t)$	$\theta_x < 2.4 \times 10^{-4}$ $\theta_z < 9 \times 10^{-3}$

7.5.2 Analysis Summary

The antenna-spacecraft relationship is illustrated in Figure 2-1; but, for analysis, coordinate systems and parameters must be defined; these are shown in Figure 7-16. The spacecraft rotates about its y_b-axis, which is oriented normal to the orbit plane, at orbital rate ($\Omega_o \approx 1.1 \times 10^{-3}$ rad/sec for a 300 n.mi. altitude circular orbit). Contributing a pitch momentum bias of 43 ft-lb/sec is the pitch momentum wheel, nominally aligned parallel to the spacecraft's pitch axis and rotating at 500 rpm. A pair of solar arrays have their drive axis also oriented parallel to the pitch axis. However, since they rotate at orbital rate, their contribution to the motion of the spacecraft is small as compared to that of the wheel. The antenna employs a three-gimbal system. Driven at orbital rate is the primary gimbal (spacecraft referenced) used to maintain the array's x_a and z_a axes fixed in inertial space. Rotation about the z_a and x_a axes represents the action of the antenna's azimuth and elevation gimbals, respectively.

The antenna consists of a planar array, 3 feet on each side, with the array and support structure (including electronic boxes mounted on the rear surface of the array) each weighing approximately 8 pounds. Correspondingly, the spacecraft will weigh from 850 to 1000 pounds. Calculated array moments of inertia, about axes fixed to the array and originating at its center of mass (CM$_A$), are $I_{x_{a_2}} = I_{z_{2_2}} = 0.25$ slug-ft^2 and $I_{y_{a_2}} = 0.5$ slug-ft^2. Note that the θ axis of rotation is displaced from the antenna's center of mass by approximately 1 foot. Estimates of minimum spacecraft inertias are $I_{y_b} = 150$ slug-ft^2 and $I_{z_b} = 140$ slug-ft^2.
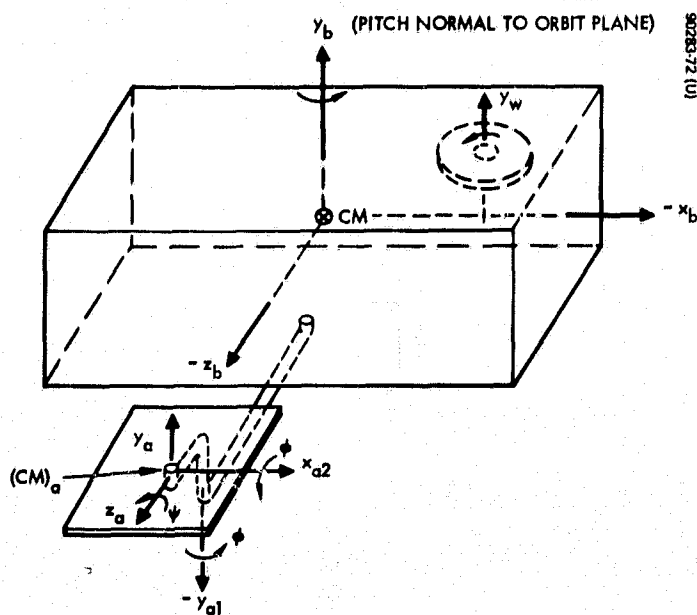

Figure 7-16. Antenna and Spacecraft Configuration

The fundamental equation of motion is given by

$$\mathcal{A} \cdot \dot{\bar{\omega}} + \bar{\omega} \; \mathcal{A} \cdot \bar{\omega} = - \left[\dot{\mathcal{A}} \right] \cdot \bar{\omega} - (\bar{\omega} \times \bar{h}) - \dot{\bar{h}}$$

where

$\mathcal{A}$ = inertia dyadic of the vehicle

$\bar{\omega}$ = angular velocity of the vehicle

$\bar{h} = \bar{h}_w + \bar{h}_a$

$\bar{h}_a$ = angular momentum of the rotating antenna

$\bar{h}_w$ = angular momentum of the rotating wheel

Antenna motion causes changes in the spacecraft inertia dyadic and results in reaction torques. Taking these effects into account, as well as the above mentioned assumption that the slewing maneuver is performed during 20 degrees of orbital motion, i.e., $-10 \le \theta \le 10$ degrees, the following equations of motion are obtained.

1) $\quad I_{x_o} \dot{\omega}_x - 0.5 \left(I_{a_y} - I_{a_x} \right) \sin 2\psi \, \dot{\omega}_y - A(\psi) \cdot \theta \, \dot{\omega}_z + \left[\left(I_{z_o} - I_{y_o} \right) \omega_y \right.$

$\left. - h_{w_o} \right] \omega_z - A(\psi)\theta \, \omega_x \omega_y - B(\psi)\theta \, \omega_y^2 + 0.5 \left(I_{a_y} - I_{a_x} \right)$

$\sin 2\psi \, \omega_x \omega_z + B(\psi)\theta \, \omega_z^2 = \left(I_{a_y} - I_{a_x} \right) \sin 2\psi \, \dot{\psi} \omega_x$

$+ \left(I_{a_y} - I_{a_x} \right) \cos 2\psi \dot{\psi} \omega_y + C(\psi, \dot{\psi}, \theta, \dot{\theta}) \, \omega_z - I_{a_z} \dot{\psi} \omega_y$

$+ I_{a_y} \omega_z \dot{\theta}$

2) $\quad I_{y_o} \dot{\omega}_y - 0.5 \left(I_{a_y} - I_{a_x} \right) \sin 2\psi \, \dot{\omega}_x - B(\psi)\theta \, \dot{\omega}_z + \left(I_{x_o} - I_{y_o} \right) \omega_x \omega_z$

$+ A(\psi) \, \omega_x^2 + B(\psi) \, \omega_x \omega_y - 0.5 \left(I_{a_y} - I_{a_x} \right) \sin 2\psi \, \omega_y \omega_z$

$- A(\psi)\theta \, \omega_z^2 = \left(I_{a_y} - I_{a_x} \right) \sin 2\psi \, \dot{\psi} \omega_y + C(\psi, \dot{\psi}, \theta, \dot{\theta}) \, \omega_x$

$+ D(\psi, \dot{\psi}, \theta, \dot{\theta}) \, \omega_z + I_{z_a} \dot{\psi} \omega_x - I_{y_a} \ddot{\theta}$

3) $I_{z_0}\dot{\omega}_z - A(\psi)\theta\,\dot{\omega}_x - B(\psi)\theta\dot{\omega}_y - \left[\left(I_{x_0} - I_{y_0}\right)\omega_y - h_{w_0}\right]\omega_x$

$\quad - 0.5\left(I_{a_y} - I_{a_x}\right)\sin 2\psi\,\omega_x^2 - B(\psi)\theta\,\omega_x\omega_z + 0.5\left(I_{a_y} - I_{a_x}\right)$

$\quad \sin 2\psi\,\omega_y^2 + A(\psi)\,\theta\omega_y\omega_z = -mr_0^2\dot{\theta}\omega_z + C(\psi,\dot{\psi},\theta,\dot{\theta})\,\omega_x$

$\quad + D(\psi,\dot{\psi},\theta,\dot{\theta})\,\omega_z - I_{a_y}\dot{\theta}\omega_x - I_{z_a}\ddot{\psi}$

where the following relationships have been noted and made use of:

$$I_{x_0} \gg \left|I_{a_x} - I_{a_y}\right| \qquad ; \qquad \left|I_{x_0} - I_{y_0}\right| \gg 2\left|I_{a_y} - I_{a_x}\right|$$

$$I_{y_0} \gg \left|I_{a_y} - I_{a_x}\right| \qquad ; \qquad \left|I_{z_0} - I_{y_0}\right| \gg \left|mr_0^2 + \left(I_{a_x} - I_{a_y}\right)\right|$$

$$I_{z_0} \gg \left|mr_0^2\,\theta\right|$$

The above equations represent a rigorous formulation of the effects of antenna rotations, during a slewing maneuver, on spacecraft motion. The set of simultaneous differential equations are inherently nonlinear and are characterized by nonlinear coefficients which are trigonometric functions of the gimbal angles ψ and θ, as well as their respective rates. Such a set of equations could best be solved utilizing computer simulation techniques.

If the ψ gimbal rotation is divided into a series of small maneuvers, a number of approximations can be made to simplify the above equations, yielding

$$I_{x_0}\dot{\omega}_x + \left[\left(I_{z_0} - I_{y_0}\right)\Omega_0 - h_{w_0} - I_{a_y}\dot{\theta}\right]\omega_z = -I_{a_z}\Omega_0\dot{\psi} + mr_0^2\Omega_0^2\theta \quad (36)$$

$$I_{z_0}\dot{\omega}_z - \left[\left(I_{x_0} - I_{y_0}\right)\Omega_0 - h_{w_0} - I_{a_y}\dot{\theta}\right]\omega_x = -I_{a_z}\ddot{\psi} \quad (37)$$

$$\omega_y = \Omega_0 \quad (38)$$

The solution to Equations 36 and 37 was obtained for two modes: 1) acceleration about the azimuth gimbal axis, and 2) constant azimuth angular rate. The solutions for the spacecraft angular rates are shown in Table 7-11, and for the particular maneuver chosen, the attitude deviation was calculated.

8. POWER SYSTEM

8.1 DESIGN REQUIREMENTS

One of the basic objectives of this conceptual design effort was to arrive at a spacecraft with power and stabilization capabilities adequate for a variety of payloads. Estimates of spacecraft power requirements were made in the initial stages of the study based upon previous experience. With the representative payload discussed in Section 3, the power required is 283 watts. It was decided to add a significant contingency requirement (about 20 percent) and to also require power to maintain all but the payload and data transmission system during eclipse. The design lifetime was set at 1 year, and the bus voltage set at 25 volts. The power system requirements are summarized below.

End of life total solar panel capability . . . . . 500 watts

End of life load capability (sunlight) . . . . . 350 watts

Minimum bus voltage at loads . . . . 25 volts dc

Mission life . . . . 1 year

(In 300 n.m, sun-synchronous 95.9 minutes orbit, with 33.6 minutes maximum eclipse).

The design analysis assumes that the eclipse load represents the greatest discharge to be experienced by the battery. It is possible that load requirements from launch until nominal orbit operation will be greater, but preliminary analysis indicates that launch and injection loads can be accommodated by the eclipse batteries.

8.2 SOLAR ARRAY CONSIDERATIONS

In a simple design, the current capability of the main bus is determined by the voltage versus current characteristics (V-I) of the solar panel. Changes in solar illumination primarily produce variations in solar panel current capability. As seen in Figure 8-1, when the solar panel current capability changes, the entire V-I characteristic changes, resulting in a bus voltage shift. For this reason, it is important that the proper V-I behavior be designed into the solar panel to account for seasonal variations, radiation damage effects, and temperature variation.
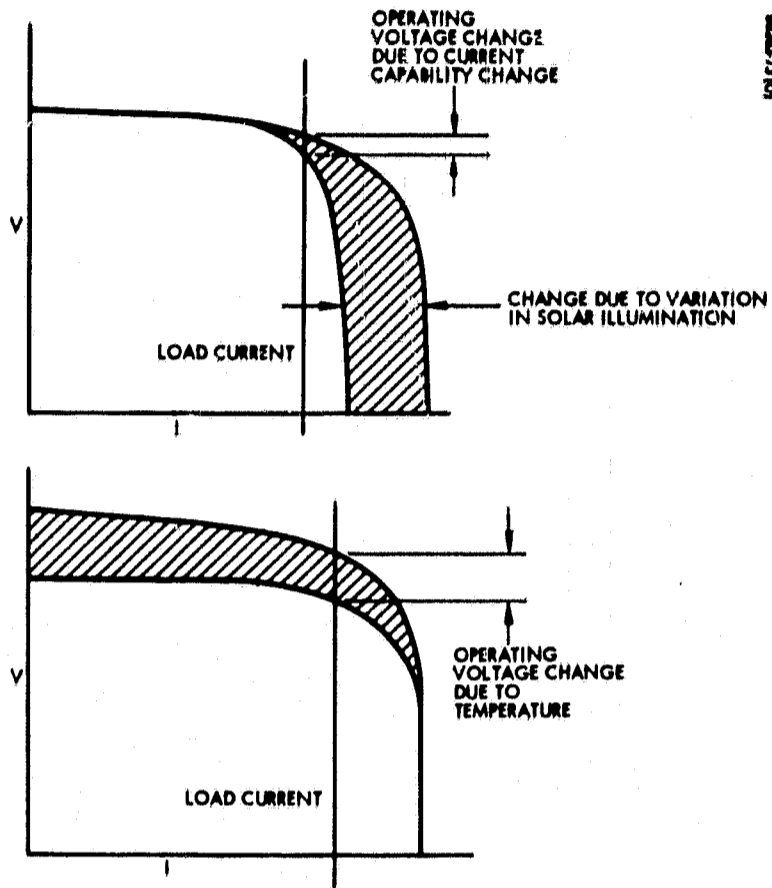
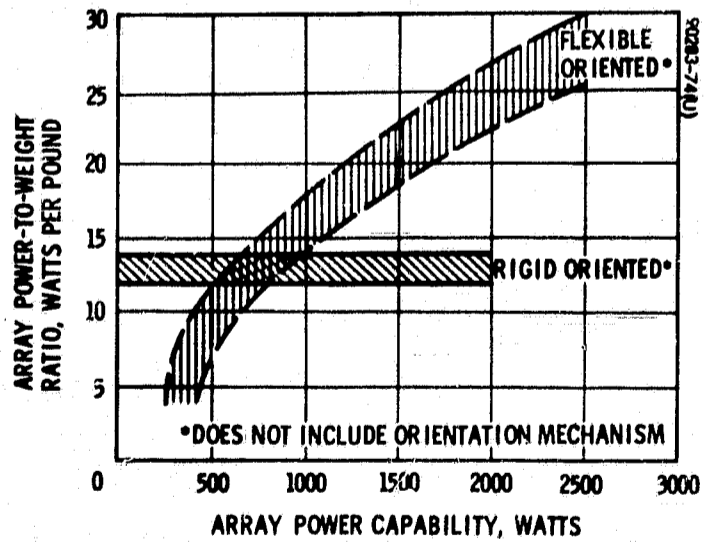Figure 8-1.   Voltage/Current Solar Panel Behavior

Figure 8-2.   Comparison of Solar Array
Specific Power Ratios

Predictions for power, current and voltage degradation for this mission assume the use of N/P, 12 mil, 10 ohm-cm silicon solar cells protected by 7 mil fused quartz coverslides. Only front side penetrating radiation has been considered, i.e., for the purpose of this analysis an infinite backshield has been assumed. In addition, it is assumed that the coverslide assembly does not degrade, and that the coverslide is an effective shield against low energy radiation. Radiation flux levels and corresponding degradation numbers are presented in Table 8-1.

Another consideration is that the additional power required for battery charging must be provided in an acceptable form. Battery voltage efficiencies, i.e., voltage on discharge, voltage on charge, and voltage losses in the control electronics must be accounted for in the design of the solar panel or the bus voltage will drop below the level required for proper system operation.

For power levels in the 0 to 2.5-kw range, three general array configurations are of practical importance: 1) cylindrical spinning, 2) rigid oriented, and 3) flexible oriented. Hybrid combinations of these configurations are also practical, particularly for power levels in the 1.5 to 2.5-kw class. Since the LAS is an earth-oriented, nonspinning vehicle, the spinning array is not applicable. Figure 8-2 presents comparative power-to-weight ratio data for the latter two configurations.

Rigid-oriented arrays are limited chiefly by the mechanical problems associated with stowage and deployment. The realizable power-to-weight ratio is essentially invariant over the power range of interest here. However, array reliability drops rapidly with increasing power level due to the corresponding increase in mechanical complexity. The orientation requirement is an additional penalty in both cost and weight.

Flexible oriented arrays offer a significant improvement in power-to weight ratio for array power levels greater than approximately 1 kw. The crossover point with rigid-oriented designs is difficult to define precisely but generally occurs in the 0.5 to 1-kw range. The fixed weights associated with stowage and deployment limit the realizable power-to-weight ratio for lower power levels.

In order to provide growth capability and for packaging ease, a flexible oriented solar array is selected. Figure 8-3 illustrates such an array, extendible in two directions from the storage drum. Due to packaging, deployment, and general configuration requirements, the LAS will have two such arrays, each extendible approximately 12 feet from the spacecraft in one direction.

TABLE 8-1. NOMINAL RADIATION ENVIRONMENT AND DEGRADATION PREDICTIONS

Time in Orbit, months	Accumulated Equivalent Flux, electrons/cm^2	Normalized Power, P/P_o	Normalized Voltage, V/V_o	Normalized Current, I/I_o
Nominal				
3	1.9×10^{13}	0.967	0.988	0.979
6	3.8×10^{13}	0.944	0.979	0.964
9	5.7×10^{13}	0.925	0.971	0.952
12	7.9×10^{13}	0.908	0.965	0.941
Worst Case				
3	4.7×10^{13}	0.934	0.975	0.958
6	1.0×10^{14}	0.891	0.958	0.930
9	1.5×10^{14}	0.868	0.949	0.915
12	2.0×10^{14}	0.847	0.941	0.901

8.3 BATTERY CELL SELECTION

Considering the number of charge-discharge cycles that the satellite secondary power source (battery) will be subjected to (in excess of 5000), the nickel-cadmium cell is the only space qualified electrolytic cell available. Refer to Figure 8-4 for a graph of nickel-cadmium cell cycle life versus temperature.

The power subsystem will be protected against the loss of the complete battery due to an open cell by shunting each cell with protective diodes, as shown in Figure 8-5.

Under normal operating conditions, the current flow during cell charging is denoted by I_c and cell discharge is denoted by I_d. If a cell without diode protection were to open, the complete battery would be lost as a source of energy. With diode protection, an open cell would be bypassed during charge by the three series-connected diodes, resulting in a current flow around the cell, denoted by I_{co}. The discharge current, I_{do}, flows through the single protective diode.

Any cell in a series string not capable of discharging at a rate set by the load will be subjected to forced voltage reversal and charged in the reverse direction. This condition of forced reversal will lead to electrolytic decomposition with gas formation, which may cause catastrophic destruction of the sealed cells. Results of preliminary tests show that the reverse critical voltage (the reverse potential below which the cell begins to produce gas), is approximately -0.2 volt. These results indicate that if the reverse cell voltage can be clamped between 0 and -0.2 volt, the cell will not generate gas. The use of germanium diodes as "antireversal" devices has been partially successful in preventing cell damage due to this phenomenon. The germanium diode reaches its conduction threshold at an approximate cell voltage of -0.3 volt. When fully conducting, the diode shunts approximately 90 percent of the load current around the cell, resulting in a decrease in the rate of gas generation. Also, the diode does not allow the cell potential to reach -1.5 volts, thereby preventing the electrolytic decomposition of water.

Define C as that charge rate in amperes for which the total battery capacity would be achieved in 1 hour. It has been shown experimentally that a desirable charge rate for a power system with very limited overcharge conditions is C/6. Continued overcharge above a nominal cell voltage of 1.43 volts at a C/6 rate and at low temperatures leads eventually to hydrogen gas production within the cell and can lead to cell damage through overpressurization. Referring to Figure 8-6, it is seen that a "tail-up" in cell voltage occurs during overcharge at temperatures below 80 degrees F. Figure 8-6 is given for a charge rate of C/8, and would be even more dramatic at C/6. To protect against cell overpressurization, battery terminal voltage will be sensed during charging and when this voltage reaches 34.32 volts (1.43 volt/cell average), a circuit within the booster will reduce the charge current to a rate of C/10, or 2.2 amperes. This is of particular significance during the noneclipse portions of the satellite mission.
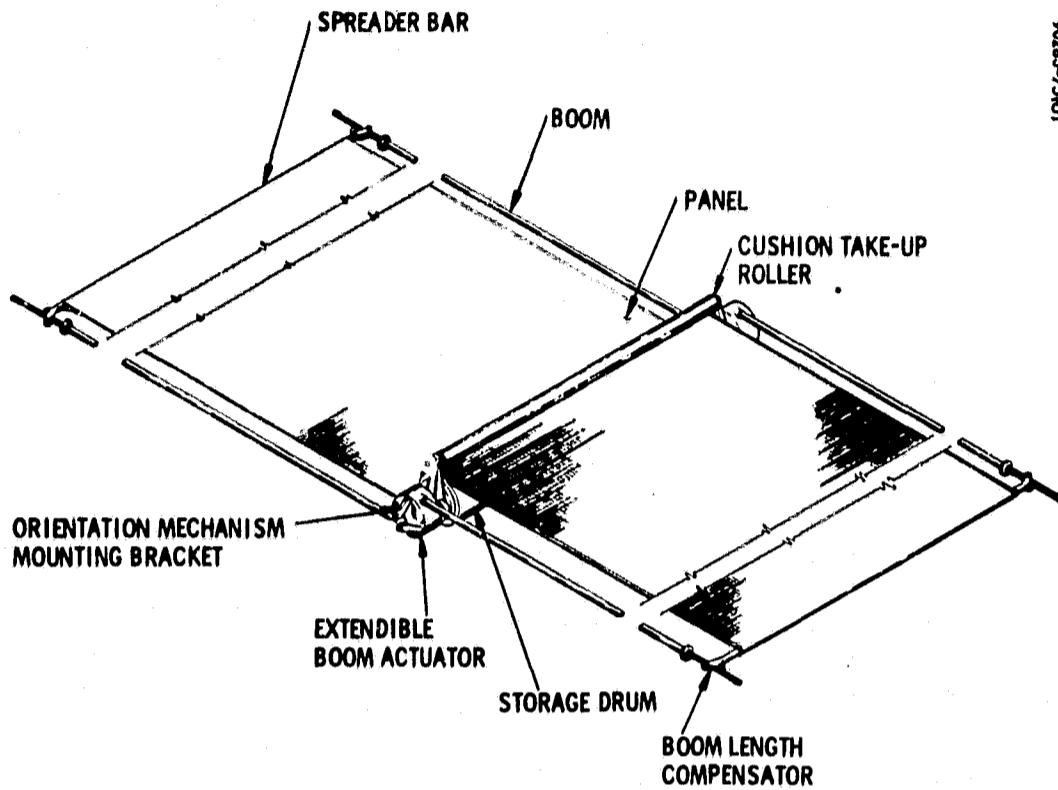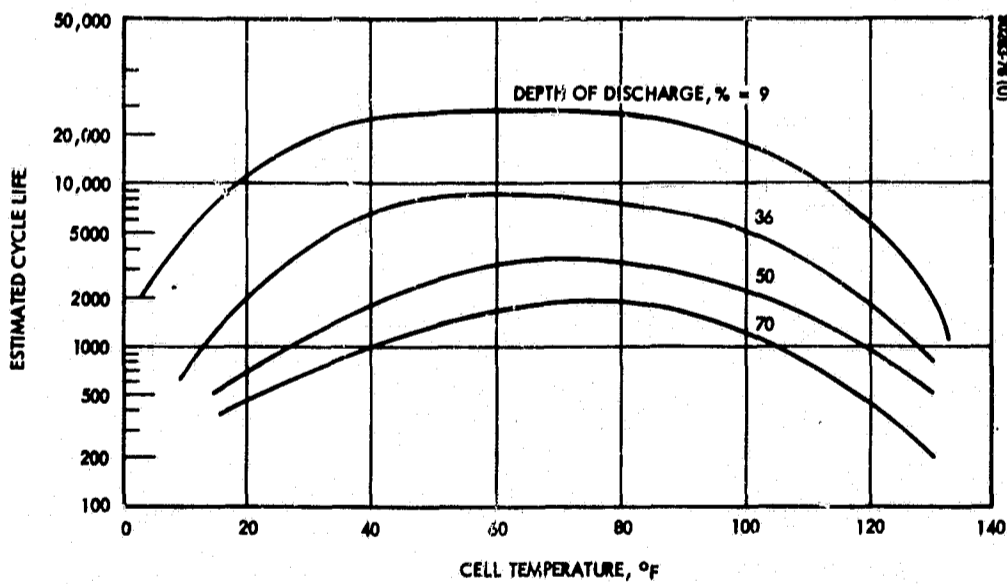
Figure 8-3. Flexible Solar Array

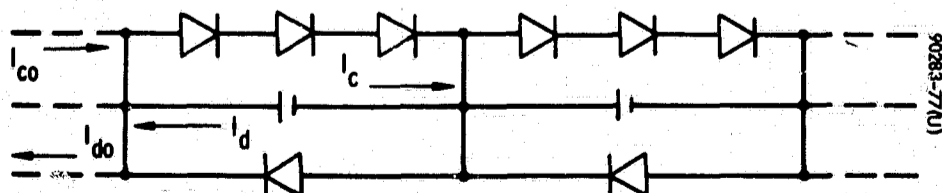Figure 8-4. Nickel-Cadmium Battery Cycle Life versus Temperature

Figure 8-5. Battery Cell Protection Method

System design, summarized shortly, yielded a battery depth of discharge of only 13.2 percent. Considering repetitive cycling to this shallow depth of discharge, it would be highly desirable to allow the spacecraft to recondition the battery approximately every 30 days. This reconditioning could be accomplished by not allowing the battery to receive any charge current for three orbits, resulting in the depth of discharge going to approximately 40 percent, and then altering the load profile so that full charge is re-established in the next few orbits.

8.4 SYSTEM DESCRIPTION

A block diagram illustration of the power system is shown in Figure 8-7. During periods of solar illumination, solar array voltage is boosted for battery charging. This precludes the necessity of battery charge solar arrays that complicate solar cell layout and slip ring requirements and reduce the total array power available for load utilization.

As the bus voltage drops, because of the beginning of eclipse, it is sensed by a circuit in the battery discharge controller and when it reaches a prescribed level, the battery is switched onto the bus. When this switching occurs, a counter in the discharge controller maintains the battery discharge state for a preset time interval equal to the eclipse period. At the end of this interval, the solar panel will again be illuminated, battery discharging will cease, and charging will begin. This technique eliminates the momentary loss of bus power due to simply switching directly between solar panel and battery discharge circuits.

The solar arrays are driven by a motor with a constant speed equal to the orbital angular velocity. Correction capability by ground command is provided.

8.5 SYSTEM DESIGN

The following is a brief summary of the approach used to design the power subsystem:

1) Beginning-of-life solar panel capability

- End of life capability — 500 watts

- According to Table 8-1 (P/P_o) worst case - 0.847

- Therefore, beginning-of-life requirement is,

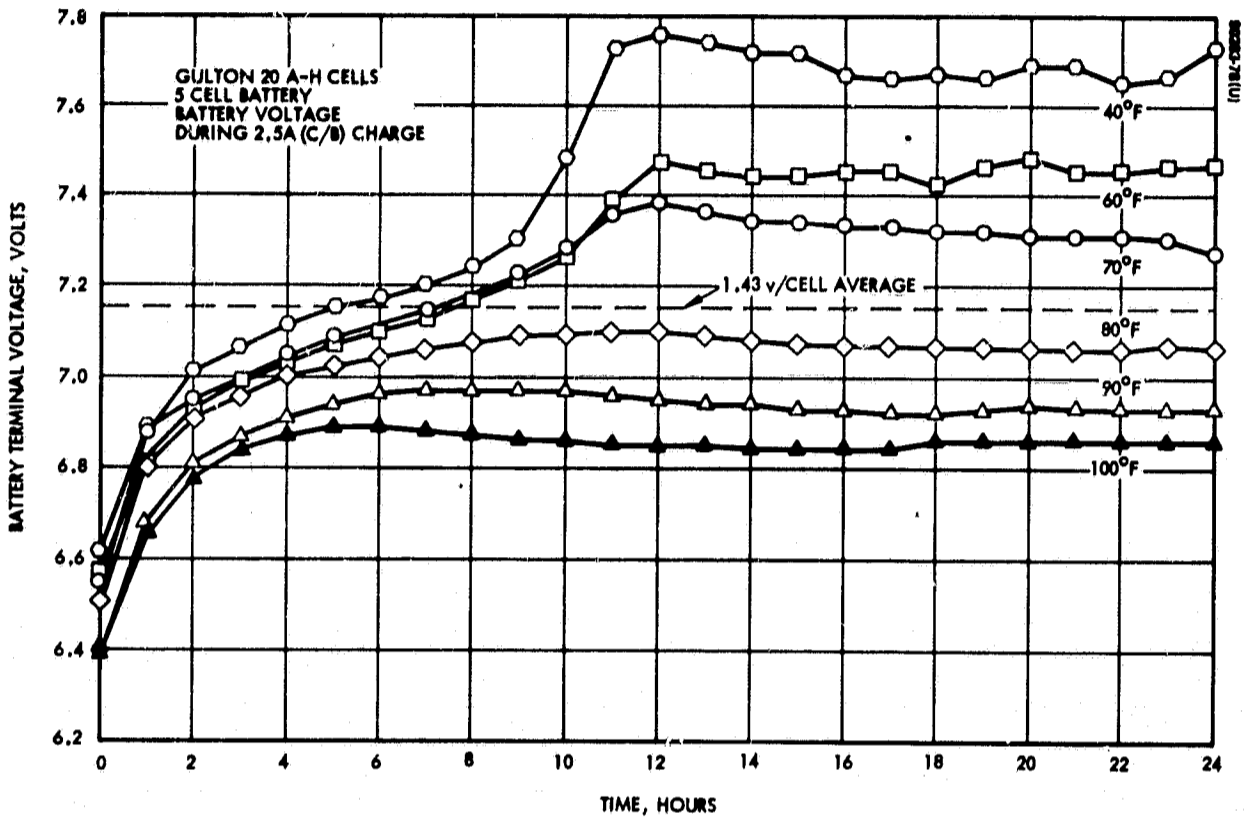$$P_o = \frac{500}{0.847} = 590 \text{ watts}$$

Figure 8-6. Nickel-Cadmium Battery Terminal Voltage
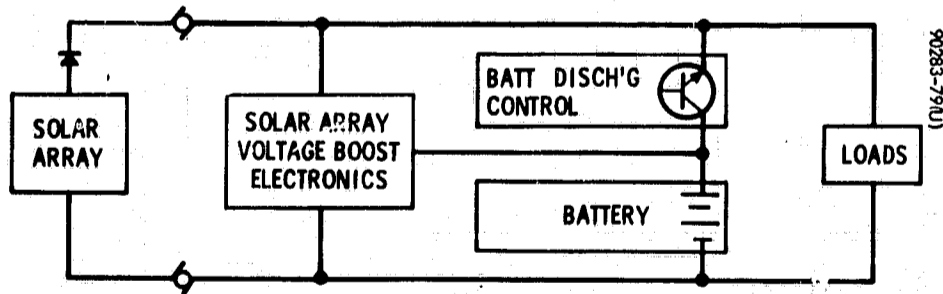versus Time During Charging

Figure 8-7. Power System Block Diagram

2) Solar panel voltage

- V_{sp} = 25 + 0.5 volt (harness drop between loads and discharge controller) + 0.5 volt (slip ring drop plus harness drop between discharge controller and solar panel) + 0.9 volt (solar panel diode)

V_{sp} = 26.9 volts

3) Solar panel voltage at input to booster

- $V_{B\ in}$ = 26.9 - 0.9 volt (diode) - 0.5 volt (harness and slip ring) = 25.5 volts

4) Required number of battery cells

- $V_{batt\ min}$ = 25 + 1.5 volts (discharge switch) + 0.5 volt (harness drop between discharge controller and loads) = 27.0 volts

- Minimum cell voltage on discharge = 1.2 volt/cell, (for shallow depth of discharge system)

- Therefore, $N = \dfrac{27 \text{ volts}}{1.2 \text{ volt/cell}} = 22.5$ cells

- Adding one cell for redundancy gives 23.5, or 24 cells

5) Battery charging capability

- Using worst case booster efficiency of 85 percent, P_{chg} = (150 watts) (0.85) = 127.5 watts

- Maximum battery terminal voltage during charge = (1.43 volt/cell)(24 cells) = 34.3 volts

- Charge current $= \dfrac{127.5 \text{ watts}}{34.3 \text{ volts}} = 3.72$ amperes

6) Battery cell size

- In order to keep charge current at a C/6 rate, which has been shown to be a desirable rate for very limited overcharge conditions, the battery cell size will be C= (6) (3.72) = 22.3 or 22 amp-hr (standard size)

7) Determination of eclipse load capability

- Considering an average charge efficiency of 75 percent (at 78 °F), through the normal range of low orbit depths of discharge (5 to 15 percent) and at a C/6 charge rate, the spacecraft eclipse load current (I_d) is calculated as follows:

$$(I_c) \, (\eta_c) \, (t_c) = (I_d) \, (t_d)$$

where:

I_c = charge current

η_c = charge efficiency

t_c = charge time

I_d = discharge current

t_d = discharge time

- $I_c = \dfrac{(I_c) \, (\eta_c) \, (t_c)}{t_d} = \dfrac{(3.72) \, (0.75) \, (62.3)}{(33.6)}$

- $I_d = 5.17$ amperes

- The eclipse load capability is then $P_d = (5.17$ amperes$) (25$ volts$)$, $= 129$ watts

8) Depth of discharge (DOD)

- Ampere hours expended during eclipse,

$$\text{Amp-hr} = (5.17 \text{ amperes}) \left(\frac{33.6 \, M}{60 \, m/h} \right) = 2.9 \text{ amp-hr}$$

- $\text{DOD} = \left(\dfrac{2.9}{22} \right) (100) = 13.2$ percent

9) Boost electronics gain factor

- $K = \dfrac{\text{maximum battery terminal voltage}}{\text{booster input voltage}} = \dfrac{34.3}{25.5} = 1.345$

10) Approximate subsystem weight, pounds

- Solar panel 53.0

- Deployment and orientation mechanisms
  and associated electronics 40.0

- Charge/discharge control electronics 5.0

- Battery. 63.5

- Total 161.5

The power system design is summarized in Table 8-2.

TABLE 8-2. POWER SYSTEM DESIGN SUMMARY

Sunlight capability	350 watts
Eclipse capability	129 watts
Beginning of life solar array capability	590 watts
End of life array capability (after 1 year)	500 watts
Bus voltage	25 volts
Solar panel voltage	27 volts
Number of battery cells	24
Depth of discharge	13.2 percent
Solar array weight	53 pounds
Deployment and orientation mechanisms	40 pounds
Electronics	5 pounds
Battery weight	64 pounds

9. CONFIGURATION AND PACKAGING

The basic configuration of the spacecraft was developed in a logical process starting with design objectives and the decision to use a Thor-Delta booster. The improved Thor-Delta booster is a relatively inexpensive vehicle, yet is capable of putting 1,300 pounds into a 500 n.mi. circular, polar orbit. The configuration is significantly influenced by the Delta shroud limitations shown in Figure 9-1.

With the size allowed by the shroud, power by conversion from incident solar energy would be inadequate for the estimated loads if only the surface of the main body was available for energy collection. Thus, solar arrays are required. Since the solar arrays are the largest appendage to the spacecraft, it was further decided to provide an orientation mechanism to obtain the greatest efficiency.

The momentum wheel technique for angular momentum bias was chosen as the basic stabilization concept, with magnetically produced torques to maintain the angular momentum and to orient its direction. A mirror, mounted to the wheel, scans the earth and reflects its field of view through the hollow wheel shaft to two sensors, thus allowing determination of the earth's leading and trailing edges at two different "latitudes." These signals are then processed to provide the required attitude error signals.

Considering the basic spacecraft shape, a flat surface facing the earth has advantages for mounting instruments and sensors. A flat side parallel to the orbit plane will allow space between it and the shroud for the protruding, earth scanning mirror. If both sides parallel to the orbit plane are flat, the stowage of the solar arrays is facilitated. In particular, if the solar arrays are flexible and rolled in tubes for stowing during launch, the tubes can be readily accommodated between flat spacecraft surfaces and the cylindrical shroud. Based upon these considerations, as well as structural simplicity, a rectangular box shape was chosen. The flexible solar array, deployable from a cylindrical tube, was chosen both for packaging ease and growth capability.

The solar arrays must be rotated 360 degrees with respect to the spacecraft body in order to maintain their sun orientation. In order to avoid interference with the data transmission system antenna, which covers the hemisphere outward from the LAS away from the earth, the solar arrays must be limited in their dimension that is parallel to the orbit plane. Then, to provide the desired power level, the solar arrays must have a much longer dimension normal to the orbit plane.

Both the solar arrays and the momentum wheel have their axis of rotation normal to the orbit plane. Since these items are relatively large,

it is apparent that the sides parallel to the orbit plane must be longer than the dimensions perpendicular to the orbit plane. In order to accommodate both the solar arrays and the momentum wheel with its earth-scanning requirements, the length was set at 88 inches. The shroud diameter then limited the cross section to 36 by 36 inches, which is a greater volume than needed for the present payload, but it allows excellent growth potential.

A hydrazine system is provided for velocity change and inclination control. The system is basically a simple low pressure, blowdown system utilizing butyl rubber diaphragms in the tanks for positive fuel expansion. The configuration shows four titanium tanks containing 80 pounds of N_2H_4 at 70 percent fill. Four tanks are used to minimize a center of gravity shift as the fuel is depleted. Two opposed jets give velocity control fore and aft and two jets normal to the orbit plane allow inclination control. These jets are approximately 5-pound thrust and are presently in use on several satellites.

The shroud constraints dictate that the data transmission antenna and the telemetry and command antenna be deployed into proper operation position. This is not considered excessively complicated, since it requires only a single, rotary 90-degree motion.

The LAS utilizes the TIROS M booster-to-spacecraft adapter. The boost loads are carried through two paths; one through a cone-cylinder central structure, the other through a column system attached to the base of the cone. These paths are mated by shelves from the cylinder to rectangular rings joined to the columns on each face. Light, stiff, tapered ribs may be used to provide support for the equipment carrying shelves. The shelf concept allows the closing faces to be relatively simple in construction and removable for access to the spacecraft interior. Booster weight allowance indicates that exotic materials for construction are not required and will probably not be required with advanced Thor boosters.

Figure 9-2 illustrates most of the major configuration, packaging, stowage, and deployment concepts.
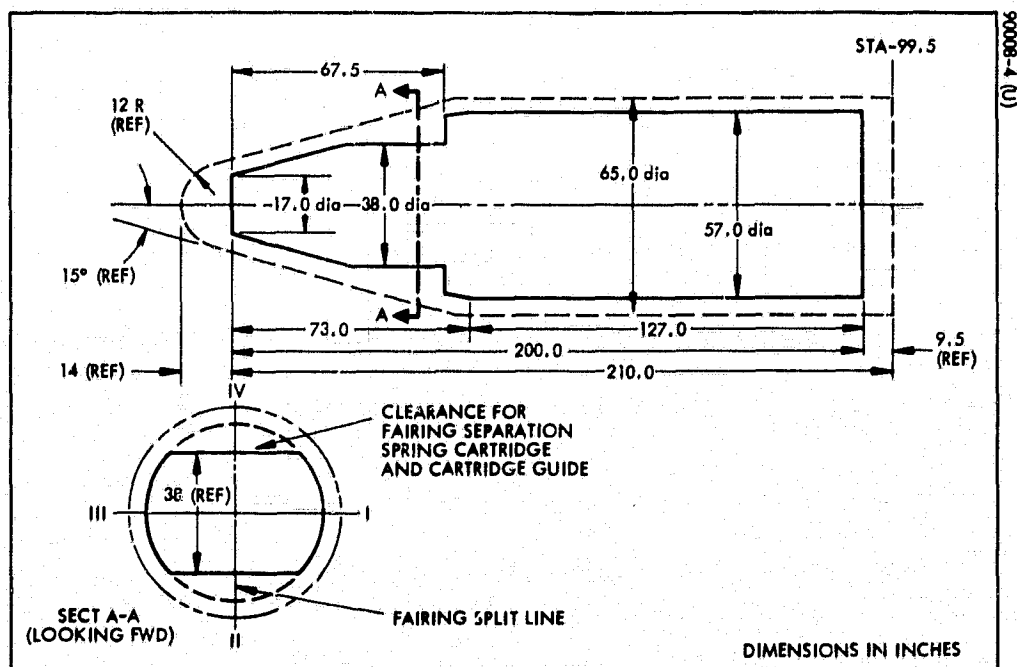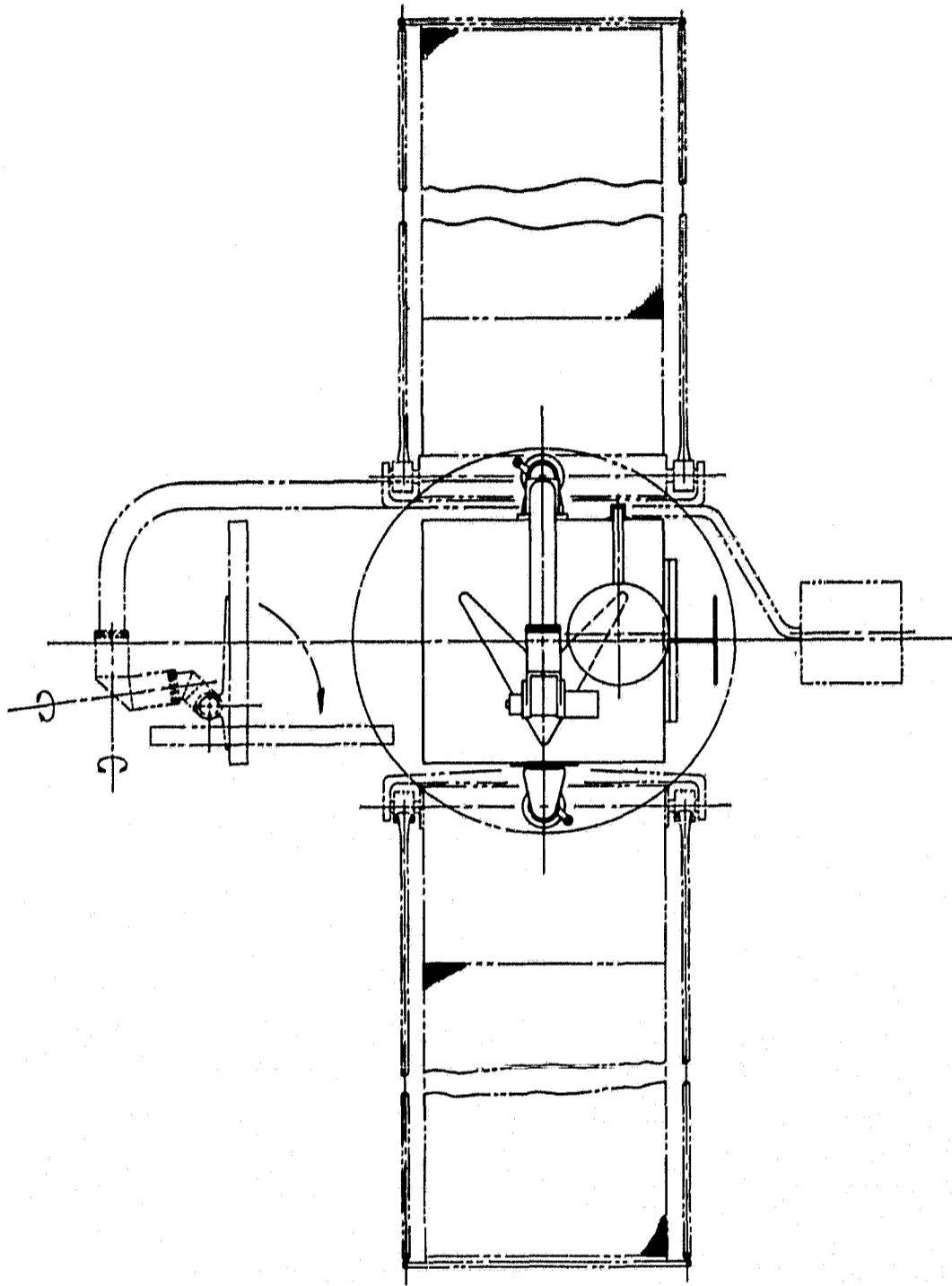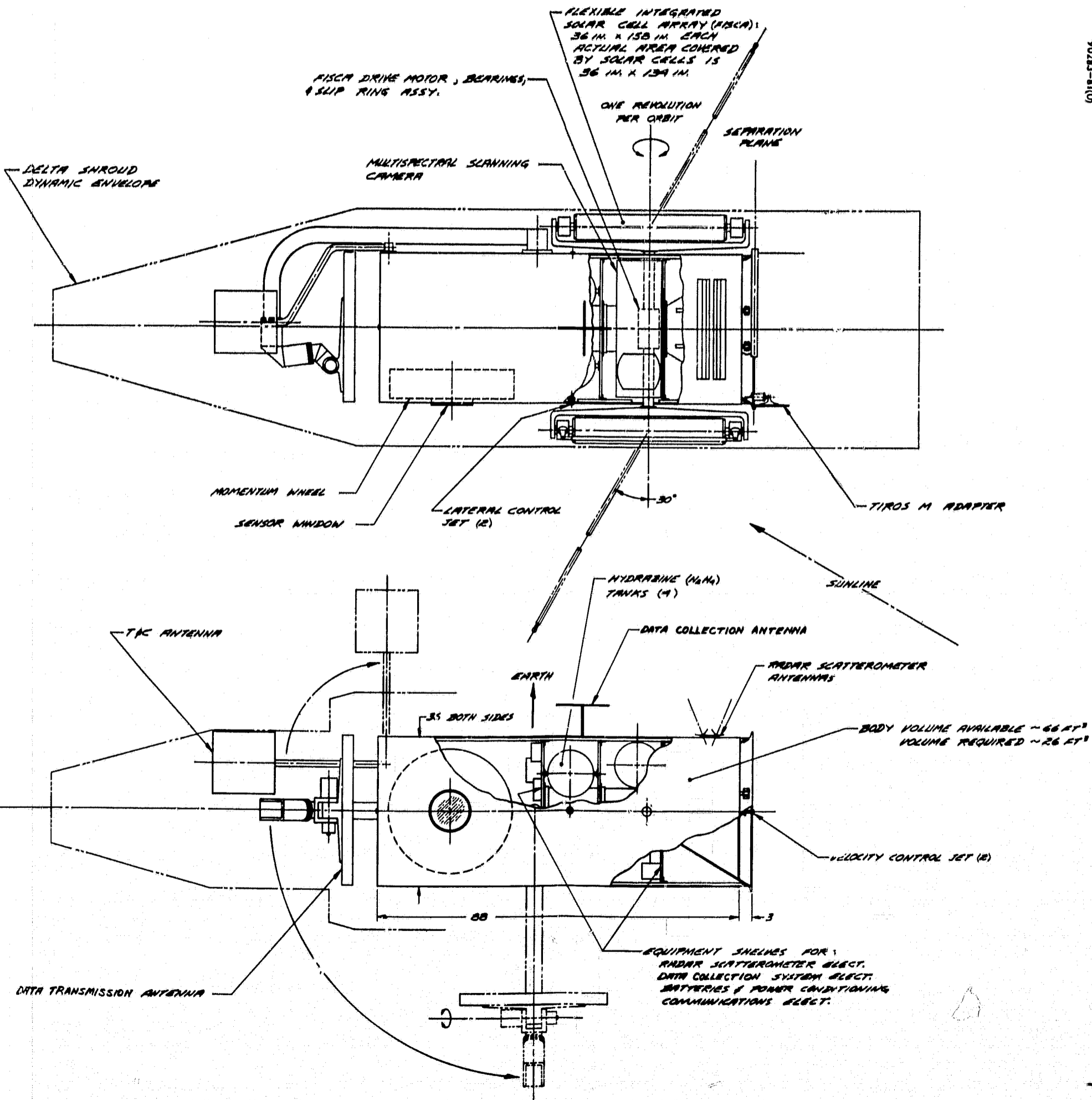

Figure 9-1. Improved Thor-Delta Booster Shroud

Payload capability = 1300 pounds

DIRECTION OF ORBIT

Figure 9-2. Packaging and Deployment Concept

FLEXIBLE INTEGRATED
SOLAR CELL ARRAY (FISCA):
36 IN. x 158 IN. EACH
ACTUAL AREA COVERED
BY SOLAR CELLS IS
36 IN. x 134 IN.

ONE REVOLUTION
PER ORBIT

SEPARATION
PLANE

FISCA DRIVE MOTOR, BEARINGS,
& SLIP RING ASSY.

MULTISPECTRAL SCANNING
CAMERA

DELTA SHROUD
DYNAMIC ENVELOPE

MOMENTUM WHEEL

SENSOR WINDOW

LATERAL CONTROL
JET (2)

30°

TIROS M ADAPTER

HYDRAZINE (N₂H₄)
TANKS (4)

SUNLINE

T&C ANTENNA

DATA COLLECTION ANTENNA

RADAR SCATTEROMETER
ANTENNAS

EARTH

35 BOTH SIDES

BODY VOLUME AVAILABLE ~66 FT³
VOLUME REQUIRED ~26 FT³

VELOCITY CONTROL JET (2)

88

3

DATA TRANSMISSION ANTENNA

EQUIPMENT SHELVES FOR:
RADAR SCATTEROMETER ELECT.
DATA COLLECTION SYSTEM ELECT.
BATTERIES & POWER CONDITIONING
COMMUNICATIONS ELECT.

FOLDOUT FRAME 2

GLOSSARY

LAS	Low altitude satellite
DRS	Data relay satellite
DRSS	Data relay satellite system
LOS	Line of sight
DTS	Data transmission system